Technische Universiteit Delft
Faculteit Elektrotechniek, Wiskunde en Informatica
Delft Institute of Applied Mathematics

Modelling and simulation of bone implant healing

Verslag ten behoeve van het
Delft Institute for Applied Mathematics
als onderdeel ter verkrijging

van de graad van

BACHELOR OF SCIENCE
in
TECHNISCHE WISKUNDE

door

MATTHEW THE

Delft, Nederland
Juni 2010

BSc verslag TECHNISCHE WISKUNDE

"Modelling and simulation of bone implant healing"

MATTHEW THE

Technische Universiteit Delft

Begeleider

Dr.ir. F.J.. Vermolen

Overige commissieleden

Prof.dr.ir. C. Vuik
Dr. J.L.A. Dubbeldam

Drs. A. Verweij

Juni, 2010

Delft

Contents

Chapter 1

Introduction

In this report a model for the ingrowth of a prosthesis in a bone will be formulated and simulated. First an overview is given of all the biological processes that are part of this healing process and what external factors can influence this process.

Then a first mathematical model is presented in which the mechanical stimuli (one of the external factors that can influence the healing process) are neglected. The model is solved by numerical means with both the finite volume method as the finite element method. For the finite element method a short introduction is first given to get familiar with this technique. Results for this model will be presented, followed by a short discussion about the results and a conclusion.

Subsequently the previous model is extended to incorporate mechanical stimuli, this is done by combining it with an elasticity equation. A short introduction will also be given to the theory of linear elasticity. The model is then solved using finite element analysis and finally also the results for this extended model will be presented, together with once again a short discussion and conclusion.

Chapter 2

Biological processes in bone implant healing

2.1 Overview

The goal of bone implant healing is the integration of the implant in the bone tissue of the patient, a process called osseointegration. This integration is achieved by the production of bone tissue that closes the gap between the bone and implant surface, which is in the order of tenths of millimeters. Other tissues than bone tissue may be produced during this process, but these are significantly weaker and therefore undesirable. The bone tissue is produced by osteoblasts that differentiate from osteogenic cells (or mesenchymal stem cells) and have migrated to the bone or implant surface. Differentiation, proliferation (cell growth and division) and migration of the osteogenic cells and osteoblasts are influenced by the mechanical state (stress and/or strain) of the tissue and by so called growth factors, which are produced by, among others, the same osteogenic cells and osteoblasts.

2.2 Cell types

All cells differentiate from stem cells which are found in bone marrow. In the production of tissues to attach the implant to the bone, three cell types are of importance: fibroblasts, chondrocytes and osteoblasts. They can either differentiate from stem cells or from each other, the directions of possible differentiation are shown in Figure 2.1.

- Fibroblasts produce fibrous tissue, which cannot withstand high tensile loads and is therefore not suitable as connective tissue in the long term.
- Chondrocytes produce an extracellular matrix in which the chondrocytes get trapped. Together they are known as cartilage, a tissue which is stiff but elastic. It is however not as stiff and hard as bone tissue and though it could serve as connective tissue between implant and bone for some time, it is not a desirable solution in the long term.
- Osteoblasts produce a bone matrix in which the osteoblasts get trapped, after which the osteoblasts become osteocytes. The osteocytes together with the bone matrix are known as bone tissue, which is a hard and stiff tissue. There are two types of bone tissue: woven bone and lamellar bone. In woven bone the fibers are not organized and it is mechanically inferior to lamellar bone, in which the fibers are neatly aligned.

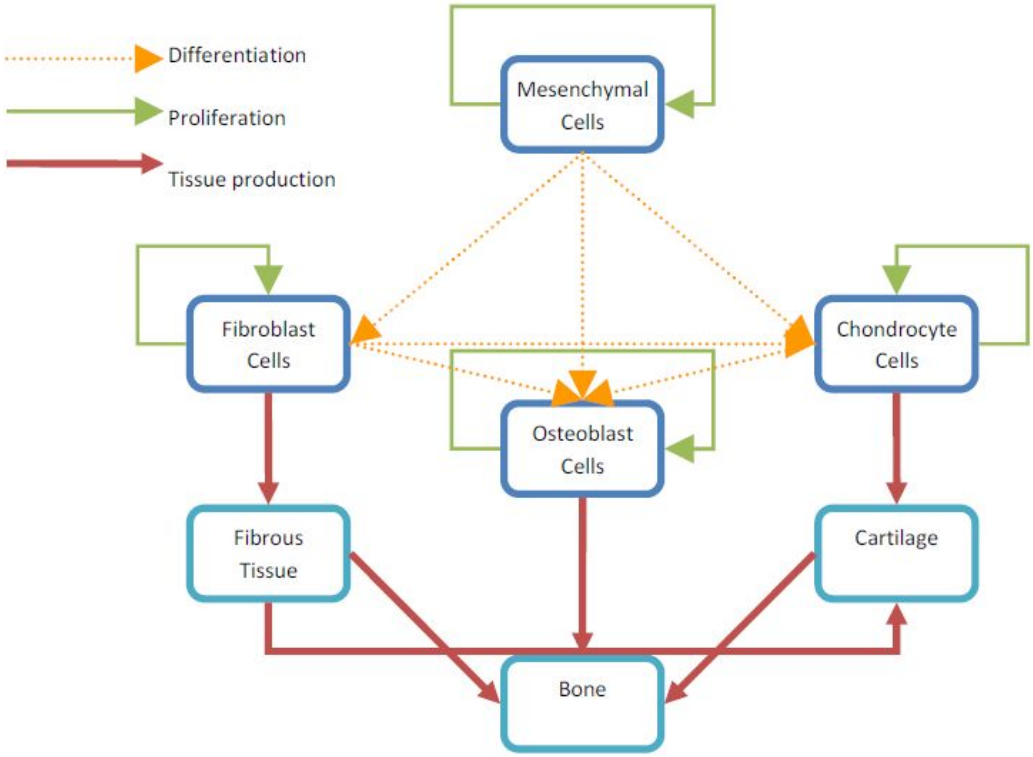

Figure 2.1: Differentiation and proliferation of osteogenic cells (stem cells), fibroblasts, chondrocytes and osteoblasts and the tissues they produce.

2.3 Healing process

Note: For a schematic graphical overview of all processes, see Appendix A.

To insert the implant, a cavity has to be drilled in the host bone. This will cause damage to blood vessels, which results in the filling of the cavity with blood. The blood contains proteins and platelets (or thrombocytes). The proteins are adsorbed at the bone and implant surfaces, the level of adsorbtion depends on the surface roughness of the surface, the rougher the surface the higher the adsorbtion. The adsorbed proteins activate the platelets, which then release different types of growth factors. These growth factors stimulate the migration and proliferation of stem cells and also stimulate the proliferation of osteoblasts. At the same time a process called hemostasis is in action, which makes the blood form clots due to the production of a fibrin network. The blood clot finally stops the bleeding. This whole process takes only a few minutes to complete.

Once the initial fase is over, the osteogenic cells migrate from the bone marrow to the cavity and differentiate into fibroblasts, chondrocytes and osteoblasts, that produce respectively fibrous tissue, cartilage and bone tissue. To which type of cell the osteogenic cells differentiates mainly depends on the mechanical state and the presence of growth factors. Moderate mechanical loading stimulates the differentiation of osteogenic cells into osteoblasts and also the secretion of growth factors by platelets, but at high mechanical loads the differentiation into ostoeblast decreases, while the differentiation into fibroblast increases. This will enhance the production of fibrous tissue in contrast to bone tissue, weakening the connection between bone and implant. Growth factors also stimulate the differentiation into osteoblasts and also stimulate the migration

of the osteogenic cells by a process called chemotaxis. Chemotaxis migrates the osteogenic cells along gradients of growth factors, in this case towards higher concentrations of growth factors. Growth factors also stimulate the secretion of new growth factors by platelets, osteogenic cells and osteoblasts.

Finally it should be noted that new tissues (fibrous tissue, cartilage or bone tissue) can only be formed on preexisting surfaces and that these tissues are of course immobile. Since bone tissue can only be formed by trapping the osteoblasts in the bone matrix, the formation of new bone can only be sustained by migration of new osteogenic cells to the surface of the implant or bone, where they will differentiate into osteoblasts again. Initially the osteoblasts form woven bone, which can be transformed into lamellar bone by a relatively slow process called bone remodelling.

Part I

Model without mechanical stimuli

Chapter 3

Mathematical model

We will use a continuum approach and look at the change in concentrations of different growth factors, cell types and tissues in time and space. This will result in a system of partial differential equations with boundary conditions, which will later be solved by numerical methods.

3.1 Assumptions and simplifications

The model was taken directly from [Moreo, 2008] with some adjustments from [Prokharau and Vermolen, 2010]. The following assumptions and simplifications have been made in this model:

- The blood clothing and the formation of the fibrin network is assumed to already have taken place. Since this is on a much smaller time scale than the process of bone tissue formation, it is not of importance in this model.
- The mechanical stresses are assumed to be optimal for the differentiation of osteogenic cells into osteoblasts, so no fibroblasts and chondrocytes will appear and cartilage and fibrous tissue will not be formed.
- Though there are many different growth factors responsible for many different mechanisms, we will model them with two generic growth factors types. The first type consists of different growth factors secreted by platelets and the second to growth factors secreted by osteogenic cells and osteoblasts.

3.2 Variables

The variables considered in this model can be divided into three categories:

- 3 cell types:
  - c: platelet density in $10^8 \frac{platelets}{ml}$
  - m: osteogenic cell density in $10^6 \frac{cells}{ml}$
  - b: ostoeblast density in $10^6 \frac{cells}{ml}$
- 2 (generic) growth factor types:
  - s_1: platelet derived growth factor in $100 \frac{ng}{ml}$
  - s_2: osteogenic derived growth factor in $100 \frac{ng}{ml}$

- 3 components of extracellular matrix
  - v_f: fibrin network volume fraction
  - v_w: woven bone volume fraction
  - v_l: lamellar bone volume fraction

Further we also have the concentration of adsorbed proteins p, this will however be a known function of space and time so this will not be a model variable.

Note that the densities have been scaled to a characteristic value (i.e. $10^8 \frac{platelets}{ml}$) so that they are dimensionless variables. The volume fractions of the components of extracellular matrix are between 0 and 1, and their sum is always equal to 1.

3.3 Computational domain

Throughout this model we will consider a dental implant that is drilled into the jaw with a metal screw (Figure 3.1).

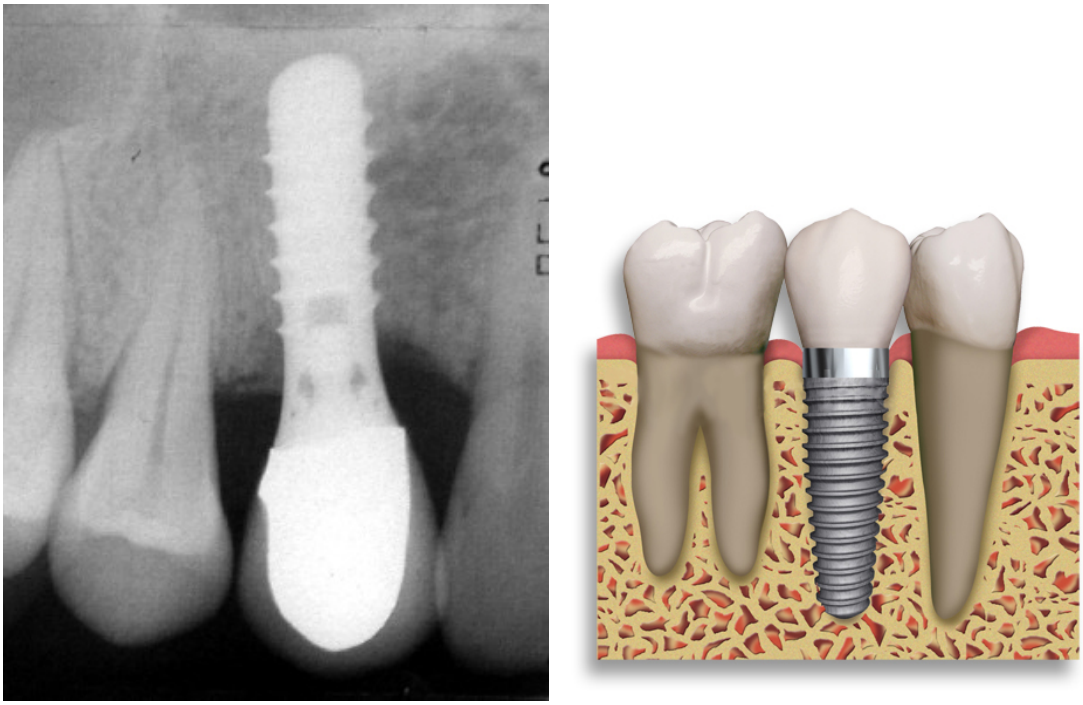

Figure 3.1: Left: X-ray of a dental implant fastened to the jaw with a metal screw. Right: schematic view of the dental implant between other teeth.

In the one dimensional case we will consider a small strip with a length of 0.6 mm, with the bone surface on the left and the implant surface on the right (see Fig. 3.2).
In the two dimensional case we will consider a rectangular area with a length of 1.4 mm and a width of 0.6 mm, with the left boundary as the bone surface and all other boundaries as implant surfaces (see Fig. 3.4). This is slightly different from the computational domain used in [Moreo, 2008], who used a trapezium area (see Fig. 3.3)

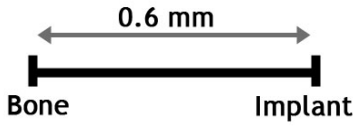

Figure 3.2: Computational domain in 1-D

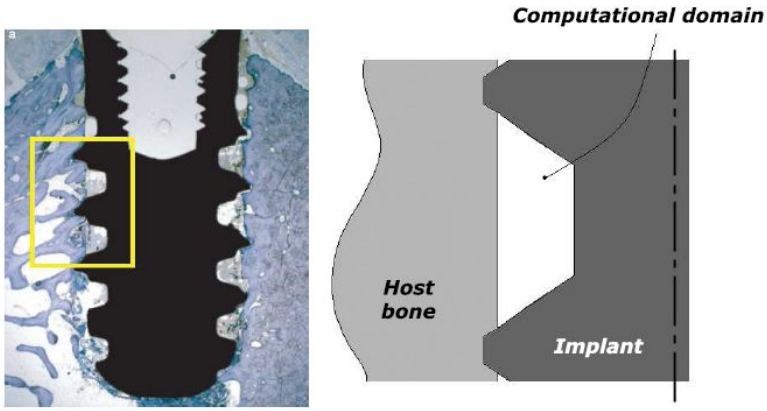

Figure 3.3: Dental implant and the accompanying computational domain in 2-D used by Moreo

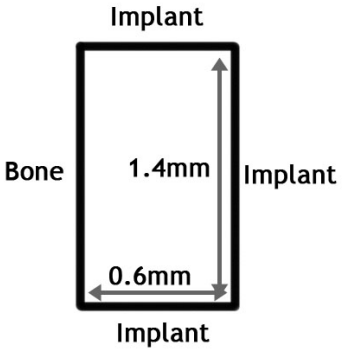

Figure 3.4: Computational domain in 2-D

3.4 Partial differential equations

3.4.1 Platelets, $c(\mathbf{x}, t)$

$$\frac{\partial c}{\partial t} = \nabla \cdot [\ \underbrace{D_c \nabla c}_{\text{Diffusion}}\ - \underbrace{H_c\ c \nabla p}_{\text{Taxis}}\ ] - \underbrace{A_c c}_{\text{Death}} \tag{3.1}$$

The flux consists of two terms: the first one is diffusion due to random migration of platelets, the second one models the movement of platelets towards a surface of adsorbed proteins by a linear 'taxis' (directed movement of cells) term. The last term simply models the cell death.

3.4.2 Osteogenic cells, $m(\mathbf{x}, t)$

$$\begin{aligned}\frac{\partial m}{\partial t} =& \nabla \cdot [\ \underbrace{D_m \nabla m}_{\text{Diffusion}} - \underbrace{m(B_{m1} \nabla s_1 + B_{m2} \nabla s_2)}_{\text{Chemotaxis}}\ ] \\ &+ \underbrace{\left(\alpha_{m0} + \frac{\alpha_m s_1}{\beta_m + s_1} + \frac{\alpha_m s_2}{\beta_m + s_2}\right) m(1-m)}_{\text{Proliferation}} - \underbrace{\frac{\alpha_{mb} s_1}{\beta_{mb} + s_1} m}_{\text{Differentiation}}\ - \underbrace{A_m m}_{\text{Death}}\end{aligned}$$

The flux once again consists of a diffusion term and a linear taxis term. The taxis term models positive chemotaxis, cell movement towards high concentrations of growth factors 1 and 2. The third term models proliferation enhanced by the presence of growth factors 1 and 2. The fourth term is the decrease in concentration due to differentiation of the osteogenic cells into osteoblasts, which depends on the concentration of growth factors 1. The last term once again models cell death.

3.4.3 Osteoblasts, $b(\mathbf{x}, t)$

$$\frac{\partial b}{\partial t} = \underbrace{\frac{\alpha_{mb} s_1}{\beta_{mb} + s_1} m}_{\text{Differentiation}}\ - \underbrace{A_b b}_{\text{Death}} \tag{3.2}$$

Osteoblasts are not mobile and can only form at a place due to the differentiation from osteogenic cells, represented by the first term (this is the counterpart of the same term in the equation for osteogenic cells). The last term represents the differentiation of osteoblasts into osteocytes once they get trapped in the extracellular matrix.

3.4.4 Growth factors 1, $s_1(\mathbf{x}, t)$

$$\frac{\partial s_1}{\partial t} = \nabla \cdot [\ \underbrace{D_{s1} \nabla s_1}_{\text{Diffusion}}\ ] + \underbrace{\left(\frac{\alpha_{c1} s_1}{\beta_{c1} + s_1} + \frac{\alpha_{c2} s_2}{\beta_{c2} + s_2}\right) c}_{\text{Secretion}} - \underbrace{A_{s1} s_1}_{\text{Decay}} \tag{3.3}$$

The growth factor flux is determined only by linear diffusion. Growth factors 1 are secreted by platelets as indicated by the second term. The secretion itself can be enhanced by the presence of both growth factors 1 and 2. The last term represents the natural decay of growth factors.

3.4.5 Growth factors 2, $s_2(\mathbf{x}, t)$

$$\frac{\partial s_2}{\partial t} = \nabla \cdot [\ \underbrace{D_{s2} \nabla s_2}_{\text{Diffusion}}\ ] + \underbrace{\frac{\alpha_{m2} s_2}{\beta_{m2} + s_2} m + \frac{\alpha_{b2} s_2}{\beta_{b2} + s_2} b}_{\text{Secretion}} - \underbrace{A_{s2} s_2}_{\text{Decay}} \tag{3.4}$$

This equation is very similar to the one for growth factors 1, the only difference lies in the second term. Growth factors 2 are secreted by osteogenic cells and osteoblasts and the secretion is only enhanced by growth factors 2.

3.4.6 Fibrin network volume fraction, $v_f(\mathbf{x}, t)$

$$\frac{\partial v_f}{\partial t} = - \underbrace{\frac{\alpha_w s_2}{\beta_w + s_2} b v_f (1 - v_w)}_{\text{Woven bone production}} \tag{3.5}$$

Fibrin network is assumed to be covering the whole area at the start of the process. As osteoblasts begin producing bone tissue this fibrin network is slowly substituted. The production of bone tissue can be enhanced by growth factors 2.

3.4.7 Woven bone volume fraction, $v_w(\mathbf{x}, t)$

$$\frac{\partial v_w}{\partial t} = \underbrace{\frac{\alpha_w s_2}{\beta_w + s_2} b v_f (1 - v_w)}_{\text{Production}} - \underbrace{\gamma v_w (1 - v_l)}_{\text{Bone remodelling}} \tag{3.6}$$

Obviously this equation contains the counterpart of the fibrin network equation. The other term models the slow substitution of woven bone into lamellar bone by the bone remodelling process.

3.4.8 Lamellar bone volume fraction, $v_l(\mathbf{x}, t)$

$$\frac{\partial v_l}{\partial t} = \underbrace{\gamma v_w (1 - v_l)}_{\text{Bone remodelling}} \tag{3.7}$$

Lamellar bone can only be formed from woven bone and the term is the counterpart of the bone remodelling term in the equation for the woven bone volume fraction.

3.4.9 Protein concentration, $p(\mathbf{x})$

We define $y = \min_{\mathbf{y} \in \Gamma_i} \{||\mathbf{x} - \mathbf{y}||\}$

$$p(\mathbf{x}) = \begin{cases} p_s(0.1 - y) & y < 0.1 \\ 0 & y \geq 0.1 \end{cases} \tag{3.8}$$

The protein concentration is a linear function of the distance from the implant surface Γ_i. At the implant surface it takes a value dependent of the microtopography of the implant surface, then it decreases linearly to zero at a certain distance from the implant surface. In the rest of the area the protein concentration is assumed to be zero.

Figure 3.5: Boundary conditions of the 2-D computational domain

3.5 Initial and boundary conditions

At all surfaces zero flux is assumed, since no movement is possible through either bone or implant surface. Only for the osteogenic cells a Dirichlet condition is taken for the first 14 days, when these cells migrate into the domain from the bone marrow. After these 14 days the zero flux condition is also placed for the osteogenic cells.

$$(D_c \nabla c(\mathbf{x},t) - H_c c(\mathbf{x},t) \nabla p(\mathbf{x})) \cdot \mathbf{n} = 0 \qquad \mathbf{x} \in \Gamma,\ t \in (0,\infty) \tag{3.9}$$

$$D_{s1} \nabla s_1(\mathbf{x},t) \cdot \mathbf{n} = 0 \qquad \mathbf{x} \in \Gamma,\ t \in (0,\infty) \tag{3.10}$$

$$D_{s2} \nabla s_2(\mathbf{x},t) \cdot \mathbf{n} = 0 \qquad \mathbf{x} \in \Gamma,\ t \in (0,\infty) \tag{3.11}$$

$$m(\mathbf{x},t) = 0.2 \qquad \mathbf{x} \in \Gamma,\ t \in (0,14] \tag{3.12}$$

$$\begin{aligned} (D_m \nabla m(\mathbf{x},t) - m(\mathbf{x},t)\,(B_{m1} \nabla s_1(\mathbf{x},t) \qquad & \{\ \mathbf{x} \in \Gamma \backslash \Gamma_b,\ t \in (0,14] \\ + B_{m2} \nabla s_2(\mathbf{x},t))) \cdot \mathbf{n} = 0 \qquad & \cup\ \mathbf{x} \in \Gamma,\ t \in (14,\infty)\ \} \end{aligned} \tag{3.13}$$

As initial conditions all concentrations are relatively low, with the exception of the platelet concentration. The volume fraction of the fibrin network is initially 1 (the whole domain is filled with fibrin network), whereas all other volume fractions are zero:

$$c(\mathbf{x},0) = 0.25, \tag{3.14}$$

$$m(\mathbf{x},0) = 0.001, \tag{3.15}$$

$$b(\mathbf{x},0) = 0.001, \tag{3.16}$$

$$s_1(\mathbf{x},0) = 0.01, \tag{3.17}$$

$$s_2(\mathbf{x},0) = 0.01, \tag{3.18}$$

$$v_f(\mathbf{x},0) = 1, \tag{3.19}$$

$$v_w(\mathbf{x},0) = 0, \tag{3.20}$$

$$v_l(\mathbf{x},0) = 0. \tag{3.21}$$

3.6 Parameters

The parameters are esimated from different in vivo and in vitro experiments, [Prokharau and Vermolen, 2010] propose the following parameters based on estimations made by [Moreo, 2008]:

$D_c = 1.365 \cdot 10^{-2}\ \frac{mm^2}{day}$ $H_c = 0.333\ \frac{mm^4}{day \cdot \mu g}$ $A_c = 0.067\ \frac{1}{day}$

$D_m = 0.133\ \frac{mm^2}{day}$ $B_{m1} = 0.667\ \frac{mm^2}{day}$ $B_{m2} = 0.167\ \frac{mm^2}{day}$
$\alpha_{m0} = 0.25\ \frac{1}{day}$ $\alpha_m = 0.25\ \frac{1}{day}$ $\beta_m = 0.1$
$\alpha_{p0} = 0.167\ \frac{1}{day}$ $\alpha_{mb} = 0.333\ \frac{1}{day}$ $\beta_{mb} = 0.1$
$A_m = 2 \cdot 10^{-3}\ \frac{1}{day}$

$D_{s1} = 0.3\ \frac{mm^2}{day}$ $\alpha_{c1} = 66.7\ \frac{1}{day}$ $\beta_{c1} = 0.1$
$\alpha_{c2} = 10\ \frac{1}{day}$ $\beta_{c2} = 0.1$ $A_{s1} = 10\ \frac{1}{day}$

$D_{s2} = 0.1\ \frac{mm^2}{day}$ $\alpha_{m2} = 25\ \frac{1}{day}$ $\beta_{m2} = 0.1$
$\alpha_{b2} = 25\ \frac{1}{day}$ $\beta_{b2} = 0.1$ $A_{s2} = 10\ \frac{1}{day}$

$\alpha_w = 0.1\ \frac{1}{day}$ $\beta_w = 0.1$ $\gamma = 0.01\ \frac{1}{day}$

$p_s = 0.1$

Chapter 4

Simulations using FVM

First the finite volume method (FVM) will be used in 1 dimension to derive a discretization of the spatial part of the PDEs presented earlier. After the discretization time integration will be done using the IMEX method and results of these simulations will be presented and interpreted.

4.1 Spatial discretization

The discretization will be done using the finite volume method, with the domain being the interval representing a cross-section of the domain from the bone surface to the implant surface (see Fig. 4.1). The interval is divided in equal subintervals e_k, $k = 1, \ldots, N$, with a nodal point x_k with function value u_k exactly in the middle of each subinterval. The length of each interval will be called h

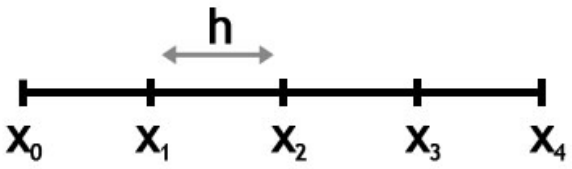

Figure 4.1: 1D domain for the FVM-discretization

The discrete equation is derived by integrating the whole PDE over each subinterval e_k.

4.1.1 General discretization of common terms

We will start with some general discretizations for terms that frequently appear in the partial differential equations presented earlier.

Partial time derivative

Taking the integral over the first partial time derivative, we can use the fact that the integral and derivative are interchangable because the integral is taken over space and the derivative over time. With the midpoint rule the discretization becomes:

$$\int_{e_n} \frac{\partial u}{\partial t}\, dV = \frac{d}{dt} \int_{e_n} u\, dV \approx \frac{d}{dt}(hu_n) = h\frac{du_n}{dt}$$

Diffusion

Diffusion is the random movement of particles in time, resulting in the spreading of this particle over a region. Diffusion is usually modeled by Fick's law:

$$\frac{\partial u}{\partial t} = D_u \nabla^2 u$$

The rate at which the spreading takes place is given by the diffusion coefficient D_u. Assuming that D_u is constant we take the integral over the test volume and apply Gauss's theorem:

$$\begin{aligned}\int_{e_n} \nabla \cdot (D_u \nabla u)\, dV = D_u \int_{\partial e_n} \frac{\partial u}{\partial n} d\Gamma &= D_u \left(\left.\frac{\partial u}{\partial x}\right|_{\Gamma_E} - \left.\frac{\partial u}{\partial x}\right|_{\Gamma_W} \right) \\ &\approx D_u \left(\frac{u_{n+1} - u_n}{h} + \frac{u_{n-1} - u_n}{h} \right) \\ &= \frac{D_u}{h} \left(u_{n-1} - 2u_n + u_{n+1} \right) \equiv \mathcal{D}(u) \end{aligned} \tag{4.1}$$

where the derivatives are approximated with central differences.

Death or decay

Cell death or growth factor decay is modeled by a decrease linear to the concentration itself by a factor A_u:

$$\frac{\partial u}{\partial t} = -A_u u$$

Taking the integral over the test volume:

$$-\int_{e_n} A_u u \; dV = -A_u \int_{e_n} u \; dV \approx -h A_u u_n \equiv \mathcal{M}(u) \tag{4.2}$$

where the integral is approximated using the midpoint rule.

Proliferation or differentiation

Proliferation and differentiation of a density or volume fraction u is modelled by a logistic growth term enhanced by a different density or volume fraction v:

$$\frac{\partial u}{\partial t} = \frac{\alpha_u v}{\beta_u + v} u$$

Taking the integral over the test volume:

$$\int_{e_n} \frac{\alpha_u v}{\beta_u + v} u \; dV \approx h \frac{\alpha_u v_n}{\beta_u + v_n} u_n \equiv \mathcal{P}(u, v) \tag{4.3}$$

where the integral is once again approximated using the midpoint rule.

Linear taxis or chemotaxis

Directed movement of cell type u in the form of a linear taxis term is modeled by an advection term along the gradient of another concentration v:

$$\frac{\partial u}{\partial t} = \nabla \cdot (-u H_u \nabla v)$$

Taking the integral over the test volume and using Gauss's theorem:

$$\begin{aligned}\int_{e_n} \nabla\cdot(-uH_u\nabla v)\,dV &= -H_u\int_{\partial e_n} u\frac{\partial v}{\partial n}d\Gamma \\ &= -H_u\left(u\left.\frac{\partial v}{\partial x}\right|_{\Gamma_E} - u\left.\frac{\partial v}{\partial x}\right|_{\Gamma_W}\right) \\ &\approx -H_u\left(\frac{u_{n+1}+u_n}{2}\frac{v_{n+1}-v_n}{h} + \frac{u_n+u_{n-1}}{2}\frac{v_{n-1}-v_n}{h}\right) \\ &= -\frac{H_u}{2h}\left[(v_{n-1}-v_n)\,u_{n-1} + (v_{n-1}-2v_n+v_{n+1})\,u_n\right. \\ &\quad \left. + (v_{n+1}-v_n)\,u_{n+1}\right] \equiv \mathcal{H}(u,v) \end{aligned} \tag{4.4}$$

where the derivatives of v are approximated with central differences.

4.1.2 Platelet concentration

$$\begin{aligned}\frac{\partial c}{\partial t} &= \nabla\cdot[D_c\nabla c - H_c\; c\nabla p\;] - A_c c \\ h\frac{dc_n}{dt} &= \mathcal{D}(c) + \mathcal{H}(c,p) + \mathcal{M}(c) \\ &= \frac{D_c}{h}(c_{n-1}-2c_n+c_{n+1}) \\ &\quad -\frac{H_c}{2h}\left[(p_{n-1}-p_n)\,c_{n-1} + (p_{n-1}-2p_n+p_{n+1})\,c_n + (p_{n+1}-p_n)\,c_{n+1}\right] - hA_cc_n \end{aligned} \tag{4.5}$$

Bone surface boundary condition

$$D_c\frac{\partial c}{\partial n} - H_c c\frac{\partial p}{\partial n} = 0, \quad \mathbf{x}\in\Gamma_b \tag{4.6}$$

Discretization:

$$D_c\frac{c_1-c_0}{h} - H_c\frac{c_1+c_0}{2}\frac{p_1-p_0}{h} = 0 \tag{4.7}$$

$$\left(\frac{D_c}{h} - \frac{H_c}{2h}(p_1-p_0)\right)c_1 = \left(\frac{D_c}{h} + \frac{H_c}{2h}(p_1-p_0)\right)c_0 \tag{4.8}$$

Define $\frac{2D_c-H_c(p_1-p_0)}{2D_c+H_c(p_1-p_0)} = C$, so that $c_0 = Cc_1$. Then the equation for $n=1$ can be written as:

$$h\frac{dc_1}{dt} = \frac{D_c}{h}(c_2-(2-C)c_1) - hA_cc_1 - \frac{H_c}{2h}\left[c_2(p_2-p_1) + c_1(p_2-(2+C)p_1+(1+C)p_0))\right] \tag{4.9}$$

Implant surface boundary condition

$$D_c\frac{\partial c}{\partial n} - H_c c\frac{\partial p}{\partial n} = 0, \quad \mathbf{x}\in\Gamma_i \tag{4.10}$$

Similar to the derivation of the left boundary we define $\frac{2D_c-H_c(p_{n+1}-p_n)}{2D_c+H_c(p_{n+1}-p_n)} = C$, so that $c_{n+1} = Cc_n$. Then the equation for $n=N$ can be written as:

$$\begin{aligned} h\frac{dc_N}{dt} &= \frac{D_c}{h}(c_{N-1}-(2-C)c_N) - hA_cc_N \\ &\quad -\frac{H_c}{2h}\left[c_{N-1}(p_{N-1}-p_N) + c_N(p_{N-1}-(2+C)p_N+(1+C)p_{N+1}))\right] \end{aligned} \tag{4.11}$$

4.1.3 Osteogenic cells

$$
\begin{aligned}
\frac{\partial m}{\partial t} &= \nabla \cdot \left[D_m \nabla m - m(B_{m1} \nabla s_1 + B_{m2} \nabla s_2) \right] \\
&\quad + \left(\alpha_{m0} + \frac{\alpha_m s_1}{\beta_m + s_1} + \frac{\alpha_m s_2}{\beta_m + s_2} \right) m(1-m) - \frac{\alpha_{mb} s_1}{\beta_{mb} + s_1} m - A_m m \\
h\frac{dm_n}{dt} &= \mathcal{D}(m) + \mathcal{H}(m, s_1) + \mathcal{H}(m, s_2) + \left(\alpha_{m0} m + \mathcal{P}(s_1, m) + \mathcal{P}(s_2, m) \right)(1-m) \\
&\quad - \mathcal{P}(s_1, m) + \mathcal{M}(m) \\
&= \frac{D_m}{h} \left(m_{n-1} - 2m_n + m_{n+1} \right) \\
&\quad - \frac{B_{m1}}{2h} \left[\left(s_{1n-1} - s_{1n} \right) m_{n-1} + \left(s_{1n-1} - 2s_{1n} + s_{1n+1} \right) m_n + \left(s_{1n+1} - s_{1n} \right) m_{n+1} \right] \\
&\quad - \frac{B_{m2}}{2h} \left[\left(s_{2n-1} - s_{2n} \right) m_{n-1} + \left(s_{2n-1} - 2s_{2n} + s_{2n+1} \right) m_n + \left(s_{2n+1} - s_{2n} \right) m_{n+1} \right] \\
&\quad + \left(h\alpha_{m0} m_n + h\frac{\alpha_m s_{1n}}{\beta_m + s_{1n}} m_n + h\frac{\alpha_m s_{2n}}{\beta_m + s_{2n}} m_n \right)(1 - m_n) - h\frac{\alpha_{mb} s_{1n}}{\beta_{mb} + s_{1n}} m_n \\
&\quad - h A_m m_n
\end{aligned} \tag{4.12}
$$

Bone surface boundary conditions

$$
\begin{cases} m(\mathbf{x}, t) = 0.2 & , \ \mathbf{x} \in \Gamma_b, \ t \in (0, 14] \\ D_m \frac{\partial m}{\partial n} - B_{m1} m \frac{\partial s_1}{\partial n} - B_{m2} m \frac{\partial s_2}{\partial n} = 0 & , \ \mathbf{x} \in \Gamma_b, \ t \in (14, \infty) \end{cases} \tag{4.13}
$$

Dirichlet boundary condition, $t \in (0, 14]$

Using linear interpolation the boundary condition becomes:

$$
\frac{m_0 + m_1}{2} = 0.2 \quad \Rightarrow \quad m_0 = 0.4 - m_1 \tag{4.14}
$$

Inserting this into the first equation $n = 1$ and taking into account the zero flux boundary conditions on growth factors 1 and 2 ($s_{11} = s_{10}$ and $s_{21} = s_{20}$), the equation becomes:

$$
\begin{aligned}
h\frac{dm_1}{dt} &= \frac{D_m}{h}(0.4 - 3m_1 + m_2) - \frac{B_{m1}}{2h}(s_{12} - s_{11})(m_1 + m_2) - \frac{B_{m2}}{2h}(s_{22} - s_{21})(m_1 + m_2) \\
&\quad + h \left(\alpha_{m0} + \frac{\alpha_m s_{11}}{\beta_m + s_{11}} + \frac{\alpha_m s_{21}}{\beta_m + s_{21}} \right) m_1(1 - m_1) - h\frac{\alpha_{mb} s_{11}}{\beta_{mb} + s_{11}} m_1 - h A_m m_1
\end{aligned} \tag{4.15}
$$

Neumann boundary, $t \in (14, \infty)$

Applying the Finite volume method to the flux term of the boundary element at the bone surface:

$$
\begin{aligned}
\Phi_{m0} &= \int_{V_1} \nabla \cdot \left[D_m \nabla m - m(B_{m1} \nabla s_1 + B_{m2} \nabla s_2) \right] dV \\
&= \left[D_m \frac{\partial m}{\partial n} - B_{m1} m \frac{\partial s_1}{\partial n} - B_{m2} m \frac{\partial s_2}{\partial n} \right]\Bigg|_{\Gamma_E} - \left[D_m \frac{\partial m}{\partial n} - B_{m1} m \frac{\partial s_1}{\partial n} - B_{m2} m \frac{\partial s_2}{\partial n} \right]\Bigg|_{\Gamma_W} \\
&= \left[D_m \frac{\partial m}{\partial n} - B_{m1} m \frac{\partial s_1}{\partial n} - B_{m2} m \frac{\partial s_2}{\partial n} \right]\Bigg|_{\Gamma_W} \\
&\approx \frac{D_m}{h}(m_2 - m_1) - \frac{B_{m1}}{2h}(m_2 + m_1)\left(s_{12} - s_{11} + s_{22} - s_{21} \right)
\end{aligned} \tag{4.16}
$$

Adding the production, differentiation and cell death terms the equation for $n = 1$ becomes:

$$h\frac{dm_1}{dt} = \frac{D_m}{h}(m_2 - m_1) - \frac{B_{m1}}{2h}\left(m_2(s_{12} - s_{11} + s_{22} - s_{21}) + m_1(s_{12} - s_{11} + s_{22} - s_{21})\right) + \left(h\alpha_{m0}m_1 + h\frac{\alpha_m s_{11}}{\beta_m + s_{11}}m_1 + h\frac{\alpha_m s_{21}}{\beta_m + s_{21}}m_1\right)(1 - m_1) - h\frac{\alpha_{mb}s_{11}}{\beta_{mb} + s_{11}}m_1 - hA_m m_1 \tag{4.17}$$

Implant surface boundary conditions

$$D_m\frac{\partial m}{\partial n} - B_{m1}m\frac{\partial s_1}{\partial n} - B_{m2}m\frac{\partial s_2}{\partial n} = 0, \quad \mathbf{x} \in \Gamma_i,\ t \in (14, \infty) \tag{4.18}$$

Similar to the case of the bone surface boundary condition, the last equation becomes

$$h\frac{dm_N}{dt} = \frac{D_m}{h}(m_N - m_{N-1}) - \frac{B_{m1}}{2h}\left[(m_N + m_{N-1})(s_{1N} - s_{1N-1} + s_{2N} - s_{2N-1})\right] + \left(h\alpha_{m0} + h\frac{\alpha_m s_{1N}}{\beta_m + s_{1N}} + h\frac{\alpha_m s_{2N}}{\beta_m + s_{2N}}\right)m_N(1 - m_N) - h\frac{\alpha_{mb}s_{1N}}{\beta_{mb} + s_{1N}}m_N - hA_m m_N \tag{4.19}$$

4.1.4 Osteoblasts

$$\begin{aligned}\frac{\partial b}{\partial t} &= \frac{\alpha_{mb}s_1}{\beta_{mb} + s_1}m - A_b b \\ h\frac{db_n}{dt} &= \mathcal{P}(s_1, m) + \mathcal{M}(b) \\ &= h\frac{\alpha_{mb}s_{1n}}{\beta_{mb} + s_{1n}}m_n - hA_b b_n\end{aligned} \tag{4.20}$$

4.1.5 Growth factors I

$$\begin{aligned}\frac{\partial s_1}{\partial t} &= \nabla \cdot [\ D_{s1}\nabla s_1\ ] + \left(\frac{\alpha_{c1}s_1}{\beta_{c1} + s_1} + \frac{\alpha_{c2}s_2}{\beta_{c2} + s_2}\right)c - A_{s1}s_1 \\ h\frac{ds_{1n}}{dt} &= \mathcal{D}(s_1) + \mathcal{P}(s_1, c) + \mathcal{P}(s_2, c) + \mathcal{M}(s_1) \\ &= \frac{D_{s_1}}{h}\left(s_{1n-1} - 2s_{1n} + s_{1n+1}\right) + h\frac{\alpha_{c1}s_{1n}}{\beta_{c1} + s_{1n}}c_n + h\frac{\alpha_{c2}s_{2n}}{\beta_{c2} + s_{2n}}c_n - hA_{s_1}s_{1n}\end{aligned} \tag{4.21}$$

Bone surface boundary conditions

$$D_{s1}\frac{\partial s_1}{\partial n} = 0, \quad \mathbf{x} \in \Gamma_b \tag{4.22}$$

Similar to the case of the osteogenic cells the flux term of the first volume can be written as:

$$\begin{aligned}\Phi_{s_1 0} &= \int_{V_1} \nabla \cdot (D_{s1}\nabla s_1)\ dV \\ &= D_{s1}\left(\left.\frac{\partial s_1}{\partial n}\right|_{\Gamma_E} - \left.\frac{\partial s_1}{\partial n}\right|_{\Gamma_W}\right) = D_{s1}\left.\frac{\partial s_1}{\partial n}\right|_{\Gamma_W} \\ &\approx \frac{D_{s1}}{h}(s_{12} - s_{11})\end{aligned} \tag{4.23}$$

Adding the production and decay terms, the equation for $n = 1$ becomes:

$$h\frac{ds_{11}}{dt} = \frac{D_{s1}}{h}(s_{12} - s_{11}) + h\frac{\alpha_{c1}s_{11}}{\beta_{c1} + s_{11}}c_1 + h\frac{\alpha_{c2}s_{21}}{\beta_{c2} + s_{21}}c_1 - hA_{s1}s_{11} \tag{4.24}$$

Implant surface boundary conditions

$$D_{s1}\frac{\partial s_1}{\partial n} = 0, \quad \mathbf{x} \in \Gamma_i \tag{4.25}$$

Similar to the bone surface boundary condition, the equation for $n = N$ becomes:

$$h\frac{ds_{1N}}{dt} = \frac{D_{s1}}{h}(s_{1N-1} - s_{1N}) + h\frac{\alpha_{c1}s_{1N}}{\beta_{c1} + s_{1N}}c_N + h\frac{\alpha_{c2}s_{2N}}{\beta_{c2} + s_{2N}}c_N - hA_{s1}s_{1N} \tag{4.26}$$

4.1.6 Growth factors II

$$\begin{aligned}
\frac{\partial s_2}{\partial t} &= \nabla \cdot [\ D_{s2}\nabla s_2\ ] + \frac{\alpha_{m2}s_2}{\beta_{m2} + s_2}m + \frac{\alpha_{b2}s_2}{\beta_{b2} + s_2}b - A_{s2}s_2 \\
h\frac{ds_{2n}}{dt} &= \mathcal{D}(s_2) + \mathcal{P}(s_2, m) + \mathcal{P}(s_2, b) + \mathcal{M}(s_2) \\
&= \frac{D_{s_2}}{h}\left(s_{2n-1} - 2s_{2n} + s_{2n+1}\right) + h\frac{\alpha_{m2}s_{2n}}{\beta_{m2} + s_{2n}}m_n + h\frac{\alpha_{b2}s_{2n}}{\beta_{b2} + s_{2n}}b_n - hA_{s_2}s_{2n}
\end{aligned} \tag{4.27}$$

Bone surface boundary conditions

$$D_{s2}\frac{\partial s_2}{\partial n} = 0, \quad \mathbf{x} \in \Gamma_b \tag{4.28}$$

Similar to the boundary condition for Growth factors I, the equation for $n = 1$ becomes:

$$h\frac{ds_{21}}{dt} = \frac{D_{s1}}{h}(s_{22} - s_{21}) + h\frac{\alpha_{m2}s_{21}}{\beta_{m2} + s_{21}}m_1 + h\frac{\alpha_{b2}s_{21}}{\beta_{b2} + s_{21}}b_1 - hA_{s2}s_{21} \tag{4.29}$$

Implant surface boundary conditions

$$D_{s2}\frac{\partial s_2}{\partial n} = 0, \quad \mathbf{x} \in \Gamma_i \tag{4.30}$$

Similar to the boundary condition for Growth factors I, the equation for $n = N$ becomes:

$$h\frac{ds_{2N}}{dt} = \frac{D_{s1}}{h}(s_{2N-1} - s_{2N}) + h\frac{\alpha_{m2}s_{2N}}{\beta_{m2} + s_{2N}}m_N + h\frac{\alpha_{b2}s_{2N}}{\beta_{b2} + s_{2N}}b_N - hA_{s2}s_{2N} \tag{4.31}$$

4.1.7 Fibrin network

$$\begin{aligned}
\frac{\partial v_f}{\partial t} &= -\frac{\alpha_w s_2}{\beta_w + s_2}bv_f(1 - v_w) \\
h\frac{dv_{f_n}}{dt} &= \mathcal{P}(s_2, b)v_f(1 - v_w) \\
&= h\frac{\alpha_w s_{2n}}{\beta_w + s_{2_n}}b_n v_{f_n}(1 - v_{w_n})
\end{aligned} \tag{4.32}$$

4.1.8 Woven bone

$$\begin{aligned}\frac{\partial v_w}{\partial t} &= \frac{\alpha_w s_2}{\beta_w + s_2} b v_f (1 - v_w) - \gamma v_w (1 - v_l) \\ h\frac{dv_{wn}}{dt} &= \mathcal{P}(s_2, b) v_f (1 - v_w) - \gamma v_w (1 - v_l) \\ &= h\frac{\alpha_w s_{2n}}{\beta_w + s_{2n}} b_n v_{f_n} (1 - v_{w_n}) - h\gamma v_{w_n} (1 - v_{l_n})\end{aligned} \tag{4.33}$$

4.1.9 Lamellar bone

$$\begin{aligned}\frac{\partial v_l}{\partial t} &= \gamma v_w (1 - v_l) \\ h\frac{dv_{ln}}{dt} &= h\gamma v_{w_n} (1 - v_{l_n})\end{aligned} \tag{4.34}$$

4.2 Time integration

Time integration was done with the Implicit-Explicit (IMEX) method, a hybrid form of implicit and explicit time integration methods. For every appearance of u_n a decision has to be made whether to evaluate it on the current or the next time step. If u_n is evaluated at the current time step, the value is known and evaluation of the corrector is easy; this corresponds to an explicit method. If u_n is evaluated at the next time step, the value is unknown and has to be solved from the resulting equation; this corresponds to an implicit method. The main disadvantage of explicit methods is the high stability requirements for the time step, whereas implicit methods are unconditionally stable. The main disadvantage of implicit methods is that the resulting equation is usually non-linear and requires a numeric scheme (Newton-Rhapson, Picard iteration) to solve, which can be very time consuming.

To prevent having to use very large matrices, all variables other than the variable being time integrated are taken on the current time step. By doing this no coupling is needed, so all variables can use their own discretization matrix of size $N \times N$ (instead of possibly $2N \times 2N$ or even $3N \times 3N$).

Platelet concentration

The only model variable present in this equation is c (p is a known function of $\mathbf{x}$) and since no non-linear terms are present, all c_k are taken on the next time step to achieve the best stability characteristics.

$$\begin{aligned}h\frac{c_n^{i+1} - c_n^i}{\Delta t} = \frac{D_c}{h}\left(c_{n-1}^{i+1} - 2c_n^{i+1} + c_{n+1}^{i+1}\right) + \frac{H_c}{2h}\left[(p_{n-1} - p_n)\, c_{n-1}^{i+1} + (p_{n-1} - 2p_n + p_{n+1})\, c_n^{i+1}\right. \\ \left. + (p_{n+1} - p_n)\, c_{n+1}^{i+1}\right] - hA_c c_n^{i+1}\end{aligned} \tag{4.35}$$

Osteogenic cells

There are three model variables present in this equation: m, s_1 and s_2. s_1 and s_2 are taken on the current time step, for reasons mentioned earlier. The only m that is taken on the current time step appears in the proliferation term, to prevent the quadratic term that would otherwise appear.

$$
\begin{aligned}
h\frac{m_n^{i+1}-m_n^i}{\Delta t} &= \frac{D_m}{h}\left(m_{n-1}^{i+1}-2m_n^{i+1}+m_{n+1}^{i+1}\right)\\
&-\frac{B_{m1}}{2h}\left[\left(s1_{n-1}^i-s1_n^i\right)m_{n-1}^{i+1}+\left(s1_{n-1}^i-2s1_n^i+s1_{n+1}^i\right)m_n^{i+1}+\left(s1_{n+1}^i-s1_n^i\right)m_{n+1}^{i+1}\right]\\
&-\frac{B_{m2}}{2h}\left[\left(s2_{n-1}^i-s2_n^i\right)m_{n-1}^{i+1}+\left(s2_{n-1}^i-2s2_n^i+s2_{n+1}^i\right)m_n^{i+1}+\left(s2_{n+1}^i-s2_n^i\right)m_{n+1}^{i+1}\right]\\
&+h\left(\alpha_{m0}+\frac{\alpha_m s1_n^i}{\beta_m+s1_n^i}+\frac{\alpha_m s2_n^i}{\beta_m+s2_n^i}\right)m_n^{i+1}(1-m_n^i)-\frac{\alpha_{mb}s1_n^i}{\beta_{mb}+s1_n^i}m_n^{i+1}-hA_m m_n^{i+1}
\end{aligned}
\tag{4.36}
$$

Osteoblasts

$$
h\frac{b_n^{i+1}-b_n^i}{\Delta t}=\frac{\alpha_{mb}s1_n^i}{\beta_{mb}+s1_n^i}m_n^i-hA_b b_n^{i+1} \tag{4.37}
$$

Growth factors I

$$
h\frac{s1_n^{i+1}-s1_n^i}{\Delta t}=\frac{D_{s1}}{h}\left(s1_{n-1}^{i+1}-2s1_n^{i+1}+s1_{n+1}^{i+1}\right)+\frac{\alpha_{c1}s1_n^{i+1}}{\beta_{c1}+s1_n^i}c_n^i+\frac{\alpha_{c2}s2_n^i}{\beta_{c2}+s2_n^i}c_n^i-hA_{s1}s1_n^{i+1} \tag{4.38}
$$

Growth factors II

$$
h\frac{s2_n^{i+1}-s2_n^i}{\Delta t}=\frac{D_{s2}}{h}\left(s2_{n-1}^{i+1}-2s2_n^{i+1}+s2_{n+1}^{i+1}\right)+\frac{\alpha_{m2}s2_n^{i+1}}{\beta_{m2}+s2_n^i}m_n^i+\frac{\alpha_{b2}s2_n^{i+1}}{\beta_{b2}+s2_n^i}b_n^i-hA_{s2}s2_n^{i+1} \tag{4.39}
$$

Fibrin network

$$
h\frac{vf_n^{i+1}-vf_n^i}{\Delta t}=\frac{\alpha_w s2_n^i}{\beta_w+s2_n^i}b_n^i vf_n^{i+1}(1-vw_n^i) \tag{4.40}
$$

Woven bone

$$
h\frac{vw_n^{i+1}-vw_n^i}{\Delta t}=\frac{\alpha_w s2_n^i}{\beta_w+s2_n^i}b_n^i vf_n^i(1-vw_n^{i+1})-h\gamma vw_n^{i+1}(1-vl_n^i) \tag{4.41}
$$

Lamellar bone

$$
h\frac{vl_n^{i+1}-vl_n^i}{\Delta t}=h\gamma vw_n^i(1-vl_n^{i+1}) \tag{4.42}
$$

4.3 Implementation

After spatial and time discretization have been done, we are left with a system of the form (with $\mathbf{u}$ the vector containing all model variables and $\mathbf{v}$ the vector containing just one of the model variables, e.g. c, m):

$$
\frac{M}{\Delta t}\mathbf{v}^{i+1}=\frac{M}{\Delta t}\mathbf{v}^i+S\mathbf{v}^{i+1}+T(\mathbf{u}^i)\mathbf{v}^{i+1}+\mathbf{f}(\mathbf{u}^i) \tag{4.43}
$$

with M, S, T matrices and $\mathbf{f}$ a vector. The matrix M is known as the *mass matrix* and the sum of matrix S and T is known as the *stiffness matrix*. Notice that M and S are constant matrices, whereas T and $\mathbf{f}$ vary with time. Seperating $\mathbf{v}^{i+1}$ and $\mathbf{v}^i$:

$$
\left(\frac{M}{\Delta t}-S-T(\mathbf{u}^i)\right)\mathbf{v}^{i+1}=\frac{M}{\Delta t}\mathbf{v}^i+\mathbf{f}(\mathbf{u}^i) \tag{4.44}
$$

Leading to the final expression for $\mathbf{v}^{i+1}$:

$$\mathbf{v}^{i+1} = \left(\frac{M}{\Delta t} - S - T(\mathbf{u}^i)\right)^{-1} \left(\frac{M}{\Delta t}\mathbf{v}^i + \mathbf{f}(\mathbf{u}^i)\right) \tag{4.45}$$

This would require an evaluation of a matrix inverse at each time step, which is not very time efficient.

Alternatively another choice in the IMEX method can be made: take all non-linear terms (including terms that have some combination of different model variables) at the current time step. This would lead to the following system:

$$\frac{M}{\Delta t}\mathbf{v}^{i+1} = \frac{M}{\Delta t}\mathbf{v}^i + S\mathbf{v}^{i+1} + T(\mathbf{u}^i)\mathbf{v}^i + \mathbf{f}(\mathbf{u}^i) \tag{4.46}$$

note that $T(\mathbf{u}^i)$ is multiplied with $\mathbf{v}^i$ instead of $\mathbf{v}^{i+1}$ now. This would result in a much easier form to calculate:

$$\mathbf{v}^{i+1} = \left(\frac{M}{\Delta t} - S\right)^{-1} \left(\left(\frac{M}{\Delta t} + T(\mathbf{u}^i)\right)\mathbf{v}^i + \mathbf{f}(\mathbf{u}^i)\right) \tag{4.47}$$

requiring that the matrix inverse only has to be calculated once at the start. The equations for this particular implementation for the IMEX method (similar to Eq. (4.35) to (4.42)) can be found in Appendix B

In summary, there are now two different approaches of implementing the IMEX method. In the first approach variables were only taken on the current time step if non-linear terms in the equation variable (i.e. c in the platelet equation, m in the osteogenic cell equation, etc.) would otherwise arise, in the second approach all terms that had two or more system variables (i.e. the set of all variables $\{c, m, \ldots\}$) were taken on the current time step. So in the first method much more variables are taken on the next time step, then in the second and therefore it is in the line of expectation that the first method will behave more like an implicit method (allowing bigger time steps) than the second method.

4.4 Results

4.4.1 Comparison of the 2 IMEX methods

The two IMEX methods described in 4.2 are compared with the parameters: $nx = 200$, $dt = 0.5$ and $T_{max} = 10$. The results for method 1 are shown in Figure 4.2 and the results for method 2 are shown in 4.3. The numerical scheme for the first method is instable and for the second method it is stable. The second method also is also faster by a factor 2, because there are a lot less matrix inversion operations. So only the second method will be used from now on.
Method 1:

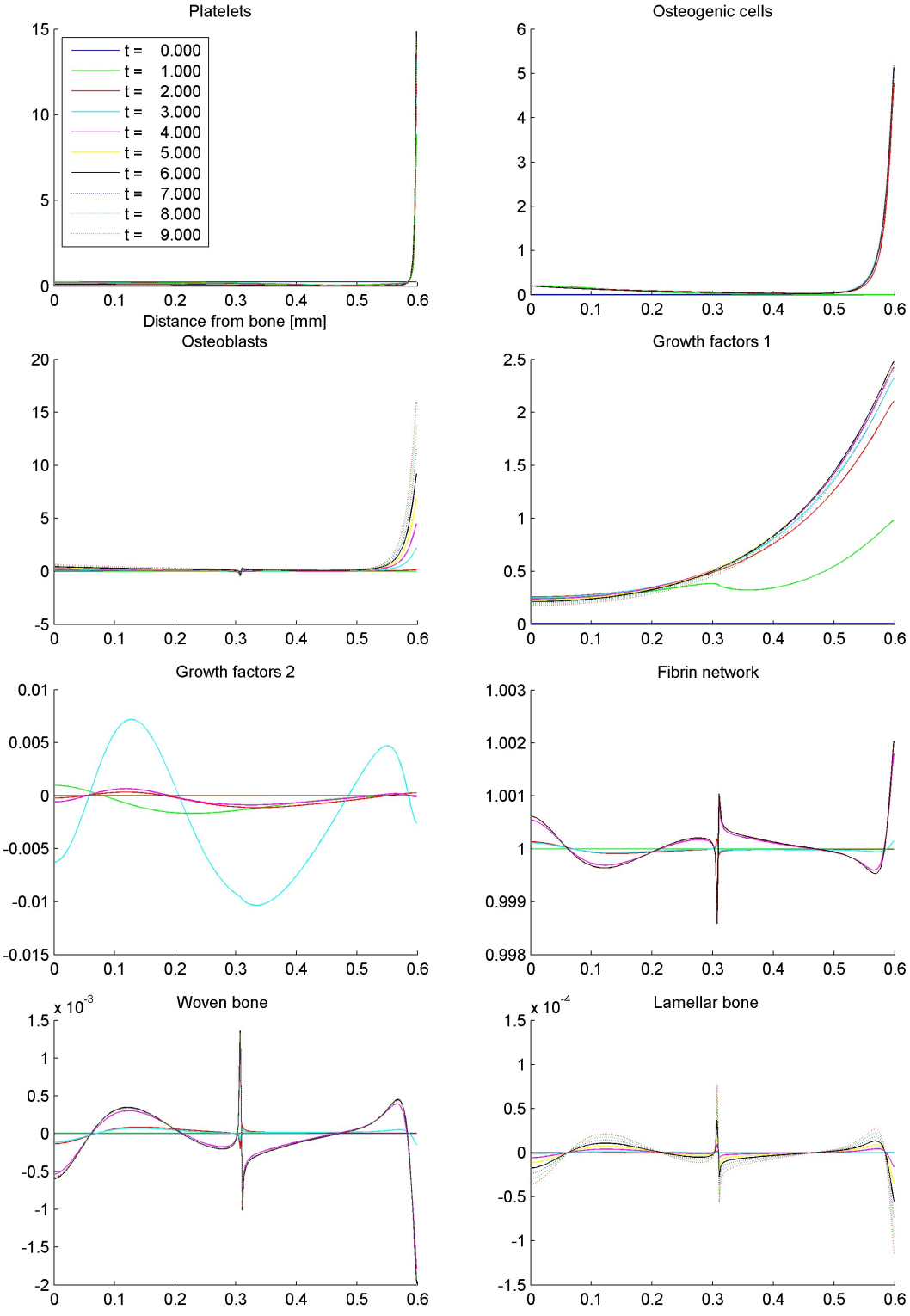

Figure 4.2: Cell densities and volume fractions of the model variables with the 1st IMEX method. $nx = 200$, $dt = 0.5$ and $T_{max} = 10$. This numerical method is instable.

Method 2:

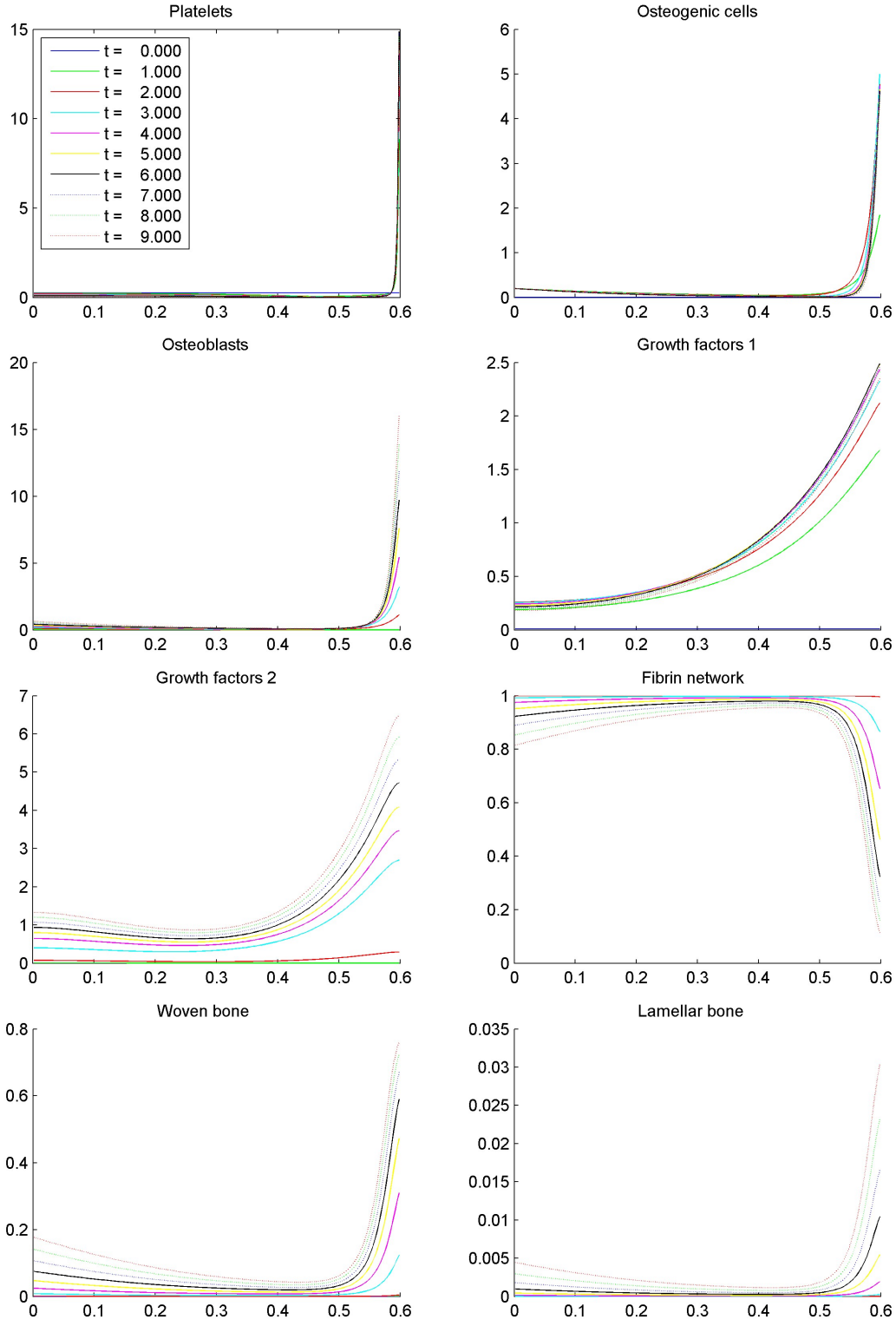

Figure 4.3: Cell densities and volume fractions of the model variables with the 2nd IMEX method. $nx = 200$, $dt = 0.5$ and $T_{max} = 10$. This numerical method is stable.

4.4.2 Comparison low vs. high surface roughness (2 months)

According to a literature study done by [Moreo, 2008] the microtopography of the surface interface is of importance in the type of healing process. With low microtopography the bone

development starts from the bone surface and with high microtopography the bone development should start from the implant surface. This difference is caused by the proteïn concentration at the implant surface, that stimulate different processes as mentioned in Section 2.3. 2 simulations have been done with $n_x = 200$, $dt = 0.02$, $T_{max} = 60$ and p_s (see Eq. (3.8)) respectively 0.1 and $0.5\frac{\mu g}{mm^2}$. The results for low microtopography are found in Figure 4.4 and for high microtopography in Figure 4.5.

It is seen that the platelet concentration at the implant surface is about a factor 10 greater for high compared to low microtopography, as can be expected from the linear taxis term. As a result also the growth factors 1 go up at the implant surface and that in turn causes a osteogenic cell density of about a factor 2 greater in the case of the high microtopography. The high bone fractions are more clotted together at the implant surface in this case, but is only slightly higher than in the case of low microtopography. In contrast the bone fractions a little further away from the implant surface are much lower in the case of the high microtopography and it is seen that the total bone volume is much lower as a result.

$p_s = 0.1$ (low microtopography):

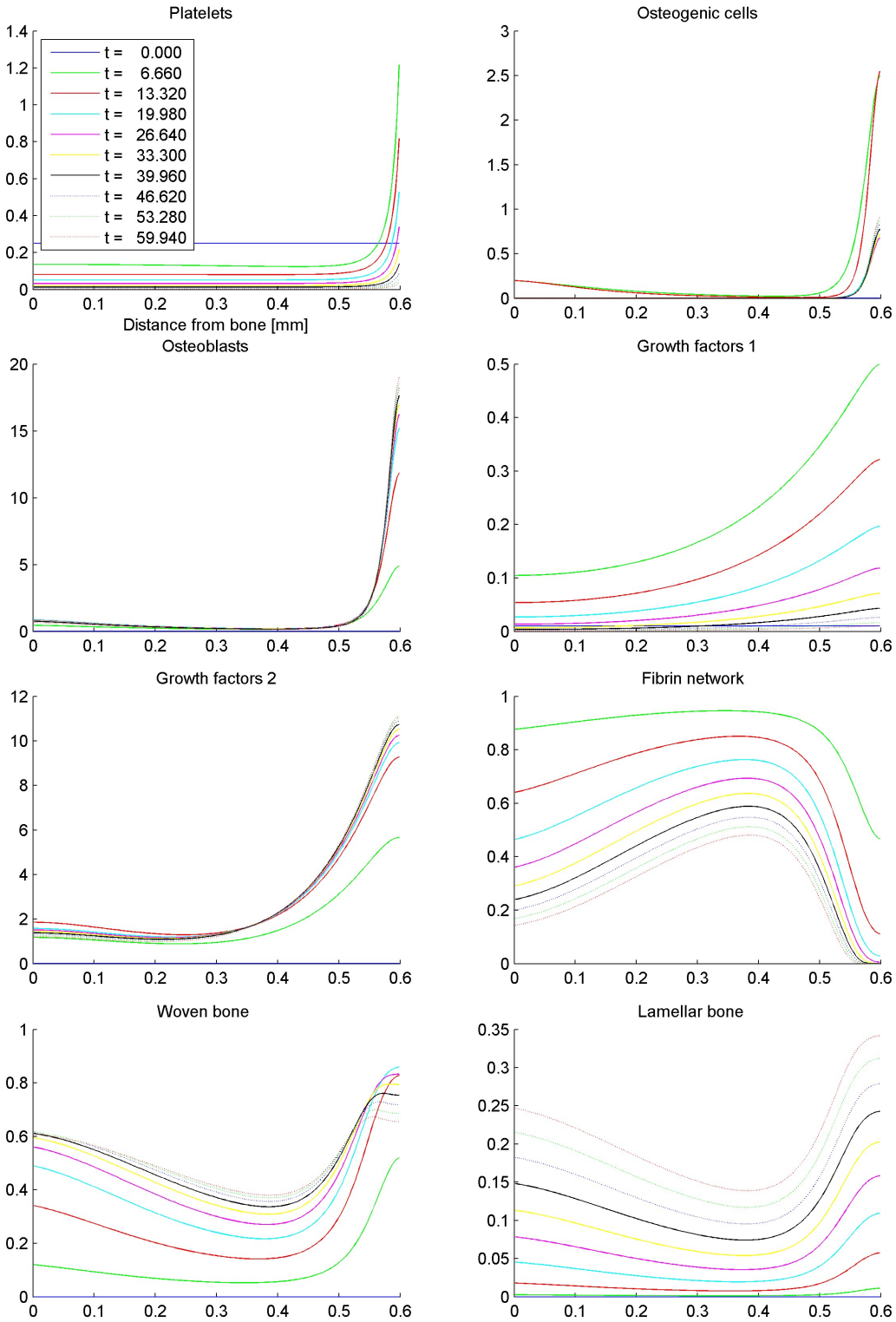

Figure 4.4: Cell densities and volume fractions of the model variables with low microtopography. $nx = 200$, $dt = 0.02$ and $T_{max} = 60$.

$p_s = 0.5$ (high microtopography):

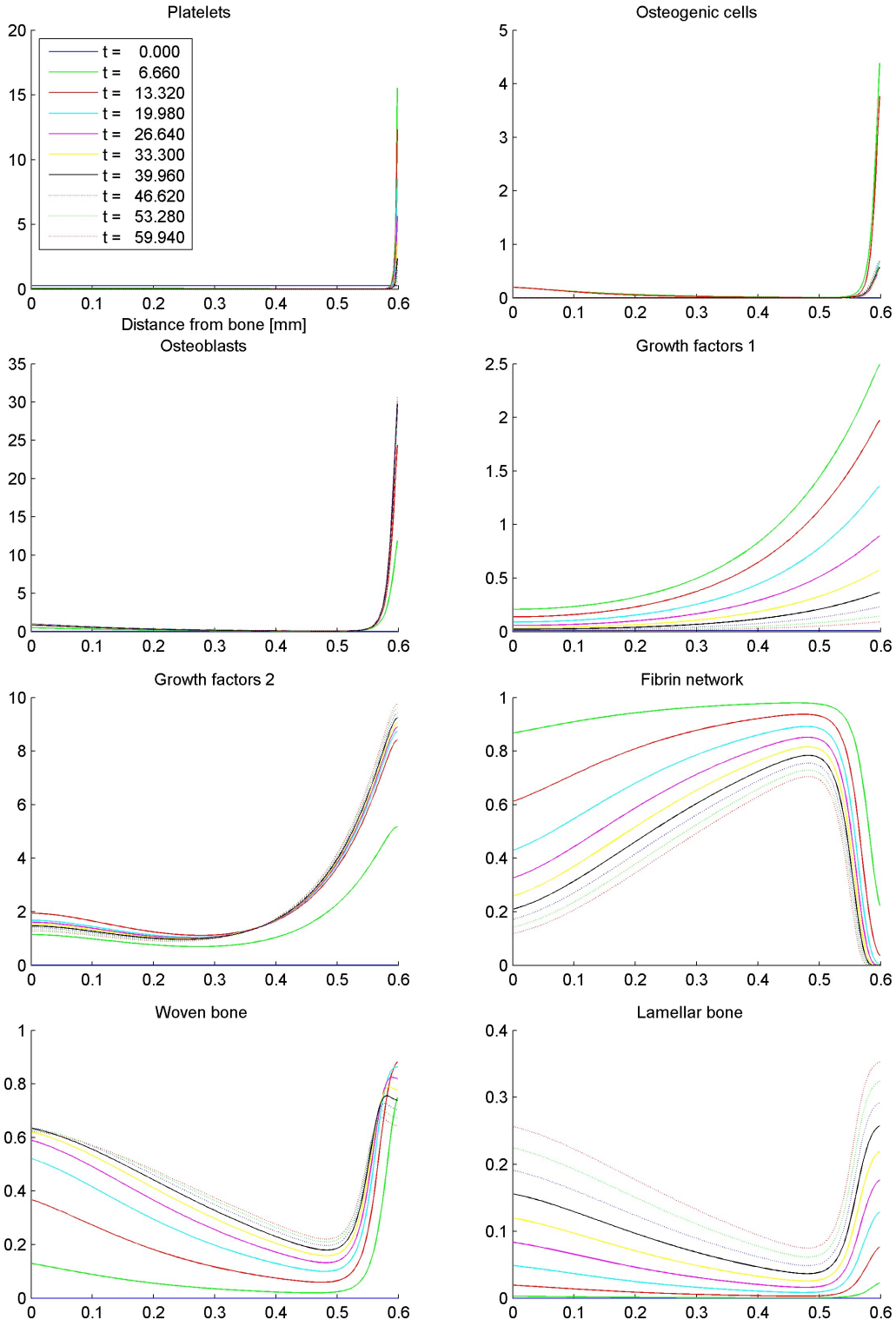

Figure 4.5: Cell densities and volume fractions of the model variables with high microtopography. $nx = 200$, $dt = 0.02$ and $T_{max} = 60$.

4.4.3 Comparison low vs. high surface roughness (10 months)

The same comparison as in the previous section is done, but now over a time span of 10 months to see the long term effects. Only the bone fractions are considered, since we are only interested in the strength of the bone implant connection. The results for low microtopography are found in Figure 4.6 and for high microtopography in Figure 4.7.

Generally the same lines are followed in this longer simulation compared to the simulation for 2 months. What does attrect attention is that the bone fraction at about $0.1mm$ from the implant surface is still only about 0.7 for high microtopography, whereas it is about 0.9 for low microtopography. The healing process for low microtopography seems to follow a much smoother bone formation over the whole domain, instead of the very localised production at the implant surface with high microtopography.

$p_s = 0.1$ (low microtopography):

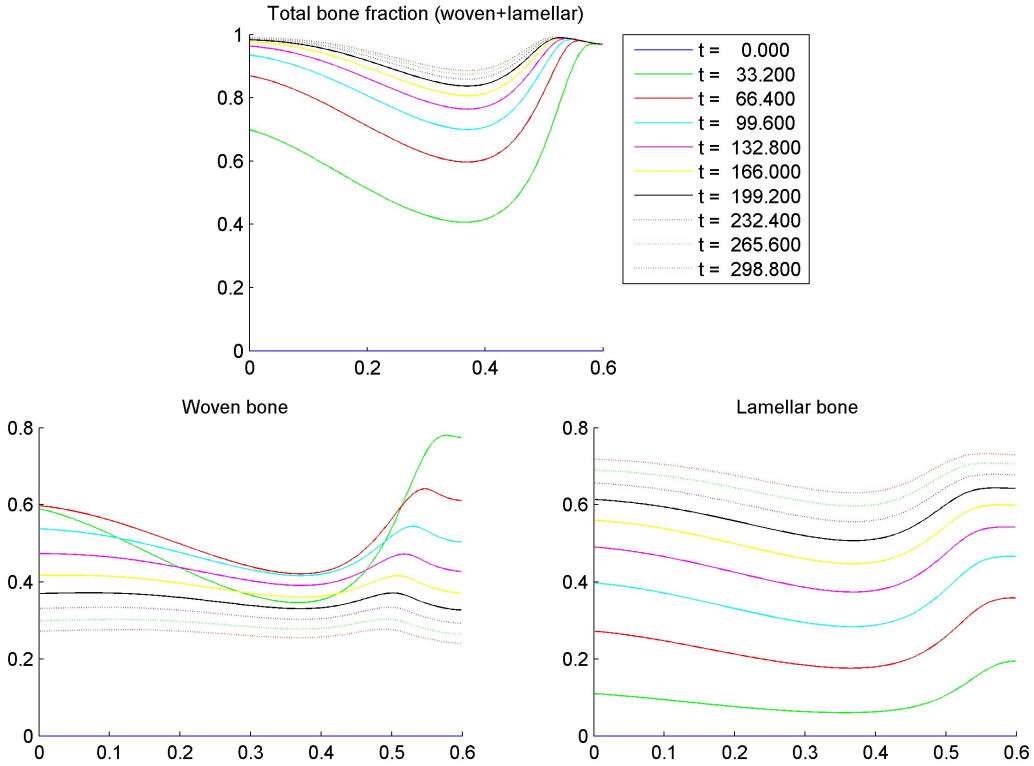

Figure 4.6: Bone fractions of the model variables with low microtopography. $nx = 200$, $dt = 0.02$ and $T_{max} = 300$.

$p_s = 0.5$ (high microtopography):

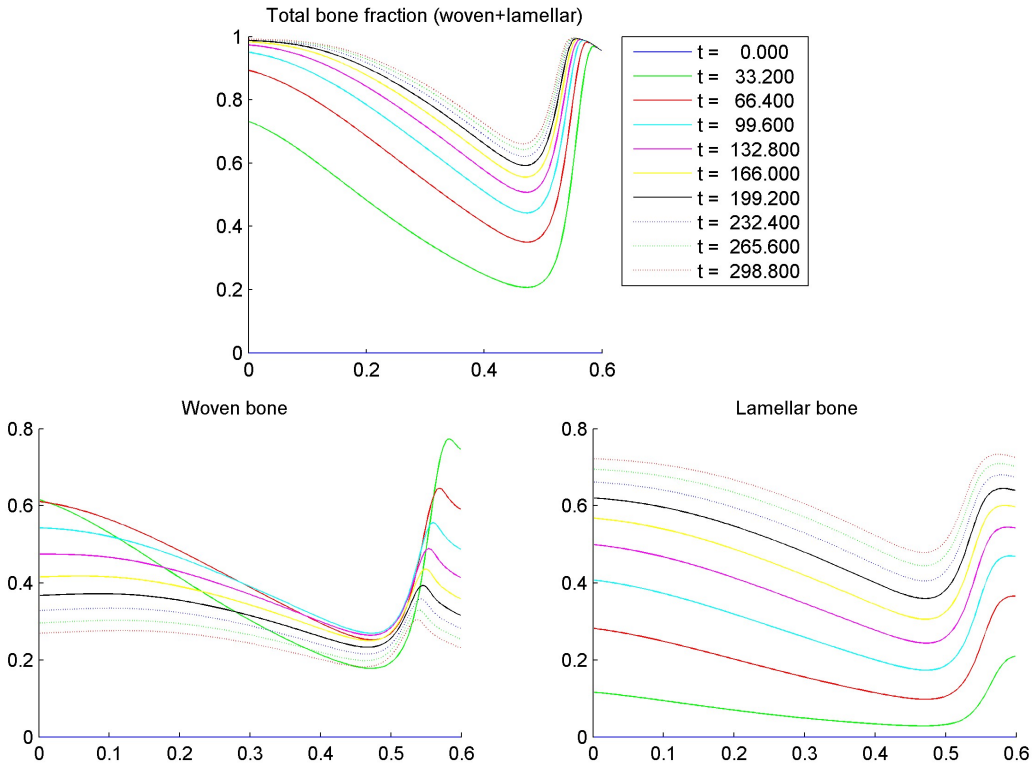

Figure 4.7: Bone fractions of the model variables with high microtopography. $nx = 200$, $dt = 0.02$ and $T_{max} = 300$.

Chapter 5

Simulations using FEM

The finite element method (FEM) is an excellent method to do calculations on complex shaped computational domains in 2 or 3 dimensions. The FEM has proved to work particularly well for calculations on mechanical stress. Since this mechanical stress will be combined with the model of [Moreo, 2008] in later stages, the system of PDEs presented earlier will also be discretized with FEM to provide a good basis for combining the two models.

First a short introduction to FEM will be given, for a more detailed explanation see [Van Kan, 2008].

5.1 Short introduction to FEM

5.1.1 Elements and basis functions

In the finite element method an 1 dimensional domain is divided into so-called elements e_k (see Fig. 5.1), with nodal points x_k and x_{k+1} at the corners of each element.

Figure 5.1: 1D domain for the FEM-discretization

The function $u(x)$ that has to be calculated on this domain, is estimated by a finite fixed set of functions $\phi_i(x)$:

$$\tilde{u}(x) = \sum_{j=1}^{n} u_j \phi_j(x) \tag{5.1}$$

The functions $\phi_i(x)$ are called basis functions.

There are many possible choices for the set of basis functions, but we will only consider piecewise linear basis functions that satisfy the following conditions:

1. $\phi_i(x)$ is linear in each element.
2. $\phi_i(x_j) = \delta_{ij}$, with δ_{ij} the Kronecker delta function.

With these two requirements the functions $\phi_i(x)$ are uniquely defined (see Fig, 5.2).

Figure 5.2: 1D domain for the FEM-discretization

5.1.2 Galerkin's method and the weak formulation

To arrive at a discretized system for the PDE we apply the frequently used Galerkin's method. The first step is deriving the so-called *weak formulation* of the PDE. This is done by multiplying the entire PDE with a so-called test function η and subsequently integrating the result over the entire computational domain. Take as an example Poisson's equation:

$$-\nabla^2 u = f, \ \mathbf{x} \in \Omega \tag{5.2}$$

with boundary conditions

$$u|_{\Gamma_1} = g_1(\mathbf{x}) \quad \text{and} \quad \left.\frac{\partial u}{\partial n}\right|_{\Gamma_2} = g_2(\mathbf{x}). \tag{5.3}$$

Multiplying with the test function η and integrating over the domain Ω results in

$$-\int_\Omega \nabla^2 u \cdot \eta \ d\Omega = \int_\Omega f \cdot \eta \ d\Omega. \tag{5.4}$$

The left hand side can be simplified with Gauss's theorem together with integration by parts (the result is also known as *Green's first identity*):

$$\begin{aligned} -\int_\Omega \nabla^2 u \cdot \eta \ d\Omega &= \int_\Omega \nabla u \cdot \nabla \eta \ d\Omega - \int_{\Gamma_2} \eta \nabla u \cdot \hat{\mathbf{n}} \ d\Gamma \\ &= \int_\Omega \nabla u \cdot \nabla \eta \ d\Omega - \int_{\Gamma_2} g_2 \cdot \eta \ d\Gamma \end{aligned} \tag{5.5}$$

(To see this use the chain rule:

$$\nabla \cdot (\eta \nabla u) = \nabla \eta \cdot \nabla u + \eta \nabla^2 u. \tag{5.6}$$

and use Gauss's theorem after taking the integral over the left hand side.)

So after combining everything, the *weak formulation* becomes:

$$\int_\Omega \nabla u \cdot \nabla \eta \ d\Omega - \int_{\Gamma_2} g_2 \cdot \eta \ d\Gamma = \int_\Omega f \cdot \eta \ d\Omega. \tag{5.7}$$

Now the estimation for the function $u(x)$ (Eq. (5.1)) can be filled into the weak formulation:

$$\sum_{j=1}^{n} u_j \int_\Omega \nabla \phi_j \cdot \nabla \eta \ d\Omega - \int_{\Gamma_2} g_2 \cdot \eta \ d\Gamma = \int_\Omega f \cdot \eta \ d\Omega. \tag{5.8}$$

The last unknown is the test-function η, which can be chosen arbitrarily. Subsequently letting η be $\phi_i(x)$, $i = 1, \ldots, n$ turns out to work very well, giving the following system of n equations:

$$\sum_{j=1}^{n} u_j \int_\Omega \nabla \phi_j \cdot \nabla \phi_i \ d\Omega - \int_{\Gamma_2} g_2 \cdot \phi_i \ d\Gamma = \int_\Omega f \cdot \phi_i \ d\Omega, \quad i = 1, \ldots, n \tag{5.9}$$

or, since we are working in 1 dimension (assuming without loss of generality that $\Omega = [0, 1]$):

$$\sum_{j=1}^{n} u_j \int_0^1 \frac{d\phi_j}{dx} \frac{d\phi_i}{dx} \ dx - g_2(1)\phi_i(1) = \int_0^1 f \phi_i \ dx, \quad i = 1, \ldots, n \tag{5.10}$$

The integrals can be worked out either analytically or numerically, resulting in a discretized system of equations which can be solved for the u_i.

5.1.3 Element matrices and vectors

The power of the finite element method lies in the orthogonality of the basis function. In particular, for one dimension:

$$\int_\Omega \phi_i \cdot \phi_j \; d\Omega = \qquad \text{if } |i-j| > 1 \tag{5.11}$$

which can easily be seen from Figure 5.2. More specifically the basis function ϕ_i is only non-zero on the elements e_i and e_{i+1}, so dividing the integral over whole Ω into integrals over all elements we get:

$$\int_\Omega \phi_i \cdot \phi_j \; d\Omega = \sum_{k=1}^{n} \int_{e_k} \phi_i \cdot \phi_j \; dx \tag{5.12}$$

where the integral over the element e_k can only be non-zero if $i \in \{k, k+1\}$ and $j \in \{k, k+1\}$. It can easily be seen that this same rule also applies to integrals over derivatives of ϕ_i and ϕ_j.

Consider the first term of Eq. (5.10), but only integrate over the element e_k:

$$\sum_{j=1}^{n} u_j \int_{e_k} \frac{d\phi_i}{dx}\frac{d\phi_j}{dx} \; dx, \quad i = 1, \ldots, n. \tag{5.13}$$

Only the equations with $i = k$ and $i = k+1$ can contain non-zero integrals, so the system of equations reduces to:

$$\sum_{j=1}^{n} u_j \int_{e_k} \frac{d\phi_k}{dx}\frac{d\phi_j}{dx} \; dx \qquad = u_k \int_{e_k} \frac{d\phi_k}{dx}\frac{d\phi_k}{dx} \; dx \qquad + u_{k+1} \int_{e_k} \frac{d\phi_k}{dx}\frac{d\phi_{k+1}}{dx} \; dx \tag{5.14}$$

$$\sum_{j=1}^{n} u_j \int_{e_k} \frac{d\phi_{k+1}}{dx}\frac{d\phi_j}{dx} \; dx \qquad = u_k \int_{e_k} \frac{d\phi_k}{dx}\frac{d\phi_{k+1}}{dx} \; dx \qquad + u_{k+1} \int_{e_k} \frac{d\phi_{k+1}}{dx}\frac{d\phi_{k+1}}{dx} \; dx \tag{5.15}$$

which can be written as the matrix multiplication:

$$\begin{bmatrix} \int_{e_k} \frac{d\phi_k}{dx}\frac{d\phi_k}{dx} \; dx & \int_{e_k} \frac{d\phi_k}{dx}\frac{d\phi_{k+1}}{dx} \; dx \\ \int_{e_k} \frac{d\phi_{k+1}}{dx}\frac{d\phi_k}{dx} \; dx & \int_{e_k} \frac{d\phi_{k+1}}{dx}\frac{d\phi_{k+1}}{dx} \; dx \end{bmatrix} \begin{bmatrix} u_k \\ u_{k+1} \end{bmatrix}. \tag{5.16}$$

We define the left matrix as the *element matrix* S^{e_k}:

$$S^{e_k} \equiv \begin{bmatrix} \int_{e_k} \frac{d\phi_k}{dx}\frac{d\phi_k}{dx} \; dx & \int_{e_k} \frac{d\phi_k}{dx}\frac{d\phi_{k+1}}{dx} \; dx \\ \int_{e_k} \frac{d\phi_{k+1}}{dx}\frac{d\phi_k}{dx} \; dx & \int_{e_k} \frac{d\phi_{k+1}}{dx}\frac{d\phi_{k+1}}{dx} \; dx \end{bmatrix} \tag{5.17}$$

Since the set $e_k{}_{k=1}^{n}$ is a disjoint set and $\cup_{k=1}^{n} e_k = \Omega$, it follows that by adding all element matrices, the integral over the whole domain Ω is calculated.

While adding the element matrices, we of course have to take into account with which elements u_i the rows of S^{e_k} are multiplied; for an example of this so called *assembly procedure* see [Van Kan, 2008, p. 102].

Similarly the integrals with just one basis function can be cast into the so called *element vector* f^{e_k}. Using the last term of Eq. (5.10) as an example:

$$\int_{e_k} f\phi_i \; dx, \quad i = 1, \ldots, n. \quad \Rightarrow \quad f^{e_k} \equiv \begin{bmatrix} \int_{e_k} f\phi_k \; dx \\ \int_{e_k} f\phi_{k+1} \; dx \end{bmatrix} \tag{5.18}$$

5.2 Weak formulation and system of equations

Following the procedure from Section 5.1.2 we can derive the weak formulation of the system of PDEs (Eq. (3.1)-(3.7)). The most important tool is *Green's first identity*, which is basically a combination of the Gauss's theorem and integration by parts (see Eq. (5.5)):

$$\int_\Omega \psi \nabla \cdot (\nabla \phi)\ d\Omega = -\int_\Omega \nabla\psi \cdot \nabla\phi\ d\Omega + \int_\Gamma \psi(\nabla\phi \cdot \mathbf{n})\ d\Gamma. \tag{5.19}$$

Most boundaries in the biological model have homogenous Neumann Boundary conditions, in which case the last boundary integral is equal to zero.

Platelet concentration
We start with the original PDE for the platelet concentration, Eq. (3.1):

$$\frac{\partial c}{\partial t} = \nabla \cdot (\ D_c \nabla c - H_c\ c \nabla p\ ) - A_c c \tag{5.20}$$

We multiply the PDE with a test function η and integrate over the whole domain Ω:

$$\int_\Omega \eta \frac{\partial c}{\partial t}\ d\Omega = \int_\Omega \eta \nabla \cdot (\ D_c \nabla c - H_c\ c \nabla p\ )\ d\Omega - \int_\Omega \eta A_c c\ d\Omega \tag{5.21}$$

Applying Green's first identity to the first term on the right hand side of Eq. (5.21) we get:

$$\int_\Omega \eta \frac{\partial c}{\partial t}\ d\Omega = -\int_\Omega \nabla\eta \cdot (\ D_c \nabla c - H_c\ c \nabla p\ )\ d\Omega + \int_\Gamma \eta\,(\ D_c \nabla c - H_c\ c \nabla p\ ) \cdot \mathbf{n}\ d\Gamma - \int_\Omega \eta A_c c\ d\Omega \tag{5.22}$$

But according to Eq. (3.9) the flux at the boundary is zero so the boundary term vanishes. This gives the final expression for the weak formulation:

$$\int_\Omega \eta \frac{\partial c}{\partial t}\ d\Omega = -\int_\Omega \nabla\eta \cdot (D_c \nabla c)\ d\Omega + \int_\Omega \nabla\eta \cdot (H_c c \nabla p)\ d\Omega - \int_\Omega \eta A_c c\ d\Omega \tag{5.23}$$

Following the approach lined out in Section 5.1.2 we now approximate the function $c(\mathbf{x}, t)$ as a linear combination of linear basis functions (Eq. (5.1)):

$$\tilde{c}(x) = \sum_{j=1}^{n} c_j \phi_j(x) \tag{5.24}$$

and replace η consecutively with each of the linear basis functions $\{\phi_i\}_{i=1}^n$.

This leads to the following system of equations:

$$\begin{aligned} \frac{d}{dt}\sum_{j=1}^{n} c_j \int_\Omega \phi_i \phi_j\ d\Omega = &-D_c \sum_{j=1}^{n} c_j \int_\Omega \nabla\phi_i \cdot \nabla\phi_j\ d\Omega + H_c \sum_{j=1}^{n} c_j \int_\Omega (\nabla\phi_i \cdot \nabla p)\,\phi_j\ d\Omega \\ &- A_c \sum_{j=1}^{n} c_j \int_\Omega \phi_i \phi_j\ d\Omega, \quad i = 1, \ldots, n \end{aligned} \tag{5.25}$$

which can be solved after evaluation of the integrals.

Osteogenic cells

Weak formulation:

$$\begin{aligned}\int_\Omega \eta \frac{\partial m}{\partial t}\ d\Omega = &- \int_\Omega \nabla\eta \cdot (D_m \nabla m)\ d\Omega + \int_\Omega \nabla\eta \cdot (m\,[B_{m1}\nabla s1 + B_{m2}\nabla s2])\ d\Omega \\ &+ \int_\Omega \eta \left(\alpha_{m0} + \frac{\alpha_m s_1}{\beta_m + s_1} + \frac{\alpha_m s_2}{\beta_m + s_2}\right) m(1-m)\ d\Omega \\ &- \int_\Omega \eta \frac{\alpha_{mb} s_1}{\beta_{mb} + s_1} m\ d\Omega - \int_\Omega \eta A_m m\ d\Omega \end{aligned} \tag{5.26}$$

System of equations ($i = 1, \ldots, n$):

$$\begin{aligned}\frac{d}{dt}\sum_{j=1}^{n} m_j \int_\Omega \phi_i\phi_j\ d\Omega = &-D_m \sum_{j=1}^{n} m_j \int_\Omega \nabla\phi_i \cdot \nabla\phi_j\ d\Omega \\ &+ \sum_{j=1}^{n} m_j \int_\Omega \left[\nabla\phi_i \cdot (B_{m1}\nabla s1 + B_{m2}\nabla s2)\right]\phi_j\ d\Omega \\ &+ \sum_{j=1}^{n} m_j \int_\Omega \phi_i\phi_j \left(\alpha_{m0} + \frac{\alpha_m s_1}{\beta_m + s_1} + \frac{\alpha_m s_2}{\beta_m + s_2}\right)(1-m)\ d\Omega \\ &- \sum_{j=1}^{n} m_j \int_\Omega \phi_i\phi_j \frac{\alpha_{mb} s_1}{\beta_{mb} + s_1}\ d\Omega - A_m \sum_{j=1}^{n} m_j \int_\Omega \phi_i\phi_j\ d\Omega \end{aligned} \tag{5.27}$$

Osteoblasts

Weak formulation:

$$\int_\Omega \eta \frac{\partial b}{\partial t}\ d\Omega = \int_\Omega \eta \frac{\alpha_{mb} s_1}{\beta_{mb} + s_1} m\ d\Omega - \int_\Omega \eta A_b b\ d\Omega \tag{5.28}$$

System of equations ($i = 1, \ldots, n$):

$$\frac{d}{dt}\sum_{j=1}^{n} b_j \int_\Omega \phi_i\phi_j\ d\Omega = \int_\Omega \phi_i \frac{\alpha_{mb} s_1}{\beta_{mb} + s_1} m\ d\Omega - A_b \sum_{j=1}^{n} b_j \int_\Omega \phi_i\phi_j\ d\Omega \tag{5.29}$$

Growth factors I

Weak formulation:

$$\int_\Omega \eta \frac{\partial s_1}{\partial t}\ d\Omega = \int_\Omega \nabla\eta \cdot (D_{s1}\nabla s_1)\ d\Omega + \int_\Omega \eta \left(\frac{\alpha_{c1} s_1}{\beta_{c1} + s_1} + \frac{\alpha_{c2} s_2}{\beta_{c2} + s_2}\right) c\ d\Omega - \int_\Omega \eta A_{s1} s_1\ d\Omega \tag{5.30}$$

System of equations ($i = 1, \ldots, n$):

$$\begin{aligned}\frac{d}{dt}\sum_{j=1}^{n} s_{1_j} \int_\Omega \phi_i\phi_j\ d\Omega = &D_{s1} \sum_{j=1}^{n} s_{1_j} \int_\Omega \nabla\phi_i \cdot \nabla\phi_j\ d\Omega + \sum_{j=1}^{n} s_{1_j} \int_\Omega \phi_i\phi_j \frac{\alpha_{c1} c}{\beta_{c1} + s_1}\ d\Omega \\ &+ \int_\Omega \phi_i \frac{\alpha_{c2} s_2 c}{\beta_{c2} + s_2}\ d\Omega - A_{s1} \sum_{j=1}^{n} s_{1_j} \int_\Omega \phi_i\phi_j\ d\Omega \end{aligned} \tag{5.31}$$

Growth factors II

Weak formulation:

$$\int_\Omega \eta \frac{\partial s_2}{\partial t}\ d\Omega = \int_\Omega \nabla\eta \cdot (D_{s2}\nabla s_2)\ d\Omega + \int_\Omega \eta \frac{\alpha_{m2} s_2}{\beta_{m2} + s_2} m\ d\Omega + \int_\Omega \eta \frac{\alpha_{b2} s_2}{\beta_{b2} + s_2} b\ d\Omega - \int_\Omega \eta A_{s2} s_2\ d\Omega \tag{5.32}$$

System of equations ($i = 1, \ldots, n$):

$$\begin{aligned}\frac{d}{dt}\sum_{j=1}^{n} s_{2_j} \int_\Omega \phi_i\phi_j\ d\Omega = D_{s2}\sum_{j=1}^{n} s_{2_j}\int_\Omega \nabla\phi_i\cdot\nabla\phi_j\ d\Omega + \sum_{j=1}^{n} s_{2_j}\int_\Omega \phi_i\phi_j \frac{\alpha_{m2} m}{\beta_{m2}+s_2}\ d\Omega \\ + \int_\Omega \phi_i\phi_j \frac{\alpha_{b2} b}{\beta_{b2}+s_2}\ d\Omega - A_{s2}\sum_{j=1}^{n} s_{2_j}\int_\Omega \phi_i\phi_j\ d\Omega\end{aligned} \tag{5.33}$$

Fibrin network

Weak formulation:

$$\int_\Omega \eta \frac{\partial v_f}{\partial t}\ d\Omega = -\int_\Omega \eta \frac{\alpha_w s_2}{\beta_w + s_2} b v_f (1 - v_w)\ d\Omega \tag{5.34}$$

System of equations ($i = 1, \ldots, n$):

$$\frac{d}{dt}\sum_{j=1}^{n} v_{f_j}\int_\Omega \phi_i\phi_j\ d\Omega = -\sum_{j=1}^{n} v_{f_j}\int_\Omega \phi_i\phi_j \frac{\alpha_w s_2}{\beta_w + s_2} b(1 - v_w)\ d\Omega \tag{5.35}$$

Woven bone

Weak formulation:

$$\int_\Omega \eta \frac{\partial v_w}{\partial t}\ d\Omega = \int_\Omega \eta \frac{\alpha_w s_2}{\beta_w + s_2} b v_f (1 - v_w)\ d\Omega - \int_\Omega \eta\gamma v_w (1 - v_l)\ d\Omega \tag{5.36}$$

System of equations ($i = 1, \ldots, n$):

$$\begin{aligned}\frac{d}{dt}\sum_{j=1}^{n} v_{w_j}\int_\Omega \phi_i\phi_j\ d\Omega = \int_\Omega \phi_i \frac{\alpha_w s_2}{\beta_w + s_2} b v_f\ d\Omega - \sum_{j=1}^{n} v_{w_j}\int_\Omega \phi_i\phi_j \frac{\alpha_w s_2}{\beta_w + s_2} b v_f\ d\Omega \\ - \sum_{j=1}^{n} v_{w_j}\int_\Omega \phi_i\phi_j\gamma(1 - v_l)\ d\Omega\end{aligned} \tag{5.37}$$

Lamellar bone

Weak formulation:

$$\int_\Omega \eta \frac{\partial v_l}{\partial t}\ d\Omega = \int_\Omega \eta\gamma v_w (1 - v_l)\ d\Omega \tag{5.38}$$

System of equations ($i = 1, \ldots, n$):

$$\frac{d}{dt}\sum_{j=1}^{n} v_{l_j}\int_\Omega \phi_i\phi_j\ d\Omega = \int_\Omega \phi_i\gamma v_w\ d\Omega - \sum_{j=1}^{n} v_{l_j}\int_\Omega \phi_i\phi_j\gamma v_w\ d\Omega \tag{5.39}$$

5.3 Element matrices and vectors in 1 dimension

In 1 dimension the linear basis functions ϕ_k are defined by

$$\phi_k(x) = \begin{cases} \dfrac{x - x_{k-1}}{x_k - x_{k-1}} & \text{for } x \in (x_{k-1}, x_k) \\ \dfrac{x_{k+1} - x}{x_{k+1} - x_k} & \text{for } x \in (x_k, x_{k+1}) \\ 0 & \text{otherwise} \end{cases} \tag{5.40}$$

An example of a linear basis function can be seen in Fig. 5.3.

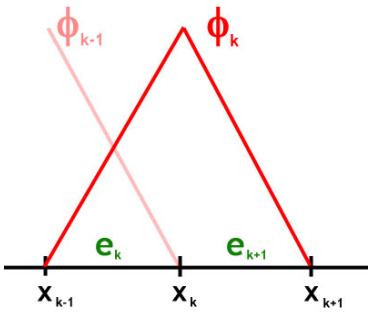

Figure 5.3: Linear basis function in 1-D

A combination of analytical and numerical methods will be used to respectively evaluate and estimate the integrals that appear in the systems of equations.

5.3.1 Analytical integral evaluation

There are two types of integrals that can be solved analytically:

$$\int \phi_i \phi_j \, dx \tag{5.41}$$

$$\int \frac{d\phi_i}{dx} \frac{d\phi_j}{dx} \, dx \tag{5.42}$$

Since we will later make use of element matrices and vectors it is only needed to evaluate the integrals on an element $e_k = (x_k, x_{k+1})$ on which only the basis functions ϕ_k and ϕ_{k+1} are non-zero.

Integral (5.41)

Let $h = x_{k+1} - x_k$ and assume without loss of generality that $x_k = 0$, the integral (5.41) becomes:

$$\int_{e_k} \phi_k \phi_k \, dx = \int_0^{x_{k+1}} \frac{-x}{h} \frac{-x}{h} dx = \frac{1}{h^2} \int_0^{x_{k+1}} x^2 dx = \frac{1}{h^2} \left[\frac{1}{3} x^3 \right]_0^h = \frac{h}{3} \tag{5.43}$$

Similarly the other integrals can be evaluated:

$$\int_{e_k} \phi_k \phi_{k+1} \, dx = \frac{h}{6} \quad \text{and} \quad \int_{e_k} \phi_{k+1} \phi_{k+1} \, dx = \frac{h}{3} \tag{5.44}$$

So the element matrix for (5.41) is:

$$S^{e_k} = \frac{h}{6} \begin{bmatrix} 2 & 1 \\ 1 & 2 \end{bmatrix} \tag{5.45}$$

Integral (5.42)

For (5.42) we get:

$$\int_{e_k} \frac{d\phi_k}{dx}\frac{d\phi_k}{dx}\,dx = \int_0^{x_{k+1}} \frac{-1}{h}\frac{-1}{h}dx = \frac{1}{h^2}\int_0^{x_{k+1}} dx = \frac{1}{h} \tag{5.46}$$

Similarly we find:

$$\int_{e_k} \frac{d\phi_k}{dx}\frac{d\phi_{k+1}}{dx}\,dx = -\frac{1}{h} \quad \text{and} \quad \int_{e_k} \frac{d\phi_{k+1}}{dx}\frac{d\phi_{k+1}}{dx}\,dx = \frac{1}{h} \tag{5.47}$$

So the element matrix for (5.42) is:

$$S^{e_k} = \frac{1}{h}\begin{bmatrix} 1 & -1 \\ -1 & 1 \end{bmatrix} \tag{5.48}$$

5.3.2 Numerical integral evaluation

All the remaining integrals can be seperated in three generic types:

$$\int \phi_i(x)\phi_j(x)f(x,t)\,dx \tag{5.49}$$

$$\int \phi_i(x)f(x,t)\,dx \tag{5.50}$$

$$\int \frac{d\phi_i(x)}{dx}\frac{\partial f(x,t)}{\partial x}\phi_j(x)\,dx \tag{5.51}$$

where $f(x,t)$ is some function of x and t, e.g. $\frac{\alpha_{mb}s_1(x,t)}{\beta_{mb}+s_1(x,t)}$ in the equation of the osteogenic cell concentration. Once again we are only interested in forming an element matrix or vector, so the integral will only be evaluated over an element $e_k = (x_k, x_{k+1})$.

(5.49) and (5.50) will be estimated using the *Newton-Cotes rule* of degree 1, also known as the trapezoid rule:

$$\int_a^b f(x)dx \approx \frac{b-a}{2}(f(a)+f(b)) \tag{5.52}$$

Newton-Cotes is often chosen in finite element analysis, because it makes optimal use of all available nodal points inside an element, in this case the two nodal points x_k and x_{k+1}.

Integral (5.49)

With $h = x_{k+1} - x_k$ and using the fact that $\phi_i(x_j) = \delta_{ij}$ (see Section 5.1.1):

$$\int_{e_k} \phi_k(x)\phi_k(x)f(x,t)\,dx \approx \frac{h}{2}\left(\phi_k(x_k)\phi_k(x_k)f(x_k,t) - \phi_k(x_{k+1})\phi_k(x_{k+1})f(x_{k+1},t)\right) = \frac{h}{2}f(x_k,t) \tag{5.53}$$

$$\int_{e_k} \phi_k(x)\phi_{k+1}(x)f(x,t)\,dx \approx \frac{h}{2}\left(\phi_k(x_k)\phi_{k+1}(x_k)f(x_k,t) - \phi_k(x_{k+1})\phi_{k+1}(x_{k+1})f(x_{k+1},t)\right) = 0 \tag{5.54}$$

$$\int_{e_k} \phi_{k+1}(x)\phi_{k+1}(x)f(x,t)\,dx \approx \frac{h}{2}\left(\phi_{k+1}(x_k)\phi_{k+1}(x_k)f(x_k,t) - \phi_{k+1}(x_{k+1})\phi_{k+1}(x_{k+1})f(x_{k+1},t)\right) = \frac{h}{2}f(x_{k+1},t) \tag{5.55}$$

The element matrix for (5.49) becomes:

$$S^{e_k} = \frac{h}{2}\begin{bmatrix} f(x_k,t) & 0 \\ 0 & f(x_{k+1},t) \end{bmatrix} \tag{5.56}$$

Integral (5.50)

Integral (5.50) can be estimated similarly with Newton-Cotes:

$$\int_{e_k} \phi_k(x) f(x,t)\ dx \approx \frac{h}{2} f(x_k,t) \tag{5.57}$$

$$\int_{e_k} \phi_{k+1}(x) f(x,t)\ dx \approx \frac{h}{2} f(x_{k+1},t) \tag{5.58}$$

with the element vector

$$f^{e_k} = \frac{h}{2}\begin{bmatrix} f(x_k,t) \\ f(x_{k+1},t) \end{bmatrix} \tag{5.59}$$

Integral (5.51)

Integral (5.51) is a little bit harder to evaluate because of the presence of an derivative. Since the function $f(x,t)$ is in this case always known in x_k and x_{k+1}, the derivative can be estimated with central differences. Now there is only one function value ($\frac{\partial f}{\partial x}\left(\frac{x_k+x_{k+1}}{2}\right)$) available, so the trapezoid rule can no longer be used and we have to step down to the *midpoint rule*:

$$\int_a^b f(x)dx \approx (b-a) f\left(\frac{a+b}{2}\right) \tag{5.60}$$

Defining $x_{k+\frac{1}{2}} = \frac{x_k+x_{k+1}}{2}$ the necessary function values of the linear basis function are:

$$\phi_k(x_{k+\frac{1}{2}}) = \phi_{k+1}(x_{k+\frac{1}{2}}) = \frac{1}{2} \quad \text{and} \quad \frac{d\phi_k}{dx} = -\frac{d\phi_{k+1}}{dx} = \frac{1}{h}. \tag{5.61}$$

Applying central differences to $f(x,t)$ in x, we get:

$$\begin{aligned} \int_{e_k} \frac{d\phi_k(x)}{dx}\frac{\partial f(x,t)}{\partial x}\phi_k(x)\ dx &\approx \frac{d\phi_k}{dx}(x_{k+\frac{1}{2}})\frac{f(x_k,t)-f(x_{k+1},t)}{h}\phi_k(x_{k+\frac{1}{2}}) \\ &= \frac{f(x_k,t)-f(x_{k+1},t)}{2h^2} \end{aligned} \tag{5.62}$$

$$\int_{e_k} \frac{d\phi_k(x)}{dx}\frac{\partial f(x,t)}{\partial x}\phi_{k+1}(x)\ dx \approx \frac{f(x_k,t)-f(x_{k+1},t)}{2h^2} \tag{5.63}$$

$$\int_{e_k} \frac{d\phi_{k+1}(x)}{dx}\frac{\partial f(x,t)}{\partial x}\phi_k(x)\ dx \approx -\frac{f(x_k,t)-f(x_{k+1},t)}{2h^2} \tag{5.64}$$

$$\int_{e_k} \frac{d\phi_{k+1}(x)}{dx}\frac{\partial f(x,t)}{\partial x}\phi_{k+1}(x)\ dx \approx -\frac{f(x_k,t)-f(x_{k+1},t)}{2h^2} \tag{5.65}$$

So the element matrix for (5.51) becomes:

$$S^{e_k} = \frac{f(x_k,t)-f(x_{k+1},t)}{2h^2}\begin{bmatrix} 1 & 1 \\ -1 & -1 \end{bmatrix} \tag{5.66}$$

5.4 Element matrices and vectors in 2 dimensions (triangular elements)

The extension of the linear line element in 1 dimension is the triangle in 2 dimensions (see Figure 5.4).

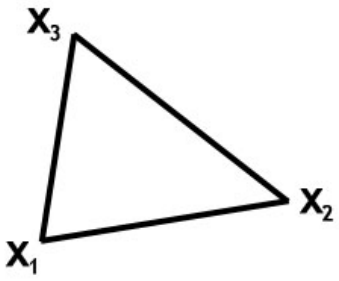

Figure 5.4: Element e_k with nodal points $\mathbf{x}_1, \mathbf{x}_2$ and $\mathbf{x}_3$.

The linear basis function satisfy the following two rules similar to the 1 dimensional case:

1. $\phi_i(\mathbf{x})$ is linear in each element.
2. $\phi_i(\mathbf{x}_j) = \delta_{ij}$, with δ_{ij} the Kronecker delta function.

In Figure 5.5 one such linear basis function can be seen.

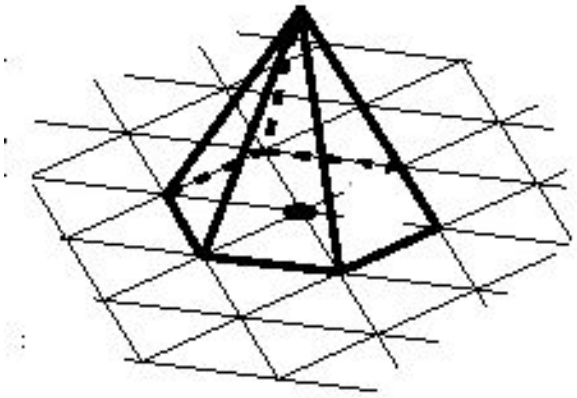

Figure 5.5: Linear basis function in 2-D

With these requirements the basis functions are uniquely defined. On the element e_k with nodal points $\mathbf{x}_i = (x_i, y_i),\ i = 1, 2, 3$ (see Figure 5.4) the basis functions are given by (see [Van Kan, 2008, p. 108] for a derivation):

$$\phi_1(\mathbf{x}) = 1 + \frac{1}{\Delta}(x - x_1)(y_2 - y_3) + \frac{1}{\Delta}(y - y_1)(x_3 - x_2) \tag{5.67}$$

$$\phi_2(\mathbf{x}) = 1 + \frac{1}{\Delta}(x - x_2)(y_3 - y_1) + \frac{1}{\Delta}(y - y_2)(x_1 - x_3) \tag{5.68}$$

$$\phi_3(\mathbf{x}) = 1 + \frac{1}{\Delta}(x - x_3)(y_1 - y_2) + \frac{1}{\Delta}(y - y_3)(x_2 - x_1) \tag{5.69}$$

where Δ is thetwo times the area of the triangle:

$$\Delta = |(x_2 - x_1)(y_3 - y_2) - (y_2 - y_1)(x_3 - x_2)| \tag{5.70}$$

Note that this only defines one of the six pieces of the linear basis function, since there are 5 other elements where the basis function is non-zero (see Figure 5.5).

Once again the integrals that appear in the system of equations from Section 5.2 have to be respectively be evaluated and estimated by analytically or numerically.

5.4.1 Analytical integral evaluation

The same two types of integrals as for the 1 dimensional case can be solved analytically:

$$\int \phi_i \phi_j \, d\Omega \tag{5.71}$$

$$\int \nabla\phi_i \cdot \nabla\phi_j \, d\Omega = \int \frac{d\phi_i}{dx}\frac{d\phi_j}{dx} \, dx + \int \frac{d\phi_i}{dy}\frac{d\phi_j}{dy} \, dy \tag{5.72}$$

Since we will later make use of element matrices and vectors it is only needed to evaluate the integrals on an element e_k with nodal points $\mathbf{x}_1$, $\mathbf{x}_2$ and $\mathbf{x}_3$ and accompanying basis functions $\phi_1(\mathbf{x})$, $\phi_2(\mathbf{x})$ and $\phi_3(\mathbf{x})$.

Integral (5.71)

The element matrix for (5.71) is:

$$S^{e_k} = \frac{\Delta}{24}\begin{bmatrix} 2 & 1 & 1 \\ 1 & 2 & 1 \\ 1 & 1 & 2 \end{bmatrix}. \tag{5.73}$$

for a method to derive this result, see [Van Kan, 2008, p. 111].

In practice the result above is seldom used. It is often more efficient to use a method called *lumping* where Newton-Cotes is used to approximate the above integral. The advantage is that the mass matrix (see Section 4.2) becomes diagonal, which greatly reduces computing time by making certain matrix inversion needed in the simulation a lot easier and faster. To calculate this lumped matrix simply use Eq. (5.79) with $f \equiv 1$.

Integral (5.72)

For (5.42) we get:

$$\int_{e_k} \frac{d\phi_1}{dx}\frac{d\phi_1}{dx} \, dx = \int_{e_k} \frac{1}{\Delta}(y_2 - y_3) \cdot \frac{1}{\Delta}(y_2 - y_3) \, dx = \frac{(y_2 - y_3)^2}{\Delta^2}\int_{e_k} dx = \frac{(y_2 - y_3)^2}{2\Delta} \tag{5.74}$$

$$\int_{e_k} \frac{d\phi_1}{dy}\frac{d\phi_1}{dy} \, dy = \int_{e_k} \frac{1}{\Delta}(x_3 - x_2) \cdot \frac{1}{\Delta}(x_3 - x_2) \, dy = \frac{(x_3 - x_2)^2}{\Delta^2}\int_{e_k} dy = \frac{(x_3 - x_2)^2}{2\Delta} \tag{5.75}$$

using $\int_{e_k} d\Omega = \frac{\Delta}{2}$.

Similarly all other integrals with $\nabla\phi_1$, $\nabla\phi_2$ and $\nabla\phi_3$ can be calculated and the element matrix for (5.72) is:

$$S^{e_k} = \frac{1}{2\Delta}\begin{bmatrix} (y_2-y_3)^2+(x_3-x_2)^2 & \\ (y_3-y_1)(y_2-y_3)+(x_1-x_3)(x_3-x_2) & \\ (y_1-y_2)(y_2-y_3)+(x_3-x_2)(x_2-x_1) & \end{bmatrix}$$
$$\begin{bmatrix} (y_2-y_3)(y_3-y_1)+(x_3-x_2)(x_1-x_3) & (y_2-y_3)(y_1-y_2)+(x_3-x_2)(x_2-x_1) \\ (y_3-y_1)^2+(x_1-x_3)^2 & (y_3-y_1)(y_1-y_2)+(x_1-x_3)(x_2-x_1) \\ (y_1-y_2)(y_3-y_1)+(x_2-x_1)(x_1-x_3) & (y_1-y_2)^2+(x_2-x_1)^2 \end{bmatrix} \tag{5.76}$$

For implementation it is easier to rewrite this matrix using the matrix D that approximates the gradient of all basis functions:

$$\begin{bmatrix}\nabla\phi_1(\mathbf{x})\\ \nabla\phi_2(\mathbf{x})\\ \nabla\phi_3(\mathbf{x})\end{bmatrix} \approx \frac{1}{\Delta}\begin{bmatrix} y_2-y_3 & x_3-x_2 \\ y_3-y_1 & x_1-x_3 \\ y_1-y_2 & x_2-x_1\end{bmatrix} \equiv D \tag{5.77}$$

so that the element matrix can be written as a matrix multiplication:

$$S^{e_k} = \frac{\Delta}{2}\, D\cdot D^T \tag{5.78}$$

5.4.2 Numerical integral evaluation

All the remaining integrals can be seperated in three generic types:

$$\int \phi_i(\mathbf{x})\phi_j(\mathbf{x})f(\mathbf{x},t)\; d\Omega \tag{5.79}$$

$$\int \phi_i(\mathbf{x})f(\mathbf{x},t)\; d\Omega \tag{5.80}$$

$$\int \left(\nabla\phi_i(\mathbf{x})\cdot\nabla f(\mathbf{x},t)\right)\phi_j(\mathbf{x})\; d\Omega \tag{5.81}$$

where $f(\mathbf{x},t)$ is some function of $\mathbf{x}$ and t. Once again we are only interested in forming an element matrix or vector, so the integral will only be evaluated over an element e_k.

Integrals (5.79) and (5.80) will be estimated using the *Newton-Cotes rule* of degree 1 in 2 dimensions:

$$\int_{e_k} f(\mathbf{x})\; d\Omega \approx \frac{\Delta}{6}(f(\mathbf{x}_1)+f(\mathbf{x}_2)+f(\mathbf{x}_3)) \tag{5.82}$$

Integral (5.79)

Making use of the basis function's property $\phi_i(\mathbf{x}_j)=\delta_{ij}$:

$$\begin{aligned}\int_{e_k} &\phi_i(\mathbf{x})\phi_j(\mathbf{x})f(\mathbf{x},t)\; d\Omega \\ &\approx \frac{\Delta}{6}\left(\phi_i(\mathbf{x}_1)\phi_j(\mathbf{x}_1)f(\mathbf{x}_1,t)+\phi_i(\mathbf{x}_2)\phi_j(\mathbf{x}_2)f(\mathbf{x}_2,t)+\phi_i(\mathbf{x}_3)\phi_j(\mathbf{x}_3)f(\mathbf{x}_3,t)\right) \\ &= \begin{cases} \frac{\Delta}{6}f(\mathbf{x}_i,t), & \text{if } i=j=1,2,3 \\ 0, & \text{otherwise}\end{cases}\end{aligned} \tag{5.83}$$

The element matrix for (5.79) becomes:

$$S^{e_k} = \frac{\Delta}{6}\begin{bmatrix} f(\mathbf{x}_1,t) & 0 & 0 \\ 0 & f(\mathbf{x}_2,t) & 0 \\ 0 & 0 & f(\mathbf{x}_3,t)\end{bmatrix} \tag{5.84}$$

Integral (5.80)

Integral (5.80) can be estimated similarly:

$$\int_{e_k} \phi_i(\mathbf{x}) f(\mathbf{x},t)\ d\Omega \approx \frac{\Delta}{6} f(\mathbf{x}_i,t) \tag{5.85}$$

with the element vector

$$f^{e_k} = \frac{\Delta}{6}\begin{bmatrix} f(\mathbf{x}_1,t) \\ f(\mathbf{x}_2,t) \\ f(\mathbf{x}_3,t) \end{bmatrix} \tag{5.86}$$

Integral (5.81)

Integral (5.81) contains a gradient that first has to be calculated. Since the function $f(\mathbf{x},t)$ is known in $\mathbf{x}_1$, $\mathbf{x}_2$ and $\mathbf{x}_3$ the gradient can be estimated by a generalized form of central differences:

$$\begin{aligned} \nabla f(\mathbf{x},t) &\approx \frac{1}{\Delta}\begin{bmatrix} y_2-y_3 & y_3-y_1 & y_1-y_2 \\ x_3-x_2 & x_1-x_3 & x_2-x_1 \end{bmatrix}\begin{bmatrix} f(\mathbf{x}_1,t) \\ f(\mathbf{x}_2,t) \\ f(\mathbf{x}_3,t) \end{bmatrix} \\ &= \frac{1}{\Delta}\begin{bmatrix} (y_2-y_3)f(\mathbf{x}_1,t)+(y_3-y_1)f(\mathbf{x}_2,t)+(y_1-y_2)f(\mathbf{x}_3,t) \\ (x_3-x_2)f(\mathbf{x}_1,t)+(x_1-x_3)f(\mathbf{x}_2,t)+(x_2-x_1)f(\mathbf{x}_3,t) \end{bmatrix} \end{aligned} \tag{5.87}$$

Using the gradient matrix of the basis functions D (Eq. (5.77)) we can write Eq. (5.87) in a much simpler form:

$$\nabla f(\mathbf{x},t) \approx D^T \cdot \mathbf{f} \tag{5.88}$$

where $\mathbf{f} = (f(\mathbf{x}_1,t), f(\mathbf{x}_2,t), f(\mathbf{x}_3,t))^T$.

Next the *midpoint rule* in 2 dimensions can be applied:

$$\int_{e_k} f(\mathbf{x})\ d\Omega \approx \frac{\Delta}{2} f\left(\frac{\mathbf{x}_1+\mathbf{x}_2+\mathbf{x}_3}{3}\right) \tag{5.89}$$

Defining $\bar{\mathbf{x}} = \frac{\mathbf{x}_1+\mathbf{x}_2+\mathbf{x}_3}{3}$ the necessary function values of the linear basis function are:

$$\phi_i(\bar{\mathbf{x}}) = \frac{1}{3} \quad \text{and} \quad \nabla\phi_i = \begin{cases} \frac{1}{\Delta}\left[y_2-y_3, x_3-x_2\right], & \text{if } i=1 \\ \frac{1}{\Delta}\left[y_3-y_1, x_1-x_3\right], & \text{if } i=2 \\ \frac{1}{\Delta}\left[y_1-y_2, x_2-x_1\right], & \text{if } i=3 \end{cases} \tag{5.90}$$

Applying 2 dimensional central differences to $f(\mathbf{x},t)$ in x, we get:

$$\int_{e_k} \nabla\phi_i(\mathbf{x})\nabla f(\mathbf{x},t)\phi_j(\mathbf{x})\ d\Omega \approx \begin{cases} \frac{1}{3\Delta}\left((y_2-y_3)f_x(\mathbf{x},t)+(x_3-x_2)f_y(\mathbf{x},t)\right), & \text{if } i=1 \\ \frac{1}{3\Delta}\left((y_3-y_1)f_x(\mathbf{x},t)+(x_1-x_3)f_y(\mathbf{x},t)\right), & \text{if } i=2 \\ \frac{1}{3\Delta}\left((y_1-y_2)f_x(\mathbf{x},t)+(x_2-x_1)f_y(\mathbf{x},t)\right), & \text{if } i=3 \end{cases} \tag{5.91}$$

where $f_x(\mathbf{x},t)$ and $f_y(\mathbf{x},t)$ are the estimated partial derivatives from Eq. (5.87).

Combining Eq. (5.91) and (5.87), the element matrix for (5.81) can now easily be formed. Using the gradient matrix of the basis functions D (Eq. (5.77)) the element matrix becomes:

$$S^{e_k} = \frac{\Delta}{2} D \cdot D^T \mathbf{f} \cdot \mathbf{1} \tag{5.92}$$

where 1 is a row vector containing only ones: $\mathbf{1} = \begin{pmatrix} 1 & 1 & 1 \end{pmatrix}$.

Note that the columns of this matrix are all the same, because the function value of $\phi_j(\mathbf{x})$ is always $\frac{1}{3}$ at $\mathbf{x} = \bar{\mathbf{x}}$.

5.5 Element matrices and vectors in 2 dimensions (quadrilateral elements)

Besides triangles we can also use quadrilateral elements in 2 dimensions (see Figure 5.6), a generlization of the rectangle. The basis functions now satisfy two conditions:

1. $\phi_i(\mathbf{x})$ is bilinear in each element.
2. $\phi_i(\mathbf{x}_j) = \delta_{ij}$, with δ_{ij} the Kronecker delta function.

With quadrilaterals it is no longer possible to produce a linear function while also satifying $\phi_i(\mathbf{x}_j) = \delta_{ij}$, so the first requirement has changed to ϕ_i being bilinear instead of a linear. A bilinear function is a function of the form:

$$\phi(x, y) = a_0 + a_1 x + a_2 y + a_3 xy \tag{5.93}$$

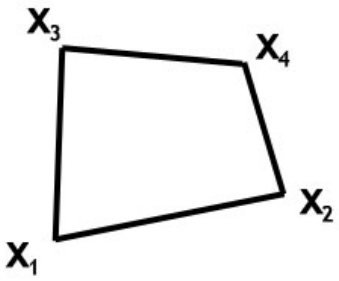

Figure 5.6: Element e_k with nodal points $\mathbf{x}_1, \mathbf{x}_2$, $\mathbf{x}_3$ and $\mathbf{x}_4$.

Construction of bilinear functions satisfying $\phi_i(\mathbf{x}_j) = \delta_{ij}$ is not trivial for general quadrilaterals, however it is quite simple for rectangles and squares. The standard technique that makes use of this observation is known as the *isoparametric transformation.*

So instead of fabricating bilinear basis functions on the quadrilateral itself (the *original frame* $\mathbf{x} = (x, y)$), we first transform the quadrilateral to the unit square and fabricate basis functions there (the *reference frame* $\boldsymbol{\xi} = (\xi, \eta)$).

The nodes of the quadrilateral are transformed in the following way:

$$\mathbf{x}_1 \to (0,0) \equiv \boldsymbol{\xi}_1, \quad \mathbf{x}_2 \to (1,0) \equiv \boldsymbol{\xi}_2, \quad \mathbf{x}_3 \to (1,1) \equiv \boldsymbol{\xi}_3 \quad \text{and} \quad \mathbf{x}_4 \to (0,1) \equiv \boldsymbol{\xi}_4 \tag{5.94}$$

furthermore we require that straight lines in the reference frame stay straight lines in the reference frame and that the inverse transformation satisfies the 2 requirements:

$$\mathbf{x} = \sum_{j=1}^{n} x_j \phi_j(\boldsymbol{\xi}) \tag{5.95}$$

$$u(\mathbf{x}) = \sum_{j=1}^{n} u_j \phi_j(\boldsymbol{\xi}) \tag{5.96}$$

From Eq. (5.95) we can derive the back transformation:

$$x = x_1 + (x_2 - x_1)\xi + (x_4 - x_1)\eta + (x_1 - x_2 + x_3 - x_4)\xi\eta \tag{5.97}$$

$$y = y_1 + (y_2 - y_1)\xi + (y_4 - y_1)\eta + (y_1 - y_2 + y_3 - y_4)\xi\eta \tag{5.98}$$

$$\tag{5.99}$$

The basis functions are defined on each element e_k (in the reference frame) with nodal points $\boldsymbol{\xi}_i = (\xi_i, \eta_i),\ i = 1, 2, 3, 4$ by:

$$\phi_1(\boldsymbol{\xi}) = (1-\xi)(1-\eta) \tag{5.100}$$
$$\phi_2(\boldsymbol{\xi}) = \xi(1-\eta) \tag{5.101}$$
$$\phi_3(\boldsymbol{\xi}) = \xi\eta \tag{5.102}$$
$$\phi_4(\boldsymbol{\xi}) = (1-\xi)\eta \tag{5.103}$$

Note that this only defines one of the four pieces of the linear basis function, since there are 3 other elements where the basis function is non-zero.

The integrals in the systems of equations are easily adapted to this transformation by using the *Jacobian* of the transformation:

$$\int_{e_{k_{\mathbf{x}}}} f(\mathbf{x})\ dxdy = \int_{e_{k_{\boldsymbol{\xi}}}} f(\boldsymbol{\xi})|J(\boldsymbol{\xi})|\ d\xi d\eta \tag{5.104}$$

with J the determinant of the Jacobian matrix $\mathbf{J}$ (using Eq. (5.99)):

$$\mathbf{J} = \begin{bmatrix} \frac{\partial x}{\partial \xi} & \frac{\partial x}{\partial \eta} \\ \frac{\partial y}{\partial \xi} & \frac{\partial y}{\partial \eta} \end{bmatrix} = \begin{bmatrix} x_2 - x_1 + A_x\eta & x_4 - x_1 + A_x\xi \\ y_2 - y_1 + A_y\eta & y_4 - y_1 + A_y\xi \end{bmatrix} \tag{5.105}$$

where $A_x = (x_1 - x_2 + x_3 - x_4)$ and $A_y = (y_1 - y_2 + y_3 - y_4)$.

For the isoparametric transformation we will only use numerical integration methods. This is done because the Jacobian is a function of ξ and η, which make the previously analytically evaluated integrals much more difficult (though certainly not impossible, but quite unnecessary).

5.5.1 Numerical integral evaluation

All the integrals can be seperated in four generic types ($\int \phi_i\phi_j|J|\ d\Omega$ is just a specific case of Eq. (5.106) with $f \equiv 1$):

$$\int \phi_i(\boldsymbol{\xi})\phi_j(\boldsymbol{\xi})f(\boldsymbol{\xi}, t)|J(\boldsymbol{\xi})|\ d\Omega \tag{5.106}$$
$$\int \phi_i(\boldsymbol{\xi})f(\boldsymbol{\xi}, t)|J(\boldsymbol{\xi})|\ d\Omega \tag{5.107}$$
$$\int \nabla\phi_i(\boldsymbol{\xi}) \cdot \nabla\phi_j(\boldsymbol{\xi})|J(\boldsymbol{\xi})|\ d\Omega \tag{5.108}$$
$$\int (\nabla\phi_i(\boldsymbol{\xi}) \cdot \nabla f(\boldsymbol{\xi}, t))\, \phi_j(\boldsymbol{\xi})|J(\boldsymbol{\xi})|\ d\Omega \tag{5.109}$$

where $f(\mathbf{x}, t)$ is some function of $\mathbf{x}$ and t. Once again we are only interested in forming an element matrix or vector, so the integral will only be evaluated over an element e_k in the reference frame. The function values of $f(\mathbf{x}, t)$ are known in the nodal points $\mathbf{x}_i,\ i = 1, 2, 3, 4$ in the original frame.

Integrals (5.106), (5.107) and (5.108) will be estimated using the *Newton-Cotes rule* of degree 1 in 2 dimensions:

$$\begin{aligned}\int_{e_k} f(\boldsymbol{\xi})|J(\boldsymbol{\xi})|\ d\Omega &\approx \frac{1}{4}\left(f(\boldsymbol{\xi}_1)|J(\boldsymbol{\xi}_1)| + f(\boldsymbol{\xi}_2)|J(\boldsymbol{\xi}_2)| + f(\boldsymbol{\xi}_3)|J(\boldsymbol{\xi}_3)| + f(\boldsymbol{\xi}_4)|J(\boldsymbol{\xi}_4)|\right) \\ &= \frac{1}{4}\left(f(\mathbf{x}_1)J_1 + f(\mathbf{x}_2)J_2 + f(\mathbf{x}_3)J_3 + f(\mathbf{x}_4)J_4\right)\end{aligned} \tag{5.110}$$

using $u(\mathbf{x}_i) = u(\boldsymbol{\xi}_i)$ (follows from Eq. (5.96)), $\int_{e_k} d\Omega = 1$ (since we are integrating over a unit square with area 1) and defining $J_i = |J(\boldsymbol{\xi}_i)|$.

Integral (5.106)

Making use of the basis function's property $\phi_i(\boldsymbol{\xi}_j) = \delta_{ij}$, the element matrix for (5.106) becomes:

$$S^{e_k} = \frac{1}{4}\begin{bmatrix} f(\mathbf{x}_1,t)J_1 & 0 & 0 & 0 \\ 0 & f(\mathbf{x}_2,t)J_2 & 0 & 0 \\ 0 & 0 & f(\mathbf{x}_3,t)J_3 & 0 \\ 0 & 0 & 0 & f(\mathbf{x}_4,t)J_4 \end{bmatrix} \tag{5.111}$$

Integral (5.107)

Integral (5.107) can be estimated similarly to the element vector

$$f^{e_k} = \frac{1}{4}\begin{bmatrix} f(\mathbf{x}_1,t)J_1 \\ f(\mathbf{x}_2,t)J_2 \\ f(\mathbf{x}_3,t)J_3 \\ f(\mathbf{x}_4,t)J_4 \end{bmatrix} \tag{5.112}$$

Integral (5.108)

With Newton-Cotes integral (5.108) reads

$$\int \nabla\phi_i(\boldsymbol{\xi}) \cdot \nabla\phi_j(\boldsymbol{\xi})|J(\boldsymbol{\xi})| \; d\Omega \approx \sum_{k=1}^{4} \nabla\phi_i(\boldsymbol{\xi}_k) \cdot \nabla\phi_j(\boldsymbol{\xi}_k)|J(\boldsymbol{\xi}_k)| \tag{5.113}$$

Integral (5.113) is very misleading. The gradients are taken with respect to x and y, where we have been evaluating everything in ξ and η so far. To facilitate this transformation we make use the inverse of the transformation Jacobian (Eq. (5.105)):

$$\mathbf{J}^{-1} = \begin{bmatrix} \frac{\partial\xi}{\partial x} & \frac{\partial\xi}{\partial y} \\ \frac{\partial\eta}{\partial x} & \frac{\partial\eta}{\partial y} \end{bmatrix} \tag{5.114}$$

Using the chain rule, the gradient with respect to x and y can be written in terms of ξ and η:

$$\nabla\phi_i = \begin{bmatrix} \frac{\partial\phi_i}{\partial x} \\ \frac{\partial\phi_i}{\partial y} \end{bmatrix} = \begin{bmatrix} \frac{\partial\phi_i}{\partial\xi}\frac{\partial\xi}{\partial x} + \frac{\partial\phi_i}{\partial\eta}\frac{\partial\eta}{\partial x} \\ \frac{\partial\phi_i}{\partial\xi}\frac{\partial\xi}{\partial y} + \frac{\partial\phi_i}{\partial\eta}\frac{\partial\eta}{\partial y} \end{bmatrix} = \begin{bmatrix} \frac{\partial\phi_i}{\partial\xi} & \frac{\partial\phi_i}{\partial\eta} \end{bmatrix} \begin{bmatrix} \frac{\partial\xi}{\partial x} & \frac{\partial\xi}{\partial y} \\ \frac{\partial\eta}{\partial x} & \frac{\partial\eta}{\partial y} \end{bmatrix} = \nabla^{\boldsymbol{\xi}}\phi_i\mathbf{J}^{-1} \tag{5.115}$$

where $\nabla^{\boldsymbol{\xi}} \equiv (\frac{\partial}{\partial\xi}, \frac{\partial}{\partial\eta})$.

The gradients with respect to ξ and η are easily derived from Eq. (5.100)-(5.103):

$$\nabla^{\boldsymbol{\xi}}\phi_1(\boldsymbol{\xi}) = [1-\eta, 1-\xi] \tag{5.116}$$

$$\nabla^{\boldsymbol{\xi}}\phi_2(\boldsymbol{\xi}) = [1-\eta, \xi] \tag{5.117}$$

$$\nabla^{\boldsymbol{\xi}}\phi_3(\boldsymbol{\xi}) = [\eta, \xi] \tag{5.118}$$

$$\nabla^{\boldsymbol{\xi}}\phi_4(\boldsymbol{\xi}) = [\eta, 1-\xi] \tag{5.119}$$

Define N and M as the matrices containing all the derivatives with respect to respectively (ξ, η) and (x, y):

$$N(\boldsymbol{\xi}) \equiv \begin{bmatrix} \nabla^{\boldsymbol{\xi}}\phi_1(\boldsymbol{\xi}) \\ \nabla^{\boldsymbol{\xi}}\phi_2(\boldsymbol{\xi}) \\ \nabla^{\boldsymbol{\xi}}\phi_3(\boldsymbol{\xi}) \\ \nabla^{\boldsymbol{\xi}}\phi_4(\boldsymbol{\xi}) \end{bmatrix} = \begin{bmatrix} \frac{\partial\phi_1}{\partial\xi} & \frac{\partial\phi_1}{\partial\eta} \\ \frac{\partial\phi_2}{\partial\xi} & \frac{\partial\phi_2}{\partial\eta} \\ \frac{\partial\phi_3}{\partial\xi} & \frac{\partial\phi_3}{\partial\eta} \\ \frac{\partial\phi_4}{\partial\xi} & \frac{\partial\phi_4}{\partial\eta} \end{bmatrix} \quad \Rightarrow \quad M(\boldsymbol{\xi}) \equiv \begin{bmatrix} \nabla\phi_1(\boldsymbol{\xi}) \\ \nabla\phi_2(\boldsymbol{\xi}) \\ \nabla\phi_3(\boldsymbol{\xi}) \\ \nabla\phi_4(\boldsymbol{\xi}) \end{bmatrix} = N\mathbf{J}^{-1} \tag{5.120}$$

Now the element matrix can be written as a simple matrix multiplication:

$$S^{e_k} = \sum_{k=1}^{4} M(\boldsymbol{\xi}_k) M^T(\boldsymbol{\xi}_k) J_k \tag{5.121}$$

Integral (5.109)

Integral (5.109) contains a gradient that first has to be calculated. Since the function $f(\boldsymbol{\xi}, t)$ is known in $\boldsymbol{\xi}_1$, $\boldsymbol{\xi}_2$, $\boldsymbol{\xi}_3$ and $\boldsymbol{\xi}_4$ the gradient with respect to ξ and η can be estimated by a generalized form of central differences:

$$\begin{aligned}\nabla^{\boldsymbol{\xi}} f(\boldsymbol{\xi}, t) &\approx \frac{1}{2}\begin{bmatrix}-1 & 1 & 1 & -1\\ -1 & -1 & 1 & 1\end{bmatrix}\begin{bmatrix}f(\mathbf{x}_1,t)\\ f(\mathbf{x}_2,t)\\ f(\mathbf{x}_3,t)\\ f(\mathbf{x}_4,t)\end{bmatrix}\\ &= \frac{1}{2}\begin{bmatrix}-f(\mathbf{x}_1,t)+f(\mathbf{x}_2,t)+f(\mathbf{x}_3,t)-f(\mathbf{x}_4,t)\\ -f(\mathbf{x}_1,t)-f(\mathbf{x}_2,t)+f(\mathbf{x}_3,t)+f(\mathbf{x}_4,t)\end{bmatrix} \equiv N_f\end{aligned} \tag{5.122}$$

Like in the case of the basis functions (Eq. (5.115)), the gradient with respect to x and y can now be calculated by multiplying with the inverse Jacobian:

$$\nabla f(\boldsymbol{\xi}, t) = \nabla^{\boldsymbol{\xi}} f(\boldsymbol{\xi}, t)\mathbf{J}^{-1} \approx N_f^T \mathbf{J}^{-1} \equiv M_f(\bar{\boldsymbol{\xi}}) \tag{5.123}$$

Next the *midpoint rule* in 2 dimensions can be applied:

$$\int_{e_k} f(\boldsymbol{\xi}) d\Omega \approx f\left(\frac{\boldsymbol{\xi}_1 + \boldsymbol{\xi}_2 + \boldsymbol{\xi}_3 + \boldsymbol{\xi}_4}{4}\right) \tag{5.124}$$

Defining $\bar{\boldsymbol{\xi}} = \frac{\boldsymbol{\xi}_1+\boldsymbol{\xi}_2+\boldsymbol{\xi}_3+\boldsymbol{\xi}_4}{4}$ the necessary function values of the linear basis function are:

$$\phi_i(\bar{\boldsymbol{\xi}}) = \frac{1}{4} \quad \text{and} \quad \nabla\phi_i(\bar{\boldsymbol{\xi}}) = M(\bar{\boldsymbol{\xi}}) \tag{5.125}$$

Applying 2 dimensional central differences to $f(\boldsymbol{\xi}, t)$ in x, we get with the midpoint rule:

$$\int_{e_k} \left(\nabla\phi_i(\boldsymbol{\xi}) \cdot \nabla f(\boldsymbol{\xi}, t)\right) \phi_j(\boldsymbol{\xi}) |J(\boldsymbol{\xi})| \; d\Omega \approx \frac{1}{4} M(\bar{\boldsymbol{\xi}}) M_f J(\bar{\boldsymbol{\xi}}) \tag{5.126}$$

Combining Eq. (5.126) and (5.122), the element matrix for (5.109) becomes:

$$S^{e_k} = \frac{1}{4} M(\bar{\boldsymbol{\xi}}) \cdot M_f^T(\bar{\boldsymbol{\xi}}) \cdot \mathbf{1} \tag{5.127}$$

where 1 is a row vector containing only ones: $\mathbf{1} = \begin{pmatrix}1 & 1 & 1 & 1\end{pmatrix}$.

Note that the columns of this matrix are all the same, because the function value of $\phi_j(\boldsymbol{\xi})$ is always $\frac{1}{4}$ at $\boldsymbol{\xi} = \bar{\boldsymbol{\xi}}$.

5.6 Time integration

Also for the FEM model the IMEX method is chosen for time integration, for the same reasons mentioned in Section 4.2. From the results of the FVM simulations we can conclude that the second method (taking all non linear terms on the current time step) performs much better, so this same approach will also be taken here.

5.7 Results

5.7.1 FEM compared to FVM in 1 dimension

Of course we expect approximately the same result for the FEM 1D simulation compared to the FVM 1D simulation, since they discretize exactly the same system. The results are shown in Figure 5.7. The results correspond very well to the 1D FVM simulations in Section 4.4.2. The only difference is the calculation time, which is about a factor 7 slower for the FEM analysis. This is due to the fact that the mass matrix (see Section 4.3) is no longer diagonal in FEM analysis, which makes matrix inversion much slower.

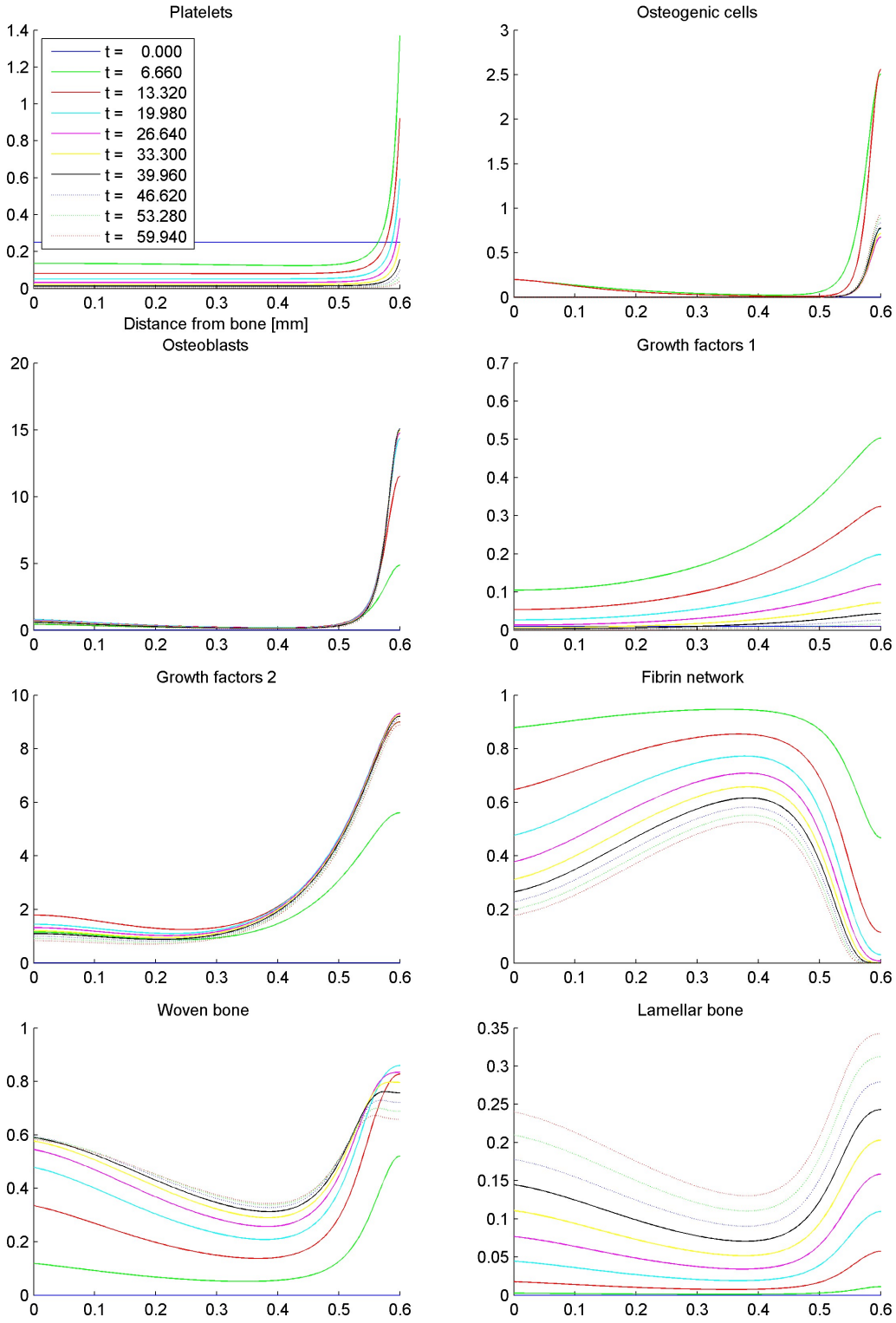

Figure 5.7: Cell densities and volume fractions of the model variables with low microtopography. $nx = 200$, $dt = 0.02$ and $T_{max} = 60$. This numerical method is instable.

5.7.2 FEM 2D grid comparison

In the initial simulation with FEM in 2D an unwanted phenomenon was observed while implementing the diffusion equation. The platelet concentration $p(\mathbf{x})$ was assumed to only be dependent of x (so no extra proteïns on the upper and lower boundaries of the implant), so the equation becomes completely symmetrical for y and is essentially reduced to its 1 dimensional counterpart. In the xz-plane we should then see the same figures as in the 1 dimensional case, but for the platelet concentration with diffusion the following was observed:

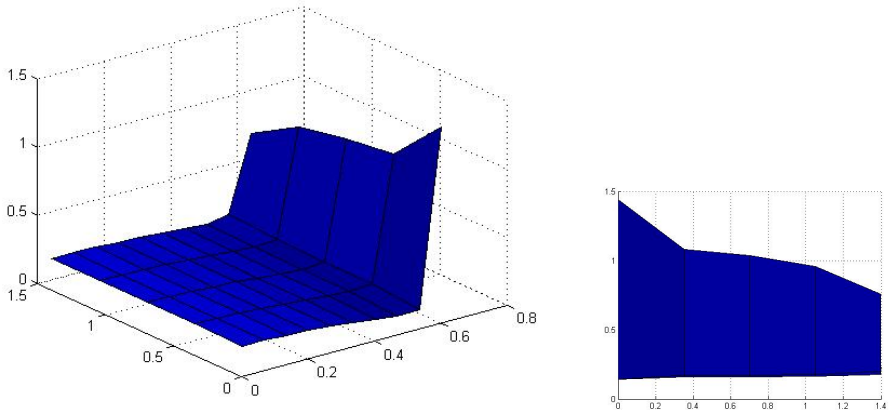

Figure 5.8: Unwanted 'diffusion' in y direction in the case $p(\mathbf{x}) = p(x)$. $nx = 10$, $ny = 5$, $t = 0.4$.

So there seems to be some kind of diffusion in y direction, which should not be there at all since concentration should be constant in y. By increasing the grid size this phenomenon can be reduced but it is still very much present:

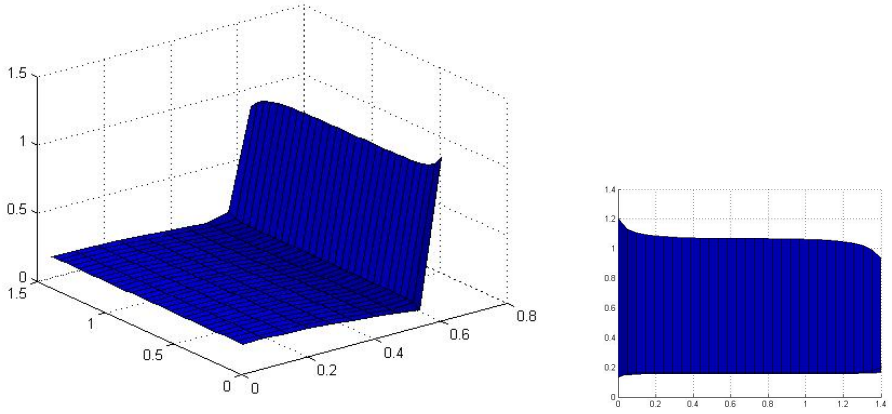

Figure 5.9: Still unwanted 'diffusion' in y direction in the case $p(\mathbf{x}) = p(x)$ with a more accurate grid. $nx = 10$, $ny = 40$, $t = 0.4$.

The problem can partially be solved by taking a different type of grid, with elements alternatively mirrored. Compare the two grids in Figure

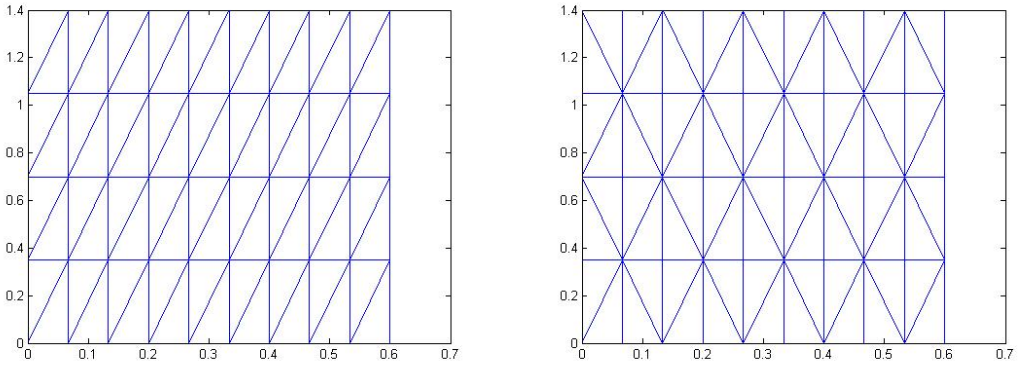

Figure 5.10: Two grid types, the left was used in the simulations above, the right is proposed as an improvement.

With a small grid there are still problems with this new grid:

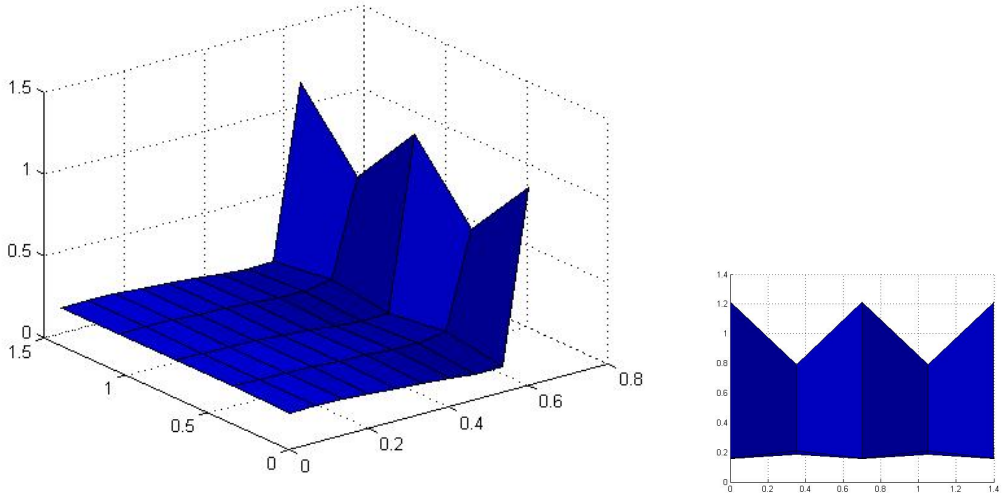

Figure 5.11: Unwanted 'diffusion' in y direction cancels out in the case $p(\mathbf{x}) = p(x)$ and the mirrored grid. $nx = 10$, $ny = 5$, $t = 0.4$.

but with a more accurate grid the contributions nullify each other to roughly reach the expected result.

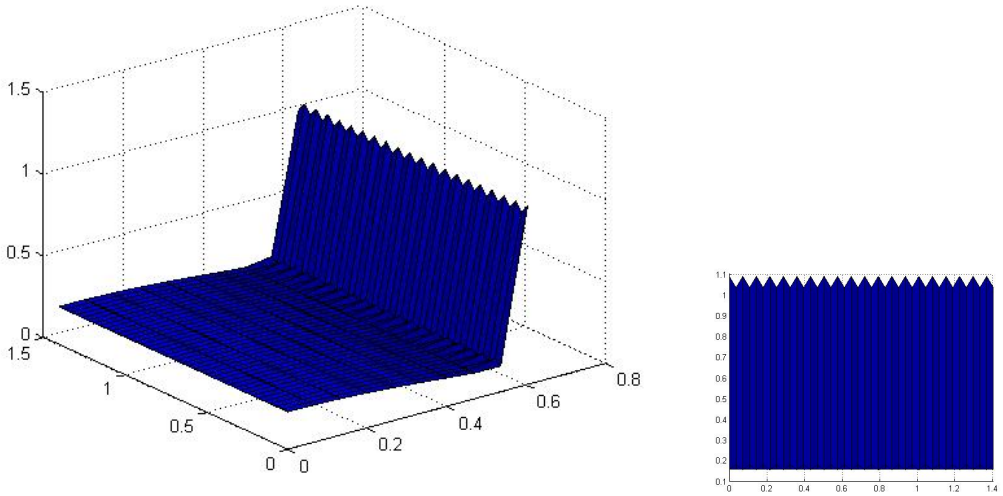

Figure 5.12: Unwanted 'diffusion' roughly dissappears in y direction in the case $p(\mathbf{x}) = p(x)$ with a more accurate mirrored grid. $nx = 10$, $ny = 40$, $t = 0.4$.

The unwanted diffusion in y-direction is a possibly serious hazard for errors, since there are different taxis terms in the model that depend on gradients of variables. So from now on the alternatively mirrored grid will be used.

Alternatively quadrilateral elements can be used and in this case this unwanted effect completely dissappears:

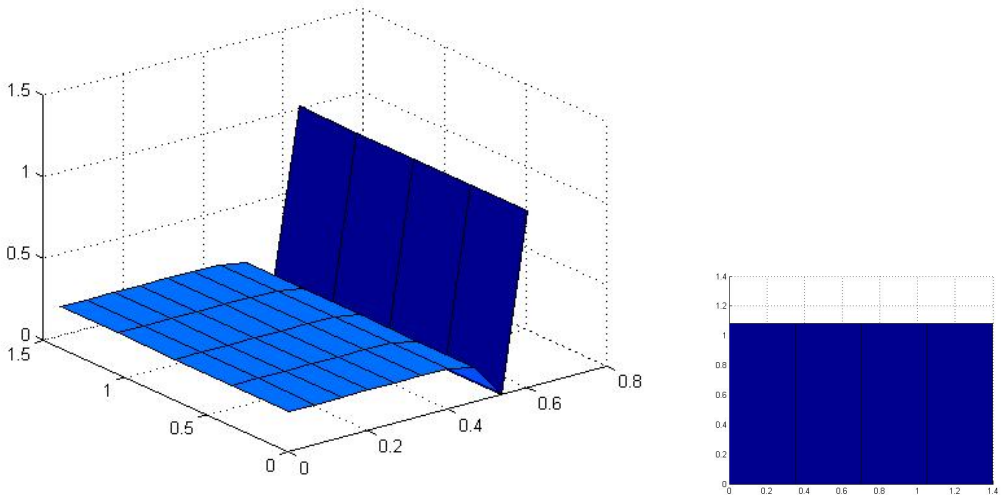

Figure 5.13: No unwanted 'diffusion' in y direction at all in the case $p(\mathbf{x}) = p(x)$ and quadrilateral elements. $nx = 10$, $ny = 5$, $t = 0.4$.

5.7.3 FEM 2D validation: comparison with 1D

As mentioned in the previous section, with $p(\mathbf{x}) = x$ the 2D equations essentially become 1D. So as a validation method we will see if there is indeed no dependency on y and if the results agree with the 1D simulation results.

As a reference we use the results from Section 4.4.1 of the second IMEX method. For the triangular elements the result is shown in Figure 5.14 and for the quadrilateral elements in 5.15. The results are in agreement with the results from the 1D simulation, so (assuming the 1D simulation was correct) the simulation in x direction is correct.

Triangular elements:

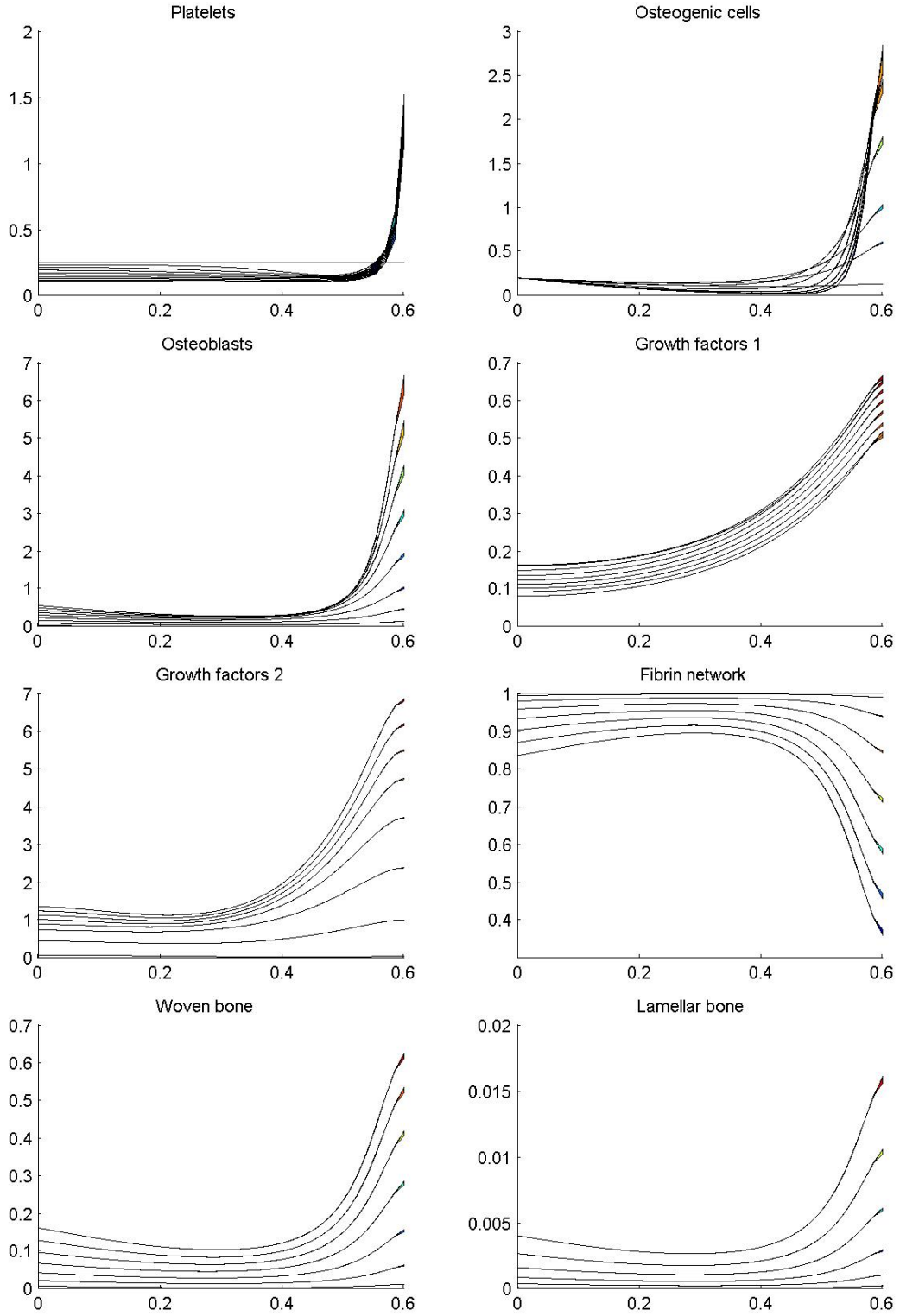

Figure 5.14: Cell densities and volume fractions of the model variables with 2D triangular elements. $nx = 40$, $ny = 50$, $dt = 0.5$ and $T_{max} = 10$. The results agree with the 1D results from Section 4.4.1.

Quadrilateral elements:

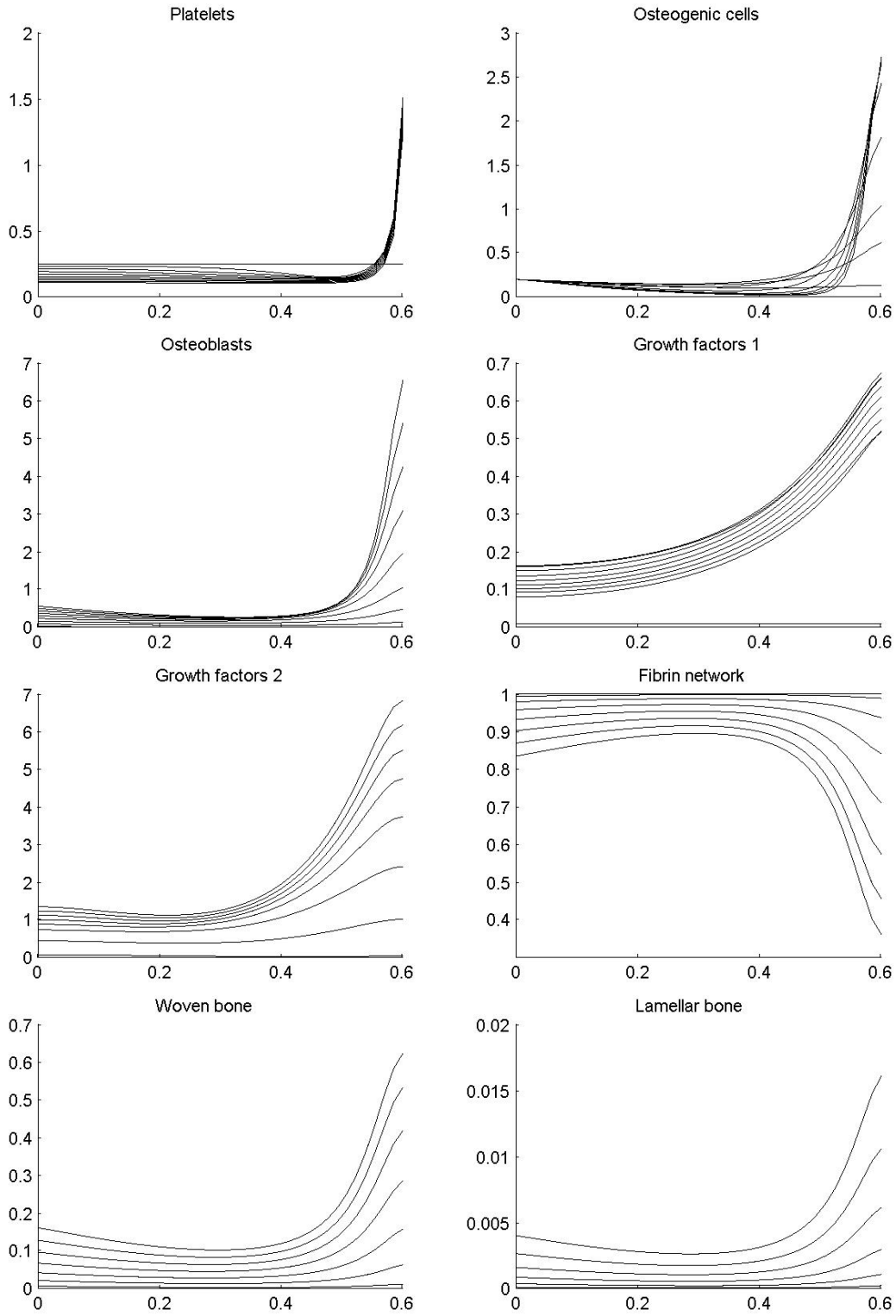

Figure 5.15: Cell densities and volume fractions of the model variables with 2D quadrilateral elements. $nx = 40$, $ny = 50$, $dt = 0.5$ and $T_{max} = 10$. The results agree with the 1D results from Section 4.4.1.

5.7.4 FEM 2D simulation triangular elements (2 months)

Simulations with FEM in 2D using triangular elements have been carried out over a time span of 60 days, a low microtopography is assumed ($p_s = 0.1$). Unfortunately it was not possible to do the same simulation for a high microtopography due to reasons explained in the discussion.

The results can be found in Figure 5.16 to 5.23. The main problem lies in the excessively high concentration of osteogenic cells at the corners of the implant surface, which causes instability in all related variables. What can still be seen quite well is the formation of bone along both host bone as implant surface. The formation at the implant surface seems to be more locally peaked, where the formation at the host bone is much more gradual and is evenly spread over the whole length of the domain.

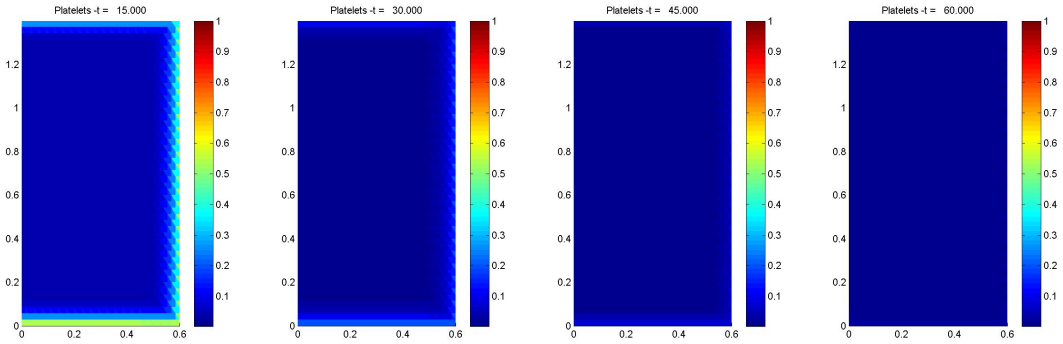

Figure 5.16: Platelet density at 4 different times ($15, 30, 45$ and 60 days). $nx = 40$, $ny = 50$, $dt = 0.02$ and $T_{max} = 60$. Initially there is a high density at the implant surfaces thanks to the higher proteïn concentration, after about 40 days the density has dropped to zero because there is no production.

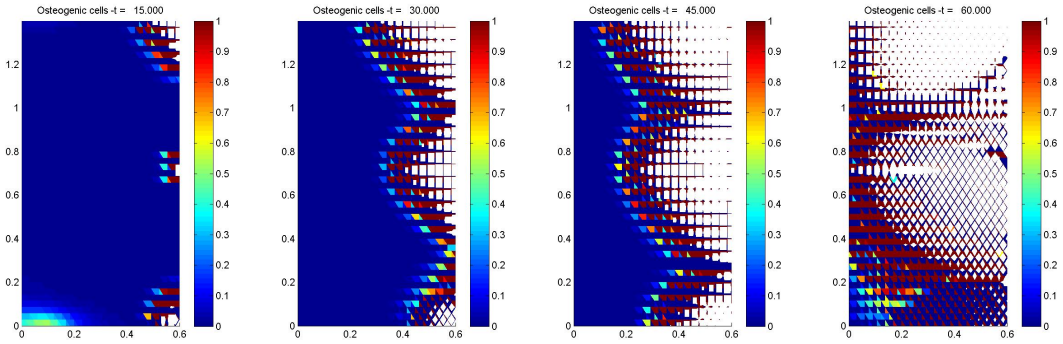

Figure 5.17: Osteogenic cell density at 4 different times ($15, 30, 45$ and 60 days). $nx = 40$, $ny = 50$, $dt = 0.02$ and $T_{max} = 60$. At first there are very high concentrations at the corners of the implant surface and also in the middle of the implant surface, after that instability arises which slowly 'spreads' over the whole domain. White areas mean that the values fall way out of the range $[0, 1]$ (in the order of 10^4).

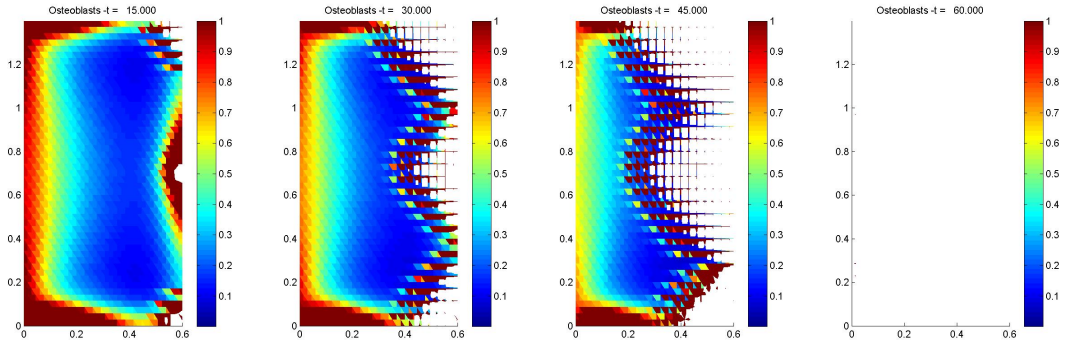

Figure 5.18: Osteoblast cell density at 4 different times (15, 30, 45 and 60 days). $nx = 40$, $ny = 50$, $dt = 0.02$ and $T_{max} = 60$. At first high osteoblast density is found at both the implant and the bone surface, after about 15 days instability arises like in the case of the osteogenic cells. White areas mean that the values fall way out of the range $[0, 1]$ (in the order of 10^4).

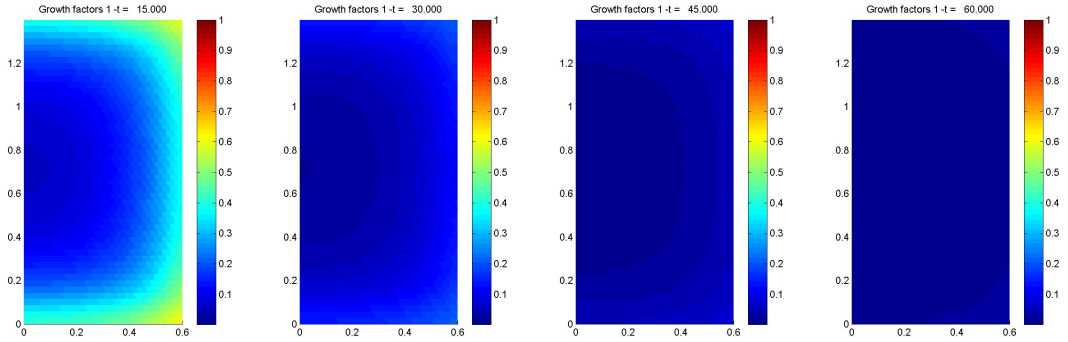

Figure 5.19: Growth factor 1 density at 4 different times (15, 30, 45 and 60 days). $nx = 40$, $ny = 50$, $dt = 0.02$ and $T_{max} = 60$. The growth factor increases in almost concentric circles towards the implant surface. After the initial production, the density slowly drops to zero while keeping the concentric circle pattern.

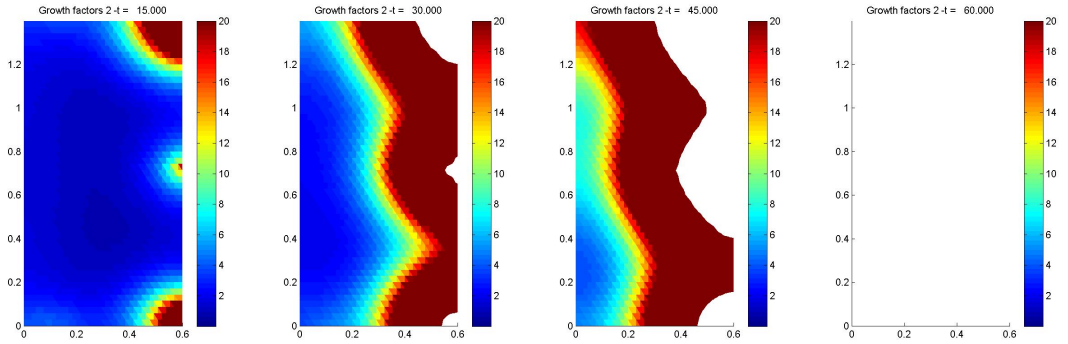

Figure 5.20: Growth factor 2 density at 4 different times (15, 30, 45 and 60 days). $nx = 40$, $ny = 50$, $dt = 0.02$ and $T_{max} = 60$. The growth factor is intially high at the implant surface corners and also somewhere in the middle (compare to the osteogenic cell density), after approximately 15 days it rises to unrealistic values most probably due to instability.

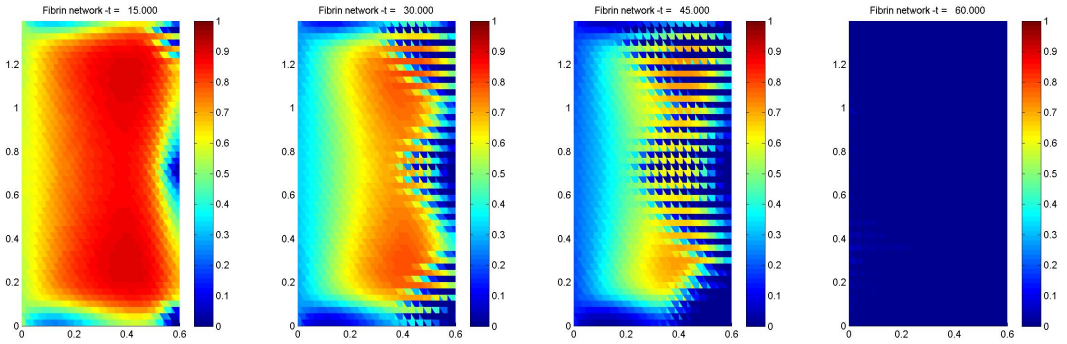

Figure 5.21: Fibrin network volume fraction at 4 different times (15, 30, 45 and 60 days). $nx = 40$, $ny = 50$, $dt = 0.02$ and $T_{max} = 60$. The fibrin network drops the quickest at the implant surface and to a lesser but still significant extent also at the bone surface, this process continues, but instabilities slowly arise from the side of the implant surface and 'spread' over the whole domain.

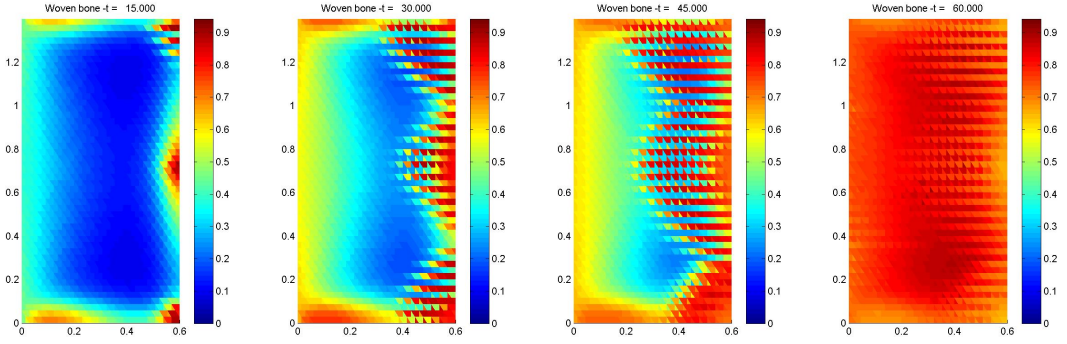

Figure 5.22: Woven bone volume fraction at 4 different times (15, 30, 45 and 60 days). $nx = 40$, $ny = 50$, $dt = 0.02$ and $T_{max} = 60$. Woven bone is formed at all surfaces (both implant and bone), very high concentrations appear at the corners of the implant surface that slowly evolve into instabilities that 'spread' over the domain.

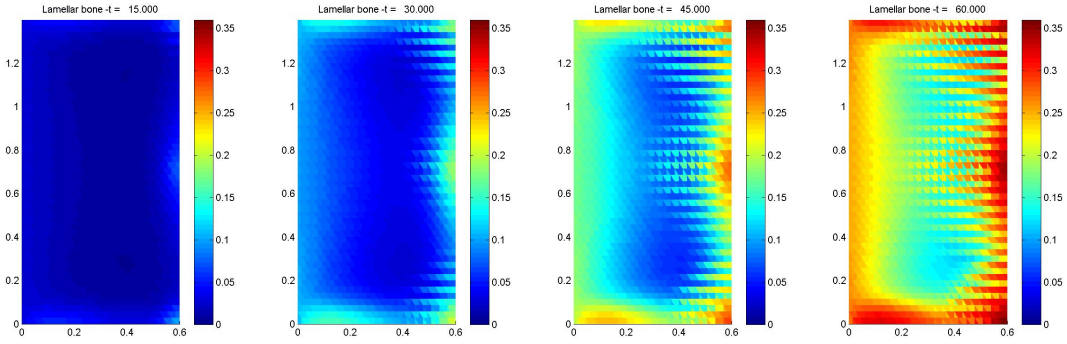

Figure 5.23: Lamellar bone volume fraction at 4 different times (15, 30, 45 and 60 days). $nx = 40$, $ny = 50$, $dt = 0.02$ and $T_{max} = 60$. Lamellar bone is formed at all surfaces (both implant and bone), in contrast to woven bone in lesser extent at the implant surfaces then at the bone surface. At 30 days there is more formation of lamellar bone at the implant surface, but again the instabilities slowly take over the whole domain.

5.7.5 FEM 2D simulation quadrilateral elements (2 months)

Simulations with FEM in 2D using quadrilateral elements have been carried out over a time span of 60 days, a low microtopography is assumed ($p_s = 0.1$). Unfortunately also for quadrilaterals it was not possible to do the same simulation for a high microtopography for reasons explained in the discussion.

The results can be found in Figure 5.24 to 5.31. The same problems arise that were found with the triangular elements, in most cases the instabilities seem to have evolved a little less over the domain, but the result will still be relatively inaccurate because of them.

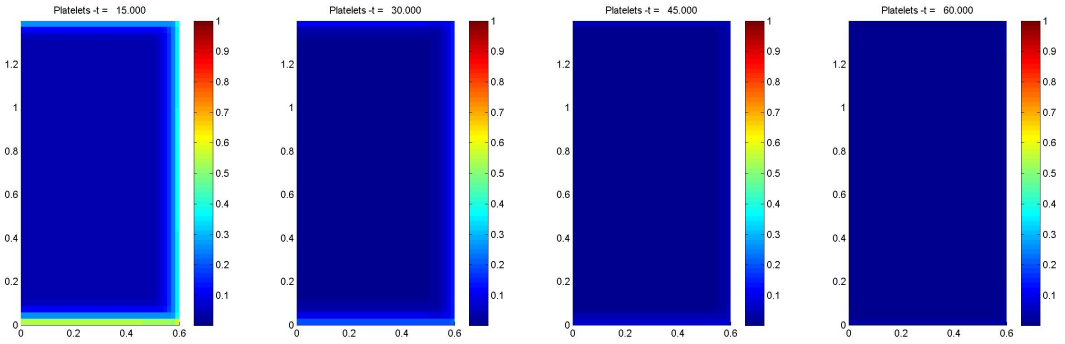

Figure 5.24: Platelet density at 4 different times (15, 30, 45 and 60 days). $nx = 40$, $ny = 50$, $dt = 0.02$ and $T_{max} = 60$. Initially there is a high density at the implant surfaces thanks to the higher proteïn concentration, after about 40 days the density has dropped to zero because there is no production.

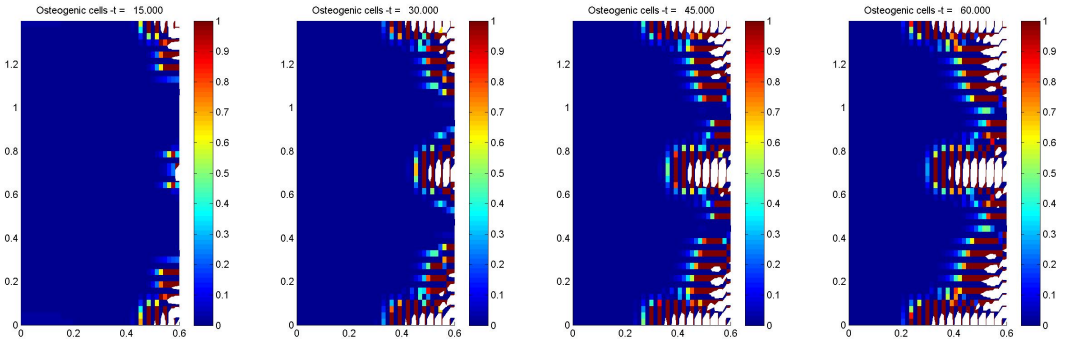

Figure 5.25: Osteogenic cell density at 4 different times (15, 30, 45 and 60 days). $nx = 40$, $ny = 50$, $dt = 0.02$ and $T_{max} = 60$. At first there are very high concentrations at the corners of the implant surface and also in the middle of the implant surface, after that these areas of instability only slowly expand, in the rest of the domain there seems to be a very low density of osteogenic cells. White areas mean that the values fall way out of the range $[0, 1]$ (in the order of 10^4).

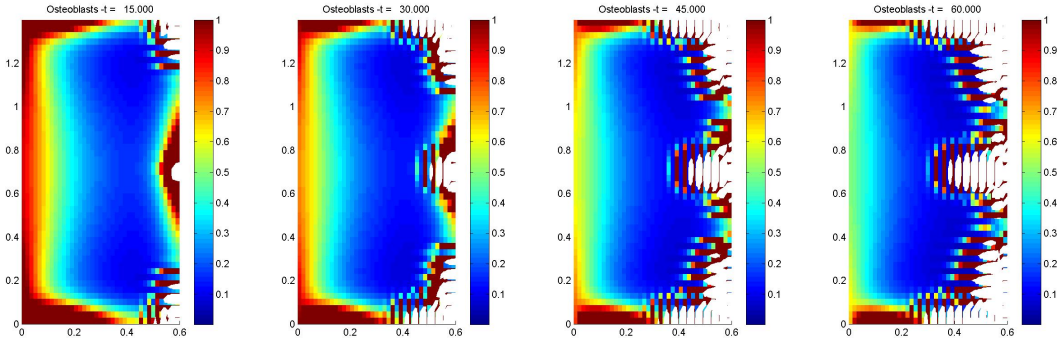

Figure 5.26: Osteoblast cell density at 4 different times (15, 30, 45 and 60 days). $nx = 40$, $ny = 50$, $dt = 0.02$ and $T_{max} = 60$. At first high osteoblast density is found at both the implant and the bone surface, after about 15 days instability arises like in the case of the osteogenic cells. The osteoblast density also slowly decrease at the bone surface. White areas mean that the values fall way out of the range $[0, 1]$ (in the order of 10^4).

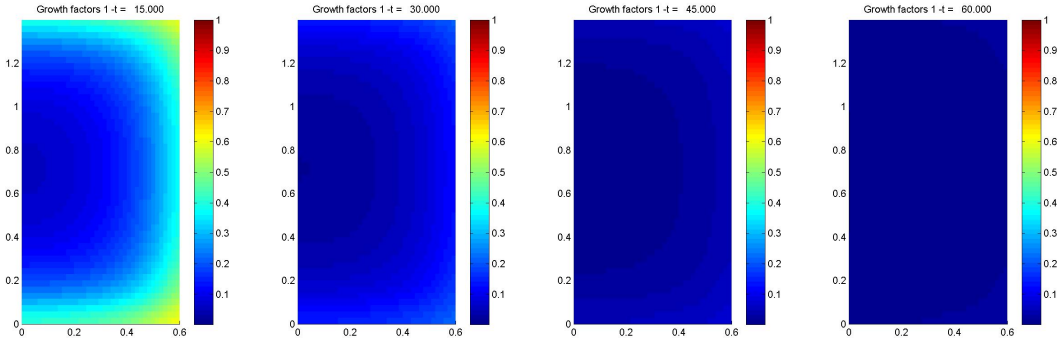

Figure 5.27: Growth factor 1 density at 4 different times (15, 30, 45 and 60 days). $nx = 40$, $ny = 50$, $dt = 0.02$ and $T_{max} = 60$. The growth factor increases in almost concentric circles towards the implant surface. After the initial production, the density slowly drops to zero while keeping the concentric circle pattern.

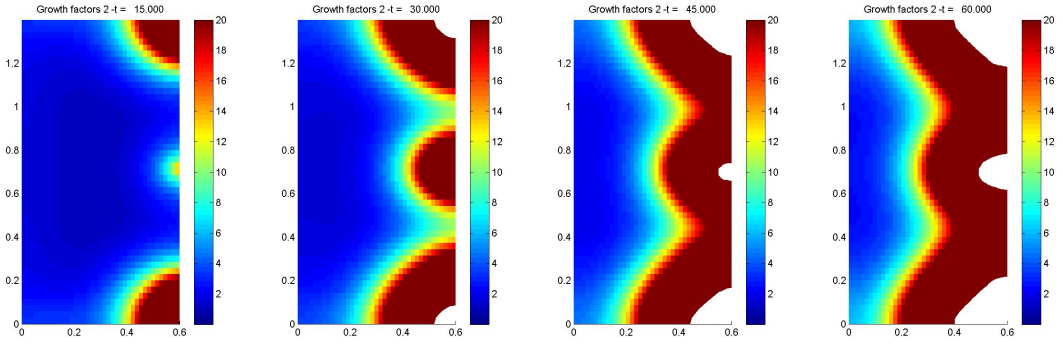

Figure 5.28: Growth factor 2 density at 4 different times (15, 30, 45 and 60 days). $nx = 40$, $ny = 50$, $dt = 0.02$ and $T_{max} = 60$. The growth factor is intially high at the implant surface corners and also somewhere in the middle (compare to the osteogenic cell density), after approximately 15 days it rises to unrealistic values most probably due to instability. White areas mean that the values fall way out of the range $[0, 1]$ (in the order of 10^4).

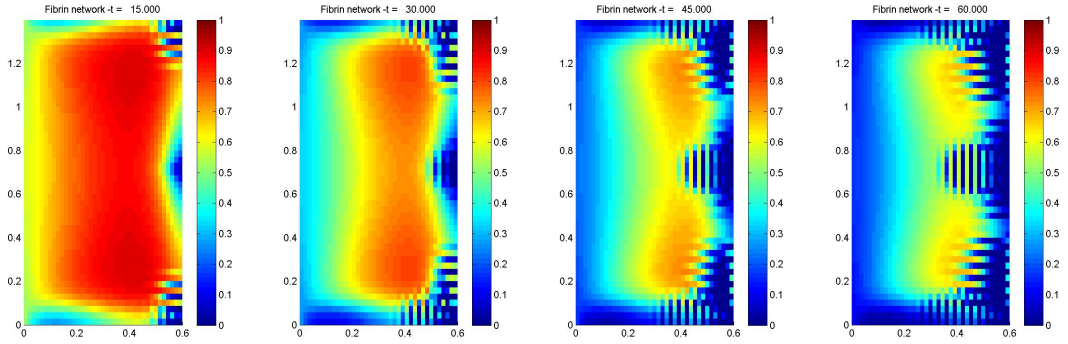

Figure 5.29: Fibrin network volume fraction at 4 different times (15, 30, 45 and 60 days). $nx = 40$, $ny = 50$, $dt = 0.02$ and $T_{max} = 60$. The fibrin network drops the quickest at the implant surface and to a lesser but still significant extent also at the bone surface, this process continues, but instabilities slowly arise from the side of the implant surface and 'spread' over the whole domain.

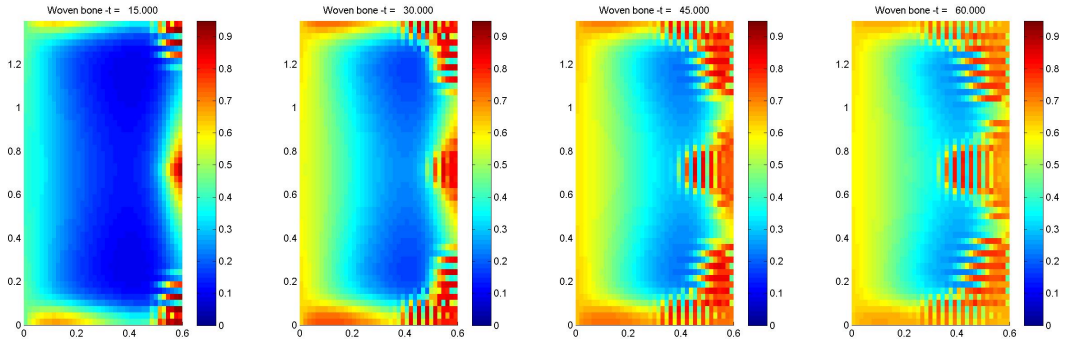

Figure 5.30: Woven bone volume fraction at 4 different times (15, 30, 45 and 60 days). $nx = 40$, $ny = 50$, $dt = 0.02$ and $T_{max} = 60$. Woven bone is formed at all surfaces (both implant and bone), very high concentrations appear at the corners of the implant surface that slowly evolve into instabilities that 'spread' over the domain. In the end the average bone fraction on the side of the bone are higher than on the side of the implant.

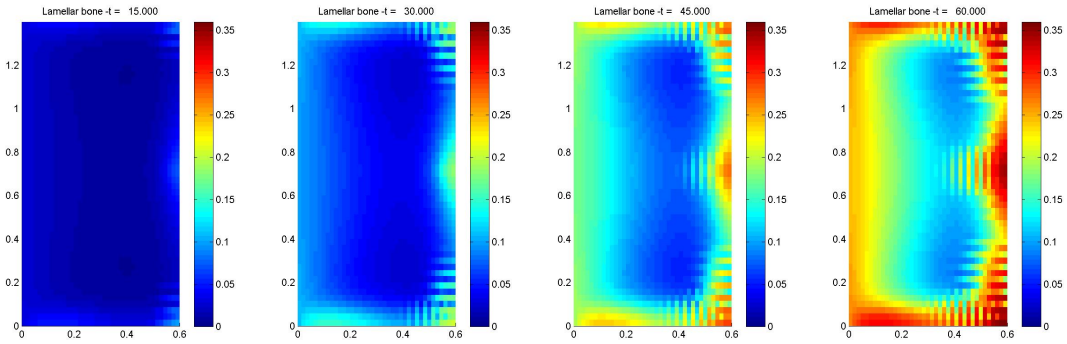

Figure 5.31: Lamellar bone volume fraction at 4 different times (15, 30, 45 and 60 days). $nx = 40$, $ny = 50$, $dt = 0.02$ and $T_{max} = 60$. Lamellar bone is formed at all surfaces (both implant and bone), in contrast to woven bone in lesser extent at the implant surfaces then at the bone surface. At 30 days there is more formation of lamellar bone at the implant surface. And like for woven bone the average bone fraction on the side of the bone are higher than on the side of the implant at 60 days.

Chapter 6

Discussion

2 conclusions related to numerical issues have already been mentioned and solved. The first was the surprising fact that for the IMEX method in the FVM simulations, the IMEX choice with lesser variables at the next time step proved to be more stable. A reason for this is not simple to give.

The second was the unwanted y-directional diffusion in the FEM 2D triangular elements simulation, which was solved by applying a mirrored grid. This could be caused by the fact that the middle of 2 neighbouring elements are actually diagonally aligned instead of horizontally or vertically (see Figure 6.1), while the proteïn concentration for example is defined on horizontal lines of equal y. If every combination of 2 such elements causes some asymmetry, the adding of all these asymmetries could lead to errors with some form of direction. What the exact cause of this error is, can be investiged further though a solution is found by using mirrored elements or even quadrilaterals.

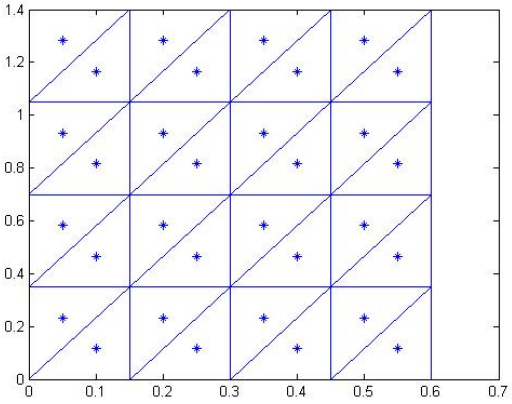

Figure 6.1: Asymmetry of the centers of elements

No real analysis has been conducted on the numerical stability of the system together with the IMEX method. This would probably be very difficult due to nonlinear terms. The convergence of the error of the numerical methods could also still be investigated.

Both the FVM and the FEM simulations reproduced the moving of the bone front from both the host bone surface as the implant surface side, as has been verified in experiments. What is remarkable is that in the 1 dimensional simulations the healing with high microtopography produces significantly worse results compared to low microtopography, whereas [Moreo, 2008]

found the exact opposite result with the same model. The major difference causing this, could be the fact that [Moreo, 2008] used a 2 dimensional model, with three implant surface boundaries with extra proteïns, instead of just 1.

Simulation of high microtopography in 2 dimensions was not succesful due to the excessively high values for the osteogenic cell density which caused singular matrices (at least to numerical precision). These high values already appeared for low microtopography, but high microtopography only increased these problems.

These high values can be traced back to the magnitude of the microtopography parameter p_s. The higher p_s the higher the concentration of platelets at the implant surface. These platelets produce more growth factors 1 and the osteogenic cell density equation contains the chemotaxis term that causes the osteogenic cell to move towards high concentrations of growth factors 1. Apparently the proteïn concentration was now formulated in such a way that the osteogenic cells clotted to the corners of the implant surface and formed excessive concentrations. It might be possible to solve this problem with a different function for the proteïn concentration or with a differently shaped computational domain ([Moreo, 2008] used a trapezoidal domain instead of a rectangular domain, it is not known if he faced the same problem with this domain).

Chapter 7

Conclusion

The model proposed by [Moreo, 2008] replicates the moving of the bone formation fronts from both the bone as the implant surface. Contrary to the findings of [Moreo, 2008] high microtopography is not favorable, but this could be caused by the fact that the findings in this report were done in a 1 dimensional simulation instead of a two dimensional. The simulations of the model experienced instability that seems to be inherent to the proposed model, but the most probable cause is the shape of the computational domain that was different in this report compared to the simulations by [Moreo, 2008].

Part II

Model with mechanical stimuli

Chapter 8

Introduction to linear elasticity

Elasticity is the physical property of a material that restores to its original shape when an external force is removed. Under certain assumptions the exact deformation of a body under external forces can be determined, described by how the points inside the material move from their original to a new position.

8.1 Stress, strain and displacement

A concept that is central in the theory of elasticity is *stress*, which is a measure of the intensity of the internal forces within the material that is being deformed as a reaction to external forces applied to the material body. There are two types of stress: *normal stress* and *shear stress* . Normal stress is the average force over an surface where the force acts perpendicular to the surface and shear stress is the average force over an surface where the force acts parallel to the surface (see Fig. 8.1).

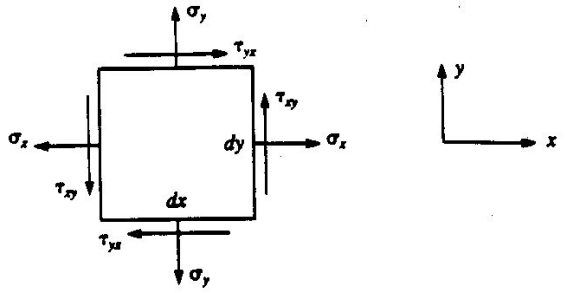

Figure 8.1: Normal (σ_x and σ_y) and shear stresses (τ_{xy} and τ_{yx}) working on a body

The theory of linear elasticity describes the deformation of a body, assuming that the deformation depends linearly on the applied force. This theory applies to almost all materials for very small forces and deformations when the first order approximation of the deformation is still accurate. In continuum mechanics infinitesimal elements are considered, so that average force over an area becomes the average force at a point under the assumption that the stress is constant over this infinitesimal element. This force of course also has a direction and to accomodate this, stress is described in a tensor known as the *Cauchy stress tensor*, $\boldsymbol{\sigma}$. In 2 dimensions the stress tensor is:

$$\boldsymbol{\sigma} \equiv \begin{bmatrix} \sigma_{xx} & \tau_{xy} \\ \tau_{xy} & \sigma_{yy} \end{bmatrix} \tag{8.1}$$

The diagonal elements describe the normal stresses on planes perpendicular to the axis of the chosen coordinate system. The off-diagonal elements describe the shear stresses along these same planes, these elements need to be equal to satisfy local conservation of angular momentum. With the stress tensor it is possible to calculate the size and direction of the force on a randomly chosen surface. Take a plane with unit normal vector $\mathbf{n}$, then $\boldsymbol{\sigma} \cdot \mathbf{n}$ gives the x and y component of the (average) force on this plane.

The stresses in the material result in small deformations, a measure of this deformation is *strain*. Strain can also be seperated into two types: *normal strain* and *shear strain*. Normal strain is the ratio of the length of the deformed element and the length of the element in undeformed state. Shear strain is the change in angle between two initially (without stresses) parallel lines. Like stress, strain has its own tensor:

$$\boldsymbol{\epsilon} \equiv \begin{bmatrix} \epsilon_{xx} & \gamma_{xy} \\ \gamma_{yx} & \epsilon_{yy} \end{bmatrix} \tag{8.2}$$

Under the *plane stress* assumption in 2 dimensions (the thickness of the material is small compared to the measurements of the surface) the relationship between stresses and strains is given by

$$\begin{bmatrix} \epsilon_{xx} \\ \epsilon_{yy} \\ \gamma_{xy} \end{bmatrix} = \frac{1}{E} \begin{bmatrix} 1 & -\nu & 0 \\ -\nu & 1 & 0 \\ 0 & 0 & 2(1+\nu) \end{bmatrix} \begin{bmatrix} \sigma_{xx} \\ \sigma_{yy} \\ \tau_{xy} \end{bmatrix} \quad \Rightarrow \quad \begin{bmatrix} \sigma_{xx} \\ \sigma_{yy} \\ \tau_{xy} \end{bmatrix} = \frac{E}{1-\nu^2} \begin{bmatrix} 1 & \nu & 0 \\ \nu & 1 & 0 \\ 0 & 0 & \frac{1-\nu}{2} \end{bmatrix} \begin{bmatrix} \epsilon_{xx} \\ \epsilon_{yy} \\ \gamma_{xy} \end{bmatrix} \tag{8.3}$$

where E is known as Young's modulus and ν as Poisson's ratio.

Finally it is possible to determine how the position of a point in the material changes under stresses. In 2 dimensions we can calculate the displacement in x and y direction, denoted with respective functions u and v, with the following relationship:

$$\begin{bmatrix} \epsilon_{xx} \\ \epsilon_{yy} \\ \gamma_{xy} \end{bmatrix} = \begin{bmatrix} \frac{\partial u}{\partial x} \\ \frac{\partial v}{\partial y} \\ \frac{\partial u}{\partial y} + \frac{\partial v}{\partial x} \end{bmatrix} \quad \Rightarrow \quad \begin{bmatrix} \sigma_{xx} \\ \sigma_{yy} \\ \tau_{xy} \end{bmatrix} = \frac{E}{1-\nu^2} \begin{bmatrix} \frac{\partial u}{\partial x} + \nu \frac{\partial v}{\partial y} \\ \nu \frac{\partial u}{\partial x} + \frac{\partial v}{\partial y} \\ \frac{1-\nu}{2} \left(\frac{\partial u}{\partial y} + \frac{\partial v}{\partial x} \right) \end{bmatrix} \tag{8.4}$$

8.2 Partial differential equations

8.2.1 Equilibrium condition

When forces change in magnitude or direction there is movement inside the material body resulting in time dependent stresses and strains. Once the force is stable and some time has passed a state of equilibrium will be reached in which the stresses and strains are no longer time dependent. In this equilibrium state the following PDE holds:

$$\nabla \cdot \boldsymbol{\sigma} + \mathbf{f} = 0 \tag{8.5}$$

which says that the sum of the divergence of the stress tensor and external *body forces* per unit volume (e.g. gravity) is zero.

Body forces are usually negligible compared to *surface forces* (e.g. applied pressure), in which case Eq. (8.5) reduces to

$$\nabla \cdot \boldsymbol{\sigma} = 0 \tag{8.6}$$

8.2.2 Boundary conditions

There are two main types of boundary conditions: displacement prescription and surface forces. In a way they are closely related because a prescribed displacement requires a (surface) force and an surface force causes a displacement.

Displacement prescriptions can be modelled with a Dirichlet boundary condition on the displacement functions u and v, i.e. $u(\mathbf{x}) = 0$ and $v(\mathbf{x}) = 0$, for a fixed edge.

Surface forces are modelled with a Neumann boundary condition of the stress tensor, i.e. $\boldsymbol{\sigma} \cdot \mathbf{n} = \begin{bmatrix} t \\ 0 \end{bmatrix}$, for a surface force in the x-direction.

8.3 Simulation using FEM

The finite element is very often used to simulate elasticity problems for its ability to handle irregular grids and relative ease in dealing with 2 and 3 dimensions. A simple problem is solved using FEM to validate the implementation for use in the next chapter.

8.3.1 Implementation validation

Since it is not easy to solve the elasticity problem analytically, instead we will prescribe a solution and calculate the body and surface forces that is then inserted into the simulation model. As computational domain the unit square is used (see Fig. 8.2.

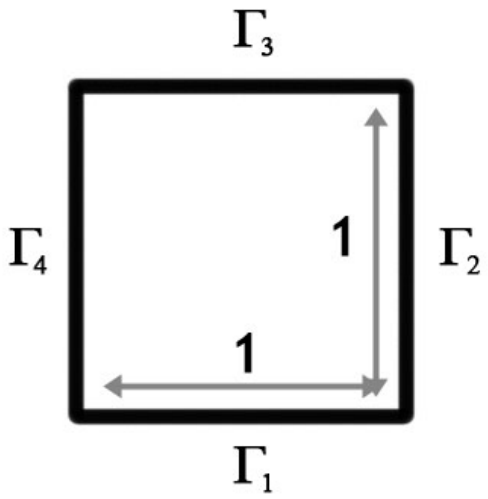

Figure 8.2: Computational domain implementation validation

As solution we prescribe

$$u(\mathbf{x}) = v(\mathbf{x}) = xy \tag{8.7}$$

The strain and stress tensor for these displacements are

$$\begin{bmatrix} \epsilon_{xx} \\ \epsilon_{yy} \\ \gamma_{xy} \end{bmatrix} = \begin{bmatrix} y \\ x \\ x+y \end{bmatrix} \quad \Rightarrow \quad \begin{bmatrix} \sigma_{xx} \\ \sigma_{yy} \\ \tau_{xy} \end{bmatrix} = \frac{E}{1-\nu^2} \begin{bmatrix} y+\nu x \\ \nu y + x \\ \frac{1-\nu}{2}(x+y) \end{bmatrix} \tag{8.8}$$

The equilibrium equation becomes:

$$\nabla \cdot \boldsymbol{\sigma} = \frac{E}{1-\nu^2} \begin{bmatrix} \nu + \frac{1-\nu}{2} \\ \nu + \frac{1-\nu}{2} \end{bmatrix} = \frac{E}{2(1-\nu)} \begin{bmatrix} 1 \\ 1 \end{bmatrix} \tag{8.9}$$

so $\mathbf{f} = -\frac{E}{2(1-\nu)} \begin{bmatrix} 1 \\ 1 \end{bmatrix}$.
The surface force boundary conditions become:

$$\begin{aligned} \boldsymbol{\sigma} \cdot \mathbf{n}|_{\Gamma_1} &= \begin{bmatrix} \sigma_{xx} n_x + \tau_{xy} n_y \\ \tau_{xy} n_x + \sigma_{yy} n_y \end{bmatrix} \Bigg|_{n_x=0, n_y=-1, x=x, y=0} \\ &= \begin{bmatrix} -\frac{E}{2(1+\nu)} x \\ -\frac{E}{1-\nu^2} x \end{bmatrix} \end{aligned} \tag{8.10}$$

and similarly for the other boundaries:

$$\boldsymbol{\sigma} \cdot \mathbf{n}|_{\Gamma_2} = \begin{bmatrix} \frac{E}{1-\nu^2}(y+\nu) \\ \frac{E}{2(1+\nu)}(1+y) \end{bmatrix} \tag{8.11}$$

$$\boldsymbol{\sigma} \cdot \mathbf{n}|_{\Gamma_3} = \begin{bmatrix} \frac{E}{2(1+\nu)}(x+1) \\ \frac{E}{1-\nu^2}(\nu+x) \end{bmatrix} \tag{8.12}$$

$$\boldsymbol{\sigma} \cdot \mathbf{n}|_{\Gamma_4} = \begin{bmatrix} -\frac{E}{1-\nu^2} y \\ -\frac{E}{2(1+\nu)} y \end{bmatrix} \tag{8.13}$$

8.3.2 Discretization

For the weak formulation of the equilibrium elasticity equation (8.5) we multiply with a test function η and integrate over the whole domain:

$$-\int_\Omega \eta \nabla \cdot \boldsymbol{\sigma} \; d\Omega = \int_\Omega \eta \cdot \mathbf{f} \; d\Omega. \tag{8.14}$$

We apply integration by parts and Gauss's theorem on the left hand side:

$$\int_\Omega \boldsymbol{\sigma} \cdot \nabla \eta \; d\Omega - \int_\Gamma \eta \boldsymbol{\sigma} \cdot \mathbf{n} \; d\Gamma = \int_\Omega \eta \cdot \mathbf{f} \; d\Omega. \tag{8.15}$$

or replacing the stress tensor with its elements:

$$\int_\Omega \sigma_{xx} \frac{\partial \eta}{\partial x} + \tau_{xy} \frac{\partial \eta}{\partial y} \; d\Omega = \int_\Omega \eta \cdot f^1 \; d\Omega + \int_\Gamma \eta \boldsymbol{\sigma}^1 \cdot \mathbf{n} \; d\Gamma \tag{8.16}$$

$$\int_\Omega \tau_{xy} \frac{\partial \eta}{\partial x} + \sigma_{yy} \frac{\partial \eta}{\partial y} \; d\Omega = \int_\Omega \eta \cdot f^2 \; d\Omega + \int_\Gamma \eta \boldsymbol{\sigma}^2 \cdot \mathbf{n} \; d\Gamma \tag{8.17}$$

where $\boldsymbol{\sigma}^i$ is the i-th row of the stress tensor and f^i is the i-th element of the body force vector.

Now the displacement derivatives can be filled in in the stress tensor components:

$$\int_\Omega \frac{E}{1-\nu^2} \left(\frac{\partial u}{\partial x} + \nu \frac{\partial v}{\partial y} \right) \frac{\partial \eta}{\partial x} + \frac{E}{2(1+\nu)} \left(\frac{\partial u}{\partial y} + \frac{\partial v}{\partial x} \right) \frac{\partial \eta}{\partial y} \; d\Omega = \int_\Omega \eta \cdot f^1 \; d\Omega + \int_\Gamma \eta \boldsymbol{\sigma}^1 \cdot \mathbf{n} \; d\Gamma \tag{8.18}$$

$$\int_\Omega \frac{E}{2(1+\nu)} \left(\frac{\partial u}{\partial y} + \frac{\partial v}{\partial x} \right) \frac{\partial \eta}{\partial x} + \frac{E}{1-\nu^2} \left(\nu \frac{\partial u}{\partial x} + \frac{\partial v}{\partial y} \right) \frac{\partial \eta}{\partial y} \; d\Omega = \int_\Omega \eta \cdot f^2 \; d\Omega + \int_\Gamma \eta \boldsymbol{\sigma}^2 \cdot \mathbf{n} \; d\Gamma \tag{8.19}$$

Next the approximation in basis functions of u and v are inserted and the test function is consecutively replaced by the basis functions $\{\phi_i\}_{i=1}^n$:

$$\sum_{j=1}^{n} u_j \int_\Omega \left(A\frac{\partial\phi_j}{\partial x}\frac{\partial\phi_i}{\partial x} + B\frac{\partial\phi_j}{\partial y}\frac{\partial\phi_i}{\partial y} \right) \, d\Omega + \sum_{j=1}^{n} v_j \int_\Omega \left(\nu A\frac{\partial\phi_j}{\partial y}\frac{\partial\phi_i}{\partial x} + B\frac{\partial\phi_j}{\partial x}\frac{\partial\phi_i}{\partial y} \right) \, d\Omega = \int_\Omega \phi_i \cdot f^1 \, d\Omega + \int_\Gamma \phi_i \boldsymbol{\sigma}^1 \cdot \mathbf{n} \, d\Gamma \tag{8.20}$$

$$\sum_{j=1}^{n} u_j \int_\Omega \left(B\frac{\partial\phi_j}{\partial y}\frac{\partial\phi_i}{\partial x} + \nu A\frac{\partial\phi_j}{\partial x}\frac{\partial\phi_i}{\partial y} \right) \, d\Omega + \sum_{j=1}^{n} v_j \int_\Omega \left(B\frac{\partial\phi_j}{\partial x}\frac{\partial\phi_i}{\partial x} + A\frac{\partial\phi_j}{\partial y}\frac{\partial\phi_i}{\partial y} \right) \, d\Omega = \int_\Omega \phi_i \cdot f^2 \, d\Omega + \int_\Gamma \phi_i \boldsymbol{\sigma}^2 \cdot \mathbf{n} \, d\Gamma \tag{8.21}$$

with $i = 1, \ldots, n$, $A \equiv \frac{E}{1-\nu^2}$ and $B \equiv \frac{E}{2(1+\nu)}$.

The integrals can be estimated with Newton-Cotes. The body and surface force terms are trivial, and though the terms on the left hand side are not hard to evaluate, some calculation is done to simplify the implementation.

8.3.3 Numerical integral approximation (triangular elements)

Take as an example the term

$$\int_\Omega \left(A\frac{\partial\phi_j}{\partial x}\frac{\partial\phi_i}{\partial x} + B\frac{\partial\phi_j}{\partial y}\frac{\partial\phi_i}{\partial y} \right) \, d\Omega \tag{8.22}$$

With Newton-Cotes this integral can be estimated to:

$$\frac{\Delta}{6}\sum_{k=1}^{3} \left(A\frac{\partial\phi_j}{\partial x}\frac{\partial\phi_i}{\partial x} + B\frac{\partial\phi_j}{\partial y}\frac{\partial\phi_i}{\partial y} \right) = \frac{\Delta}{2} \left(A\frac{\partial\phi_j}{\partial x}\frac{\partial\phi_i}{\partial x} + B\frac{\partial\phi_j}{\partial y}\frac{\partial\phi_i}{\partial y} \right) \tag{8.23}$$

since the derivatives of the basis functions are constant on the element.

Using the matrix D defined in Section 5.4.1:

$$D = \frac{1}{\Delta}\begin{bmatrix} y_2 - y_3 & x_3 - x_2 \\ y_3 - y_1 & x_1 - x_3 \\ y_1 - y_2 & x_2 - x_1 \end{bmatrix} \approx \begin{bmatrix} \frac{\partial\phi_1}{\partial x} & \frac{\partial\phi_1}{\partial y} \\ \frac{\partial\phi_2}{\partial x} & \frac{\partial\phi_2}{\partial y} \\ \frac{\partial\phi_3}{\partial x} & \frac{\partial\phi_3}{\partial y} \end{bmatrix} \tag{8.24}$$

the element matrix can be written as:

$$S_{11}^{e_k} = D\begin{bmatrix} A & 0 \\ 0 & B \end{bmatrix} D^T \tag{8.25}$$

Similarly the element matrices from the other integrals can be put in this form:

$$\int_\Omega \left(\nu A\frac{\partial\phi_j}{\partial y}\frac{\partial\phi_i}{\partial x} + B\frac{\partial\phi_j}{\partial x}\frac{\partial\phi_i}{\partial y} \right) \, d\Omega \quad \Rightarrow \quad S_{12}^{e_k} = D\begin{bmatrix} 0 & B \\ \nu A & 0 \end{bmatrix} D^T \tag{8.26}$$

$$\int_\Omega \left(B\frac{\partial\phi_j}{\partial y}\frac{\partial\phi_i}{\partial x} + \nu A\frac{\partial\phi_j}{\partial x}\frac{\partial\phi_i}{\partial y} \right) \, d\Omega \quad \Rightarrow \quad S_{21}^{e_k} = D\begin{bmatrix} 0 & \nu A \\ B & 0 \end{bmatrix} D^T \tag{8.27}$$

$$\int_\Omega \left(B\frac{\partial\phi_j}{\partial x}\frac{\partial\phi_i}{\partial x} + A\frac{\partial\phi_j}{\partial y}\frac{\partial\phi_i}{\partial y} \right) \, d\Omega \quad \Rightarrow \quad S_{22}^{e_k} = D\begin{bmatrix} B & 0 \\ 0 & A \end{bmatrix} D^T \tag{8.28}$$

Putting this all together the combined element matrix becomes:

$$S^{e_k} = \begin{bmatrix} S_{11}^{e_k} & S_{12}^{e_k} \\ S_{21}^{e_k} & S_{22}^{e_k} \end{bmatrix} = \begin{bmatrix} D & 0 \\ 0 & D \end{bmatrix} \begin{bmatrix} A & 0 & 0 & B \\ 0 & B & \nu A & 0 \\ 0 & \nu A & B & 0 \\ B & 0 & 0 & A \end{bmatrix} \begin{bmatrix} D^T & 0 \\ 0 & D^T \end{bmatrix} \tag{8.29}$$

8.3.4 Numerical integral approximation (quadrilateral elements)

For quadrilateral elements it is a little bit harder, because the derivative is no longer constant over the whole element. Instead of D we can use $M(\xi)$ (Eq. (5.123)) and now Newton-Cotes forces us to add the function values in all the four nodes:

$$S^{e_k} = \sum_{k=1}^{4} \begin{bmatrix} M(\xi_k) & 0 \\ 0 & M(\xi_k) \end{bmatrix} \begin{bmatrix} A & 0 & 0 & B \\ 0 & B & \nu A & 0 \\ 0 & \nu A & B & 0 \\ B & 0 & 0 & A \end{bmatrix} \begin{bmatrix} M^T(\xi_k) & 0 \\ 0 & M^T(\xi_k) \end{bmatrix} \tag{8.30}$$

8.4 Results

The simulation of the elasticity equation was done with both triangular as quadrilateral elements. For the results of the triangular elements see Figure 8.3 and for the quadrilateral elements see Figure 8.4. Both methods give the same solution, which is of course the proposed solution $u = v = xy$.

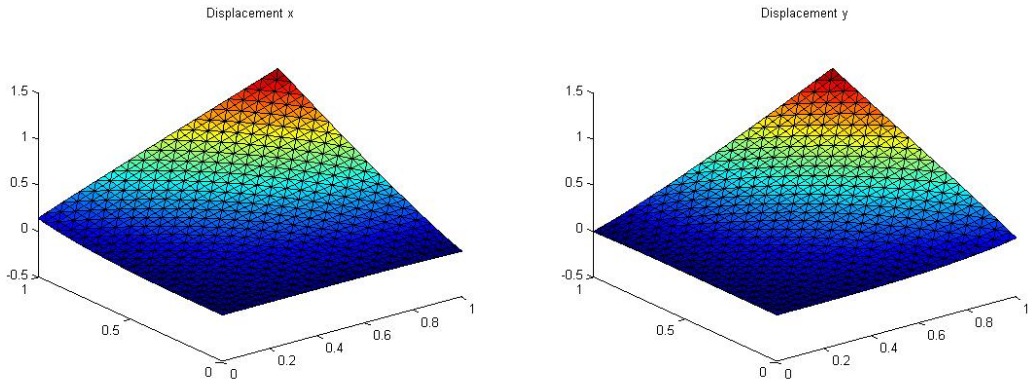

Figure 8.3: Simulation of the elasticity equation with FEM triangular elements. Both results are in agreement with the proposed solution $u = v = xy$

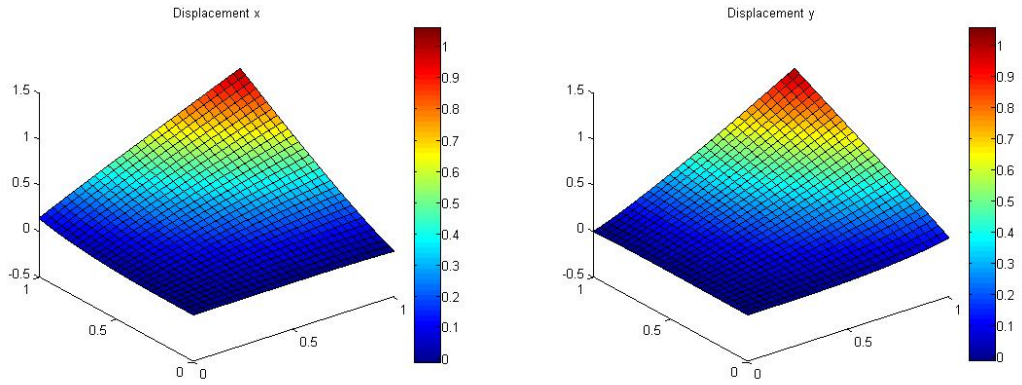

Figure 8.4: Simulation of the elasticity equation with FEM quadrilateral elements. Both results are in agreement with the proposed solution $u = v = xy$

Chapter 9

Mathematical model

We will once more use a continuum approach and extend the biological model with mechanical characteristics. The theory of elasticity will be combined with the partial differential equations presented earlier in this report and this combined model will be solved by numerical methods.

9.1 Assumptions and simplifications

The model presented is an extension of the [Moreo, 2008] model (presented in Chapter 3) proposed by [Prokharau et al., 2010]. This extension also takes mechanical stimuli into account due to internal and external forces applied to the domain. The assumption in the [Moreo, 2008] model of optimal mechanical stress is removed, though new assumptions about these mechanical stresses have to be made.

In addition to the two remaining assumptions from Section 3.1, the following assumptions and simplifications have been made in the extended model. The first four are as proposed by [Prokharau et al., 2010], the last two only apply to the model used in this report.

- The mechanical stimulus will only be determined by shear. Compression is assumed to be negligible and since cartilage is formed in regions under compression only, the production of cartilage will also be neglected.
- Formation of bone will only take place under moderate mechanical stimulus. Formation of fibroblasts only takes place under high mechanical stimulus.
- Woven bone will only be produced at low to moderate mechanical stimulus, bone remodelling (production of lamellar bone) only takes place at low mechanical stimulus and fibrous tissue is only generated at high mechanical stimulus.
- Differentiation of fibroblasts to osteoblasts is negligible.
- Fluid flow for elasticity (*poro-elasticity*) is neglected.
- Time scales are large enough to assume the mechanical state is always in equilibrium.

9.2 Variables

In addition to the variables presented in Section 3.2, we now also have fibroblasts density f in $10^6 \frac{cells}{ml}$ and fibrous tissue volume fraction v_t. For the mechanical state the variables u and v for respectively displacement in x and y direction are added, from which the stresses and strains can be calculated.

9.3 Computational domain

The computational domain is the same as in the [Moreo, 2008] model.

9.4 Partial differential equations

The changes made to the PDEs consist of the elasticity equation and a set of multiplication factors that depend on the mechanical stimulus.

9.4.1 Elasticity

Equilibrium state is assumed and gravity is neglected:

$$\nabla \cdot \boldsymbol{\sigma} = 0 \tag{9.1}$$

The values for Young's modulus and Poisson's ratio now vary over the domain, since different types of tissues are fabricated over time and space. Within an element these properties are assumed to be constant and the *rule of mixtures* is used to calculate them:

$$E(e_k, t) = E_f v_f(\bar{\mathbf{x}}, t) + E_w v_w(\bar{\mathbf{x}}, t) + E_l v_l(\bar{\mathbf{x}}, t) + E_t v_t(\bar{\mathbf{x}}, t) \tag{9.2}$$

$$\nu(e_k, t) = \nu_1(v_f(\bar{\mathbf{x}}, t) + v_t(\bar{\mathbf{x}}, t)) + \nu_2(v_w(\bar{\mathbf{x}}, t) + v_l(\bar{\mathbf{x}}, t)) \tag{9.3}$$

where $\bar{x}$ is the center of the element e_k. E_f is Young's modulus of fibrin network, E_w for woven bone, E_l for lamellar bone and E_t for fibrous tissue; ν_1 is Poisson's ratio for fibrin network and fibrous tissue and ν_2 for woven and lamellar bone.

9.4.2 Mechanical stimulus

The mechanical stimulus ψ is given by the maximum shear strain:

$$\psi = \frac{1}{2}(\epsilon_1 - \epsilon_2) \tag{9.4}$$

with ϵ_1 and ϵ_2 the eigenvalues of the strain tensor.

The mechanical stimulus is divided into three regions:

- $0 \leq \psi < \psi_1$: Low mechanical stimulus,
- $\psi_1 \leq \psi < \psi_2$: Moderate mechanical stimulus,
- $\psi \geq \psi_2$: High mechanical stimulus.

There is also an upper boundary $\hat{\psi} \in (\psi_1, \psi_2)$ for woven bone generation inside the moderate mechanical stimulus region.

9.4.3 Platelets, $c(\mathbf{x}, t)$

The platelet density is left unchanged:

$$\frac{\partial c}{\partial t} = \nabla \cdot [\ \underbrace{D_c \nabla c}_{\text{Diffusion}}\ - \underbrace{H_c\ c \nabla p}_{\text{Taxis}}\ ] - \underbrace{A_c c}_{\text{Death}} \tag{9.5}$$

9.4.4 Osteogenic cells, $m(\mathbf{x}, t)$

Mechanical stimulation influences the proliferation and differentiation of the osteogenic cells. To model these influences three multiplication factors are introduced: $g_m(\psi)$, $g_{mb}(\psi)$ and $g_{fib}(\psi)$, respectively for the proliferation, differentiation to osteoblasts and differentiation to fibroblasts.

$$\begin{aligned}\frac{\partial m}{\partial t} =& \nabla \cdot [\ \underbrace{D_m \nabla m}_{\text{Diffusion}} - \underbrace{m(B_{m1}\nabla s_1 + B_{m2}\nabla s_2)}_{\text{Chemotaxis}}\ ] \\ &+ \underbrace{g_m(\psi)\left(\alpha_{m0} + \frac{\alpha_m s_1}{\beta_m + s_1} + \frac{\alpha_m s_2}{\beta_m + s_2}\right) m(1-m)}_{\text{Proliferation}} - \underbrace{g_{mb}(\psi)\left(\alpha_{p0} + \frac{\alpha_{mb} s_1}{\beta_{mb} + s_1}\right) m}_{\text{Differentiation Osteoblasts}} \\ &- \underbrace{g_{fib}(psi)\alpha_{mf} m}_{\text{Differentiation Fib.}} - \underbrace{A_m m}_{\text{Death}}\end{aligned}$$

The multiplication factors are defined as:

$$g_m(\psi) = \frac{\psi^2 + g_{m0}\tau_m^2}{\psi^2 + \tau_m^2} \tag{9.6}$$

which increases monotonically with increasing ψ.

$$g_{mb}(\psi) = \begin{cases} g_{mb0}, & 0 \le \psi \le \psi_1 \\ 16\dfrac{(\psi-\psi_1)^2(\psi-\psi_2)^2}{(\psi_2-\psi_1)^4}(1-g_{mb0}) + g_{mb0}, & \psi_1 \le \psi < \frac{\psi_1+\psi_2}{2} \\ 16\dfrac{(\psi-\psi_1)^2(\psi-\psi_2)^2}{(\psi_2-\psi_1)^4}, & \frac{\psi_1+\psi_2}{2} \le \psi < \psi_2 \\ 0, & \psi \ge \psi_2 \end{cases} \tag{9.7}$$

which has a peak in the moderate mechanical stimulus region, where differentiation to osteoblasts will be enhanced.

$$g_{fib}(\psi) = \begin{cases} 0, & \psi < \psi_2 \\ \frac{(\psi-\psi_2)^2}{(\psi-\psi_2)^2+\tau_{fib}^2}, & \psi \ge \psi_2 \end{cases} \tag{9.8}$$

which is only non-zero in the high mechanical stimulus region, where differentiation to fibroblasts takes place. The function increases monotonically with the mechanical stimulus in this region.

9.4.5 Osteoblasts, $b(\mathbf{x}, t)$

The multiplication factor for differentiation to osteoblasts also makes an appearance in this equation:

$$\frac{\partial b}{\partial t} = \underbrace{g_{mb}(\psi)\frac{\alpha_{mb} s_1}{\beta_{mb} + s_1} m}_{\text{Differentiation}} - \underbrace{A_b b}_{\text{Death}} \tag{9.9}$$

9.4.6 Fibroblasts, $f(\mathbf{x}, t)$

Fibroblasts migrate, proliferate and die, giving the following terms in the PDE:

$$\frac{\partial f}{\partial t} = \nabla \cdot [\ \underbrace{D_f \nabla f}_{\text{Diffusion}}\ ] + \underbrace{g_{fib}(\psi)\alpha_{mf} m}_{\text{Differentiation}} + \underbrace{\alpha_f f(1-f)}_{\text{Division}} - \underbrace{A_f f}_{\text{Death}} \tag{9.10}$$

9.4.7 Growth factors 1, $s_1(\mathbf{x}, t)$

Secretion of growth factors 1 is also enhanced by mechanical stimulus, with the multiplication factor $g_{s1,c}(\psi)$:

$$\frac{\partial s_1}{\partial t} = \nabla \cdot [\ \underbrace{D_{s1} \nabla s_1}_{\text{Diffusion}}\ ] + \underbrace{g_{s1,c}(\psi) \left(\frac{\alpha_{c1} s_1}{\beta_{c1} + s_1} + \frac{\alpha_{c2} s_2}{\beta_{c2} + s_2} \right) c}_{\text{Secretion}} - \underbrace{A_{s1} s_1}_{\text{Decay}} \tag{9.11}$$

This multiplication factor is defined as:

$$g_{s1,c}(\psi) = \frac{\psi^2 + g_{s1,c0} \tau_{s1,c}^2}{\psi^2 + \tau_{s1,c}^2} \tag{9.12}$$

which increases monotonically with increasing ψ, similar to the proliferation multiplication factor of the osteogenic cell density.

9.4.8 Growth factors 2, $s_2(\mathbf{x}, t)$

Like growth factors 1, the secretion of growth factors 2 is also enhanced by mechanical stimulus by multiplication factors $g_{s2,b}(\psi)$ and $g_{s2,m}(\psi)$:

$$\frac{\partial s_2}{\partial t} = \nabla \cdot [\ \underbrace{D_{s2} \nabla s_2}_{\text{Diffusion}}\ ] + \underbrace{g_{s2,b}(\psi) \frac{\alpha_{m2} s_2}{\beta_{m2} + s_2} m + g_{s2,m}(\psi) \frac{\alpha_{b2} s_2}{\beta_{b2} + s_2} b}_{\text{Secretion}} - \underbrace{A_{s2} s_2}_{\text{Decay}} \tag{9.13}$$

Both multiplication factors follow the same pattern as the multiplication factor for secretion of growth factors 1:

$$g_{s2,b}(\psi) = \frac{\psi^2 + g_{s2,b0} \tau_{s2,b}^2}{\psi^2 + \tau_{s2,b}^2} \tag{9.14}$$

$$g_{s2,m}(\psi) = \frac{\psi^2 + g_{s2,m0} \tau_{s2,m}^2}{\psi^2 + \tau_{s2,m}^2} \tag{9.15}$$

9.4.9 Fibrin network volume fraction, $v_f(\mathbf{x}, t)$

A multiplication factor $g_w(\psi)$ is introduced for the production of woven bone and a term including another multiplication factor $g_{ft}(\psi)$ is added to model the production of fibrous tissue.

$$\frac{\partial v_f}{\partial t} = \underbrace{- g_w(\psi) \frac{\alpha_w s_2}{\beta_w + s_2} b v_f (1 - v_w)}_{\text{Woven bone production}} \underbrace{- g_{ft}(\psi) \alpha_{ft} f (1 - v_t) v_f}_{\text{Fibrous tissue production}} \tag{9.16}$$

The multiplication factors are given by:

$$g_{fib}(\psi) = \begin{cases} \frac{1}{2} \left(1 + \cos \left(\frac{\pi \psi}{\hat{\psi}} \right) \right), & \psi \leq \hat{\psi} \\ 0, & \psi \geq \hat{\psi} \end{cases} \tag{9.17}$$

which decreases monotonically with the mechanical stimulus all the way down to zero at $\hat{\psi}$.

$$g_{ft}(\psi) = \begin{cases} 0, & \psi < \psi_2 \\ \frac{(\psi - \psi_2)^2}{(\psi - \psi_2)^2 + \tau_{ft}^2}, & \psi \geq \psi_2 \end{cases} \tag{9.18}$$

which increases monotonically with the mechanical stimulus above ψ_2, similar to the multiplication factor for differentiation of osteogenic cells to fibroblasts.

9.4.10 Woven bone volume fraction, $v_w(\mathbf{x}, t)$

The multiplication factor for production of woven bone $g_w(\psi)$ also appears in this equation, together with a multiplication factor for the bone remodelling process $g_\gamma(\psi)$:

$$\frac{\partial v_w}{\partial t} = \underbrace{g_w(\psi)\frac{\alpha_w s_2}{\beta_w + s_2} b v_f (1 - v_w)}_{\text{Production}} - \underbrace{g_\gamma(\psi)\gamma v_w(1 - v_l)}_{\text{Bone remodelling}} \tag{9.19}$$

The bone remodelling multiplication factor is similar to the production of woven bone multiplication factor, only in this case the upper boundary is already reached at ψ_1 instead of $\hat{\psi}$:

$$g_\gamma(\psi) = \begin{cases} \frac{1}{2}\left(1 + \cos\left(\frac{\pi\psi}{\psi_1}\right)\right), & \psi \leq \psi_1 \\ 0, & \psi \geq \psi_1 \end{cases} \tag{9.20}$$

which decreases monotonically with the mechanical stimulus all the way down to zero at $\hat{\psi}$.

9.4.11 Lamellar bone volume fraction, $v_l(\mathbf{x}, t)$

The bone remodelling multiplication factor of course also has to be incorporated in this equation:

$$\frac{\partial v_t}{\partial t} = \underbrace{g_\gamma(\psi)\gamma v_w(1 - v_l)}_{\text{Bone remodelling}} \tag{9.21}$$

9.4.12 Fibrous tissue volume fraction, $v_t(\mathbf{x}, t)$

Finally the production of fibrous tissue by fibroblasts is added:

$$\frac{\partial v_l}{\partial t} = \underbrace{g_{ft}(\psi)\alpha_{ft} f v_f (1 - v_t)}_{\text{Production}} \tag{9.22}$$

9.5 Initial and boundary conditions

The initial and boundary conditions of the variables from the [Moreo, 2008] model remain unchanged, for the fibroblast density a zero flux boundary condition is added:

$$D_f \nabla f(\mathbf{x}, t) \cdot \mathbf{n} = 0, \quad \mathbf{x} \in \Gamma,\ t \in (0, \infty). \tag{9.23}$$

As initial conditions, the fibroblast density is taken the same as the osteoblast density and no fibrous tissue is present at the start:

$$f(\mathbf{x}, 0) = 0.001, \tag{9.24}$$

$$v_t(\mathbf{x}, 0) = 0. \tag{9.25}$$

The external force models static pressure that arise when the teeth are on top of each other (jaw is closed) but without chewing or any other extra activity that clenches the teeth together. On top of this static pressure there is for a limited time per day an extra pressure due to chewing or other extra activities that require clenching of the teeth. This extra pressure follows a sinusoidal function in time everyday from 0 until 0.2 of each day, after this the extra pressure is removed for the rest of the day.

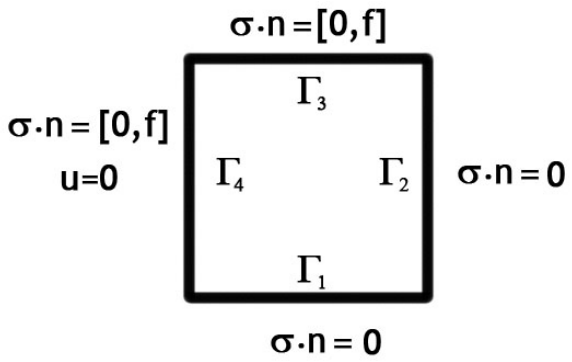

Figure 9.1: Elasticity boundary conditions

See Figure 9.1 for the boundaries and their boundary conditions: For simplicity we assume that there is only a normal external force on the top boundary Γ_3 and a shear stress is placed on the left boundary Γ_4 to fulfill conservation of (linear) momentum on the whole domain and can be seen to model the small relative movement of the implant with respect to the host bone. The other two boundaries are left free since, as they are part of the implant, they move together with the top boundary. Note that conservation of angular momentum is actually violated with these external forces. There is also a no displacement condition in x-direction at the left boundary Γ_4:

$$\boldsymbol{\sigma} \cdot \mathbf{n}|_{\Gamma_1} = 0 \tag{9.26}$$
$$\boldsymbol{\sigma} \cdot \mathbf{n}|_{\Gamma_2} = 0 \tag{9.27}$$
$$\boldsymbol{\sigma} \cdot \mathbf{n}|_{\Gamma_3} = [F(t), 0]^T \tag{9.28}$$
$$\boldsymbol{\sigma} \cdot \mathbf{n}|_{\Gamma_4} = [F(t) \cdot \frac{x_{Max}}{y_{Max}}, 0]^T \tag{9.29}$$
$$u(\mathbf{x})|_{\Gamma_4} = 0 \tag{9.30}$$

9.6 Parameters

The values of the parameters from the [Moreo, 2008] model remain unchanged. Values for Young's modulus and Poisson ratios were taken from [Andrekiv, 2006]. Boundaries for mechanical stimulus regions (ψ_1 and ψ_2) were taken from [Huisket et al., 1997]. The values of the other new parameters are determined by an educated guess, verification by comparison with experimental data still has to be done.

$E_{fn} = 0.188e6\ Pa$	$E_{ft} = 2e6\ Pa$	$E_w = 1e9\ Pa$
$E_l = 6e9\ Pa$	$\nu_1 = 0.167$	$\nu_2 = 0.325$
$\psi_1 = 0.0375$	$\psi_2 = 0.1125$	$\hat{\psi} = 0.09375$
$D_f = 0.1\ \frac{mm^2}{day}$	$\alpha_f = 0.15\ \frac{1}{day}$	$\alpha_{mf} = 0.25\ \frac{1}{day}$
$\alpha_{ft} = 0.05$		
$\tau_m = 0.1$	$g_{m0} = 0.2$	$g_{mb0} = 0.1$
$\tau_{fib} = 0.1$	$g_{s1,c0} = 0.2$	$\tau_{s1,c} = 0.1$
$g_{s2,b0} = 0.2$	$\tau_{s2,b} = 0.1$	$g_{s2,m0} = 0.2$
$\tau_{s2,m} = 0.1$	$\tau_{ft} = 0.1$	

The low external pressure is estimated at $5kPa$ and the pressure under chewing is estimated at $0.5MPa$, the last value is an educated guess based on several articles found about biting forces of a human.

Chapter 10

Simulations using FEM

10.1 Discretization

We will use triangular elements for the spatial discretization. The discretization of the biological equations will not differ from the approach used in the model without mechanical stimuli (see Section 5.3). The discretization of the elasticity equations will be done exactly the same as in the previous chapter (see Section 8.3.2). For the two new equations in the biological PDE system, we will derive a weak formulation and the system of equations will be derived.

Fibroblasts

Weak formulation:

$$\int_\Omega \eta \frac{\partial f}{\partial t}\ d\Omega = \int_\Omega \nabla\eta \cdot (D_f \nabla f)\ d\Omega + \int_\Omega \eta g_{fib}(\psi)\alpha_{mf} m\ d\Omega + \int_\Omega \eta \alpha_f f(1-f)\ d\Omega - \int_\Omega \eta A_f f\ d\Omega \tag{10.1}$$

System of equations ($i = 1, \ldots, n$):

$$\begin{aligned}\frac{d}{dt}\sum_{j=1}^{n} f_j \int_\Omega \phi_i\phi_j\ d\Omega = D_f \sum_{j=1}^{n} f_j \int_\Omega \nabla\phi_i \cdot \nabla\phi_j\ d\Omega + \int_\Omega \phi_i g_{fib}(\psi)\alpha_{mf} m\ d\Omega \\ + \sum_{j=1}^{n} f_j \int_\Omega \phi_i\phi_j \alpha_f(1-f)\ d\Omega - A_f \sum_{j=1}^{n} f_j \int_\Omega \phi_i\phi_j\ d\Omega\end{aligned} \tag{10.2}$$

Fibrous tissue

Weak formulation:

$$\int_\Omega \eta \frac{\partial v_t}{\partial t}\ d\Omega = \int_\Omega \eta g_{ft}(\psi)\alpha_{ft} f v_f (1-v_t)\ d\Omega \tag{10.3}$$

System of equations ($i = 1, \ldots, n$):

$$\frac{d}{dt}\sum_{j=1}^{n} v_{t_j} \int_\Omega \phi_i\phi_j\ d\Omega = \int_\Omega \phi_i \gamma g_{ft}(\psi)\alpha_{ft} f v_f\ d\Omega - \sum_{j=1}^{n} v_{t_j} \int_\Omega \phi_i\phi_j g_{ft}(\psi)\alpha_{ft} f v_f\ d\Omega \tag{10.4}$$

10.2 Time integration

For the biological equations the same IMEX method will be used as for the FEM in the model without mechanical stimuli (taking all non linear terms on the current time step). Before each

time step of the biological equations, the current mechanical state is calculated using the function values of the last time step. Next, the multiplication factors are calculated and after that the biological equations are evaluated (see Figure 10.1).

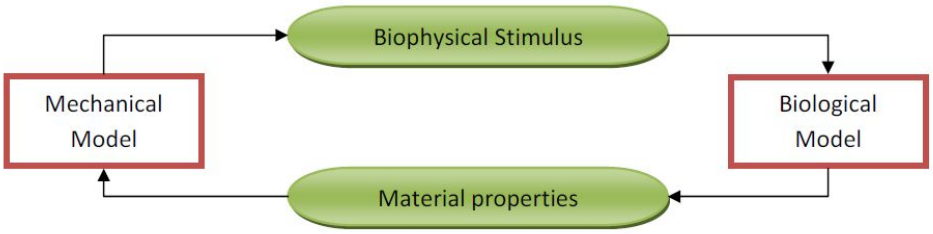

Figure 10.1: Implementation scheme model with mechanical stimuli

10.3 Results

10.3.1 FEM 2D simulation triangular elements (2 months)

The biological model extended with the elasticity equations was simulated using the FEM with triangular elements in 2D. The results are shown in Figure 10.2 to 10.11. Surprisingly enough the instabilities that arose without the mechanical stimuli have now dissappeared. The bone volume fractions are now also a lot lower than they were before, but this might have more to do with calibration of the parameters than an actual error. The maximum shear strain over the area doesn't change much more after 15 days and doesn't really seem to affect the other concentrations (since you would expect some form of asymmetry).

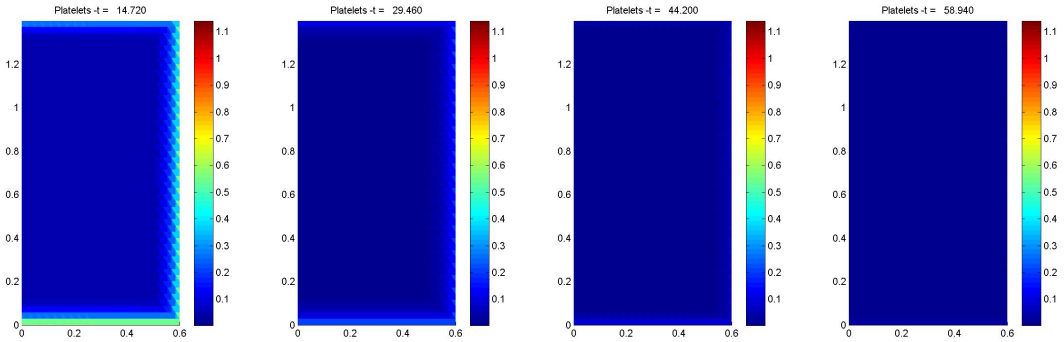

Figure 10.2: Platelet density at 4 different times ($15, 30, 45$ and 60 days). $nx = 40$, $ny = 50$, $dt = 0.02$ and $T_{max} = 60$. Initially there is a high density at the implant surfaces thanks to the higher proteïn concentration, after about 40 days the density has dropped to zero because there is no production.

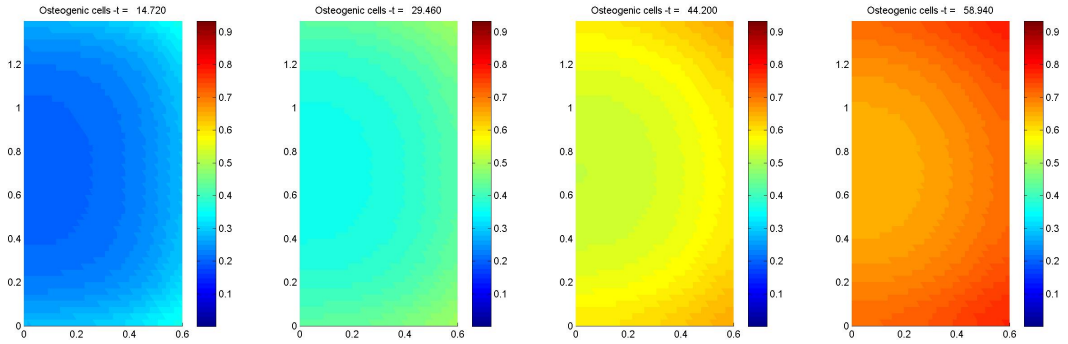

Figure 10.3: Osteogenic cell density at 4 different times (15, 30, 45 and 60 days). $nx = 40$, $ny = 50$, $dt = 0.02$ and $T_{max} = 60$. The osteogenic cell density is at its highest close to the implant surface and the spatial density rise goes with almost concentric circles. As time passes the density gets higher everywhere at about the same rate.

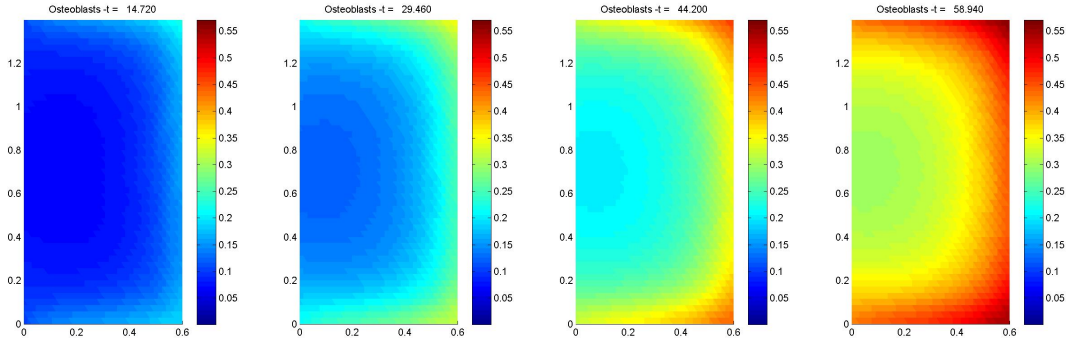

Figure 10.4: Osteoblast cell density at 4 different times (15, 30, 45 and 60 days). $nx = 40$, $ny = 50$, $dt = 0.02$ and $T_{max} = 60$. Osteoblasts first appear close to the implant surface and gradually the other areas in the direction of the bone surface are also filled with osteoblasts. The difference between the concentrations at the bone surface and the implant surface stay about the same after 30 days.

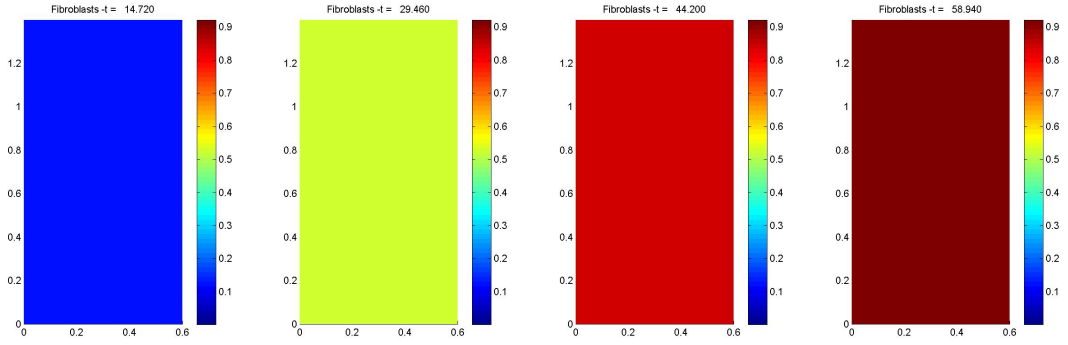

Figure 10.5: Fibroblast cell density at 4 different times (15, 30, 45 and 60 days). $nx = 40$, $ny = 50$, $dt = 0.02$ and $T_{max} = 60$. The fibroblast density is constant over the whole domain and increases with time.

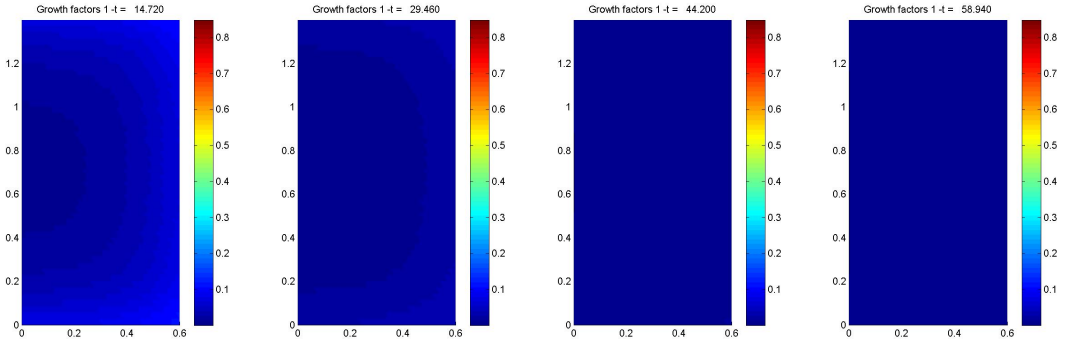

Figure 10.6: Growth factor 1 density at 4 different times (15, 30, 45 and 60 days). $nx = 40$, $ny = 50$, $dt = 0.02$ and $T_{max} = 60$. The growth factor increases in almost concentric circles towards the implant surface. After the initial production, the density slowly drops to zero while keeping the concentric circle pattern.

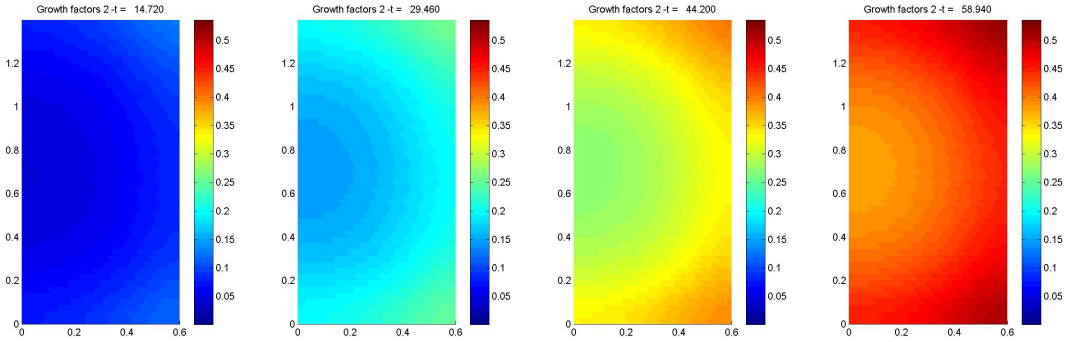

Figure 10.7: Growth factor 2 density at 4 different times (15, 30, 45 and 60 days). $nx = 40$, $ny = 50$, $dt = 0.02$ and $T_{max} = 60$. Like the growth factors 1, growth factors 2 now also form concentric circles with higher concentrations towards the implant surface. Here the concentrations rise with time however, but the difference between the concentration at the bone and implant surface also don't change much here after 30 days.

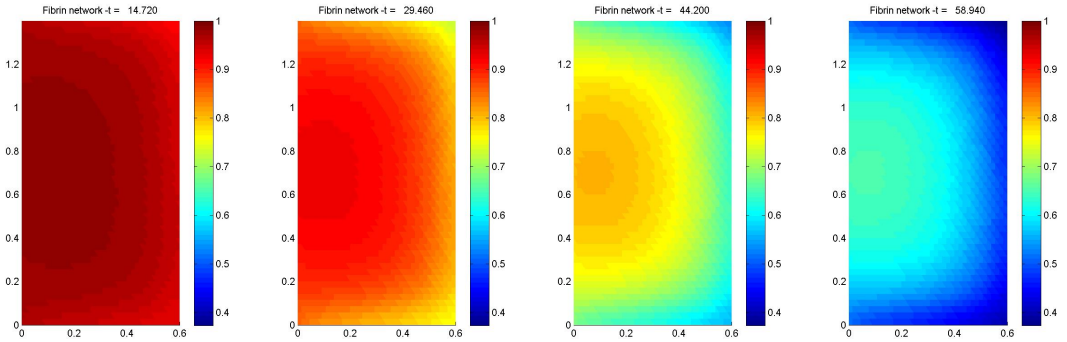

Figure 10.8: Fibrin network volume fraction at 4 different times (15, 30, 45 and 60 days). $nx = 40$, $ny = 50$, $dt = 0.02$ and $T_{max} = 60$. The fibrin network drops the quickest at the implant surface and now almost doesn't seem to drop from the side of the bone surface, this process continues and differences between volume fractions at the implant surface and bone surface stay approximately constant as time passes by.

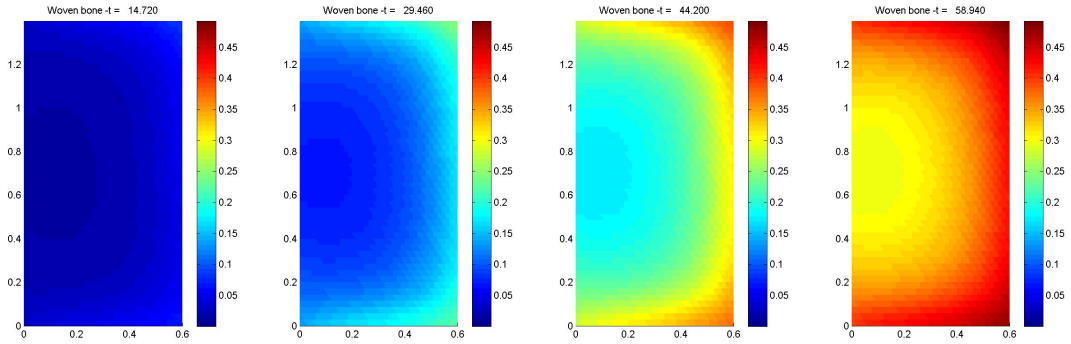

Figure 10.9: Woven bone volume fraction at 4 different times (15, 30, 45 and 60 days). $nx = 40$, $ny = 50$, $dt = 0.02$ and $T_{max} = 60$. Woven bone follows the exact opposite track of the fibrin network. The most bone tissue is created at the implant surface and almost not bone is generated at the side of the host bone. The generation of bone tissue therefore seems to go from implant surface to host bone.

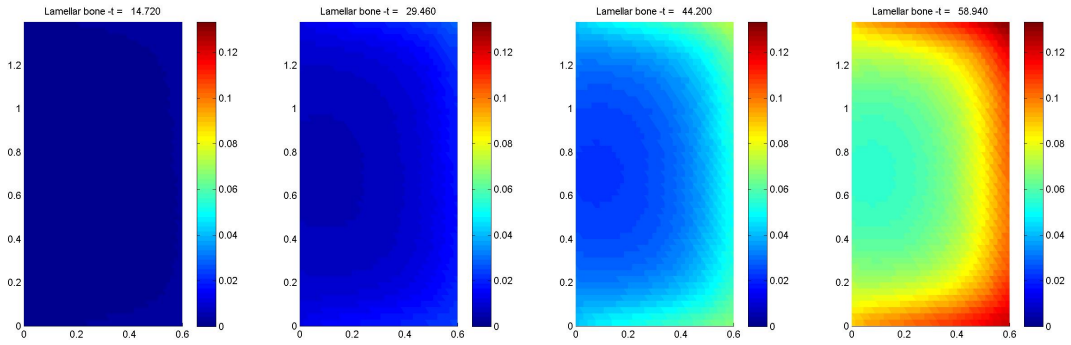

Figure 10.10: Lamellar bone volume fraction at 4 different times (15, 30, 45 and 60 days). $nx = 40$, $ny = 50$, $dt = 0.02$ and $T_{max} = 60$. Lamellar bone follows the same track as woven bone, only the volume fractions are about a factor 3 lower.

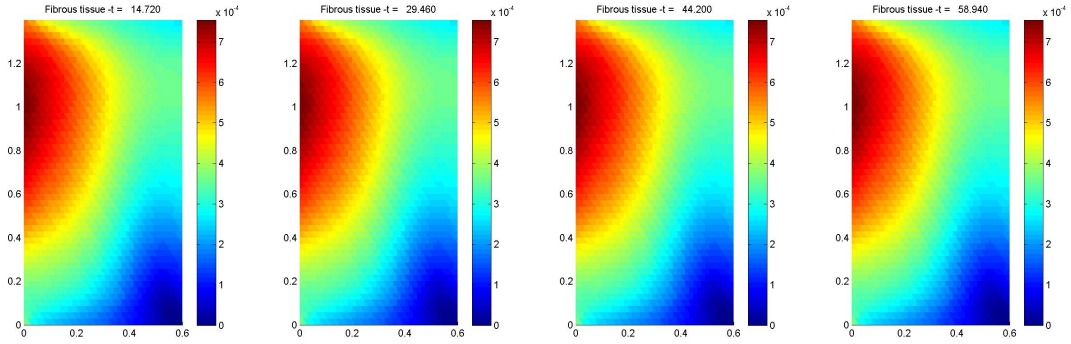

Figure 10.11: Fibrous tissue volume fraction at 4 different times (15, 30, 45 and 60 days). $nx = 40$, $ny = 50$, $dt = 0.02$ and $T_{max} = 60$. Fibrous tissue is formed mostly in the northwest corner of the domain, after 15 days nothing much changes in this volume fraction.

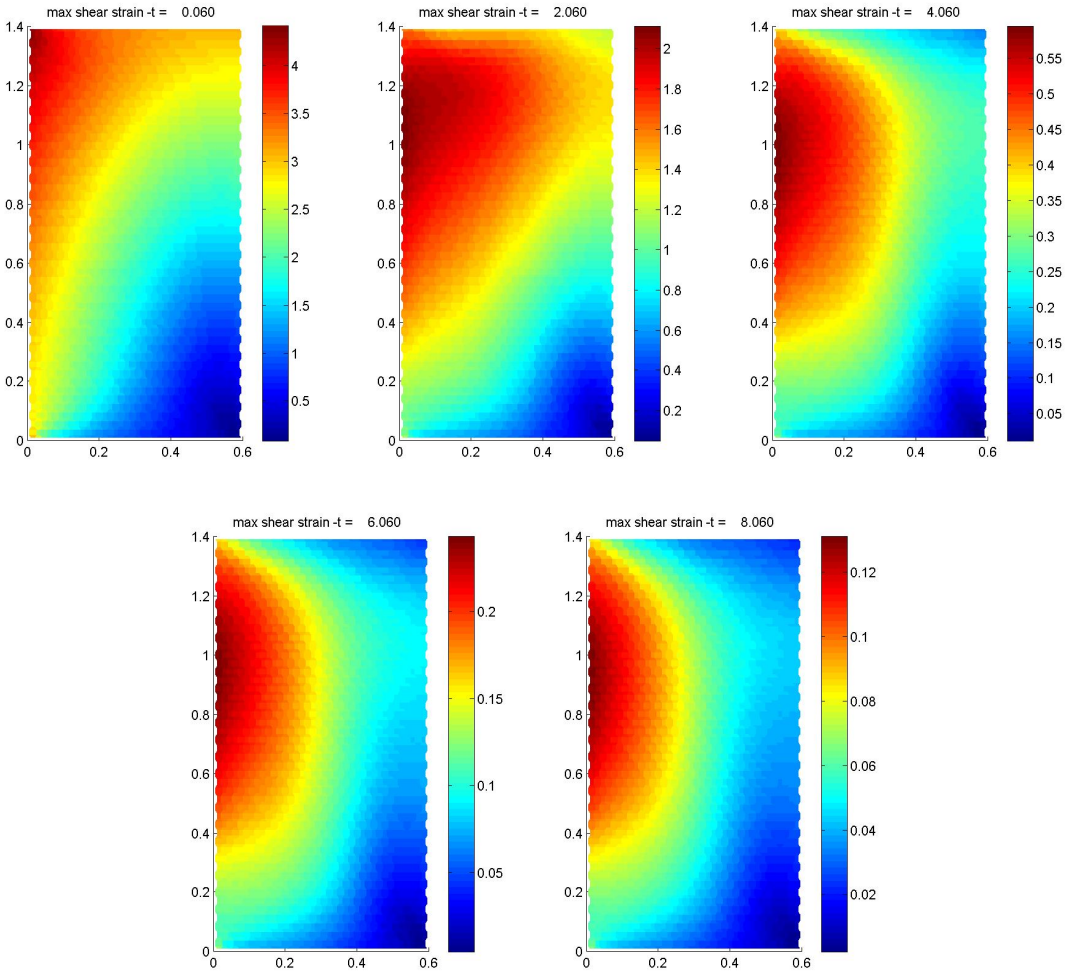

Figure 10.12: Maximum shear strain at 5 different times (0.1, 2.1, 4.1, 6.1 and 8.1 days) a time of the day when extra load caused by chewing is applied. $nx = 40$, $ny = 50$, $dt = 0.02$ and $T_{max} = 60$. At the start the strain is highest in the north west corner and gradually decreases diagonally to the south east corner. As time goes by the highest strain forms in a certain spot just below the north west corner, from which it decreases in a concentric like form. Note that the last few figures look like the fibrous tissue volume fraction, which is logical because fibrous tissue can only be generated at high strains. Note that already after 6 days the strain doesn't reach above ψ_1 anywhere in the domain.

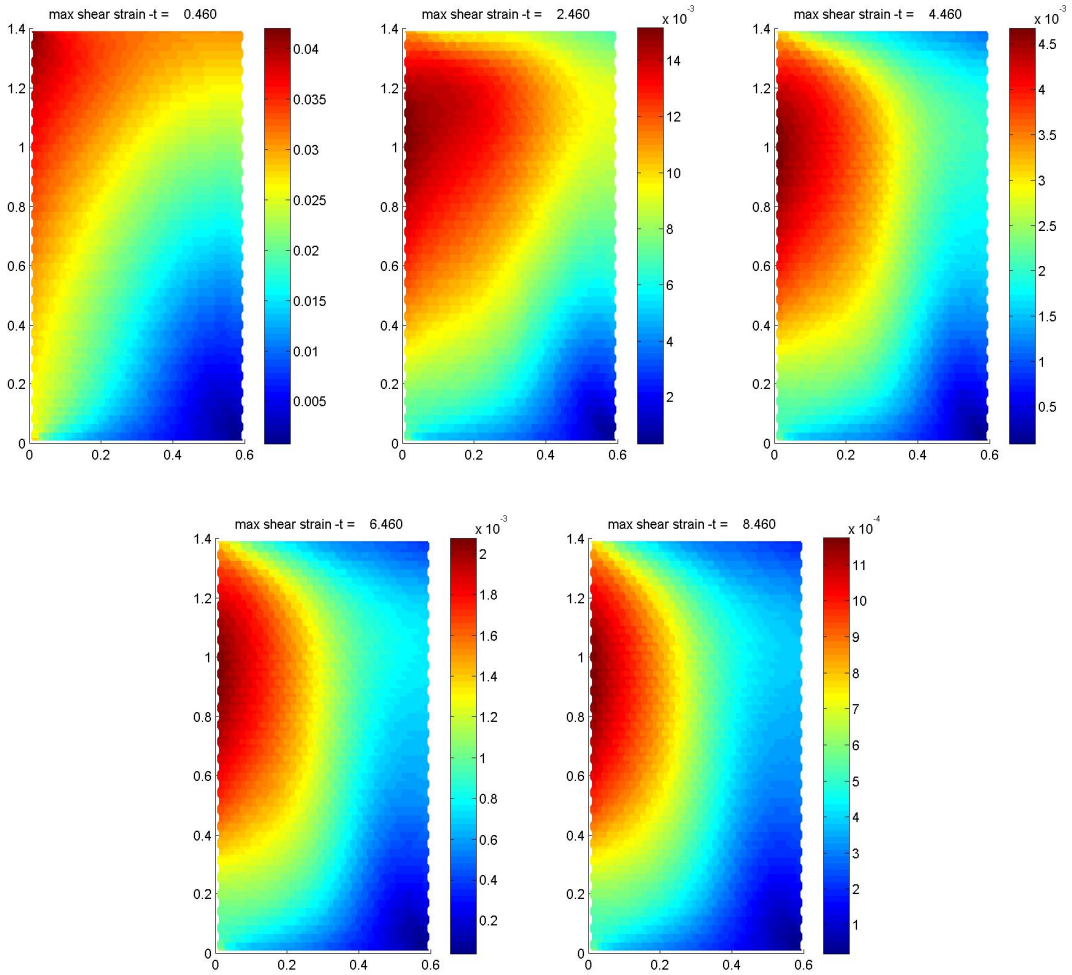

Figure 10.13: Maximum shear strain at 5 different times (0.3, 2.3, 4.3, 6.3 and 8.3 days) a time of the day when there is only the normal load. $nx = 40$, $ny = 50$, $dt = 0.02$ and $T_{max} = 60$. It follows the same pattern as the strains under extra load, but then about a factor 10 smaller. Note that here already after 2 days the strain doesn't reach above ψ_1 anywhere in the domain.

Chapter 11

Discussion

For reasons not yet known the model with mechanical stimuli doesn't experience the same instabilities as the biological model without mechanical stimuli. The bone fractions are however a lot lower than previously, but this is more a matter of changing the parameters than a fault in the model. The main problem is that the strains don't seem to have a lot of influence, since after 6 days the lower boundary for moderate strain ψ_1 is never reached again. Higher extra loads have been tried, but don't make a significant difference. It could be tried to raise the load under normal conditions, but this would be even more unrealistic than what is chosen now.

The assumption that there is no fluid flow is also debatable, [Khoe, 2009] proved that for a different model for bone ingrowth presented in [Andrekiv, 2006] neglection of fluid flow leads to large errors in the final result. How this affects the current model is not known, but it is certainly probable that the same behaviour will arise.

The boundary conditions that were taken now are somewhat arbitrary, so there could also be problems there. A better approach would be to also model the host bone and the implant materials as elements or maybe even calculate on the whole prothesis, with the cavities as special elements in which the model from this report can be used.

Chapter 12

Conclusion

The model with mechanical stimuli is numerically stable in contrast to the pure biological model. However the effect of strains doesn't seem to affect any of the other variables, other than the production of fibrous tissue which is negligible now anyway. Different loading conditions might be a solution to this problem. The best approach would be to consider the dental implant as a whole (see Figure **??**) and also discretize the bone and the implant and apply loads to certain points in the system to model the movement of the jaw as accurately as possible, where the domains presented in this report could serve as extra detailed elements.

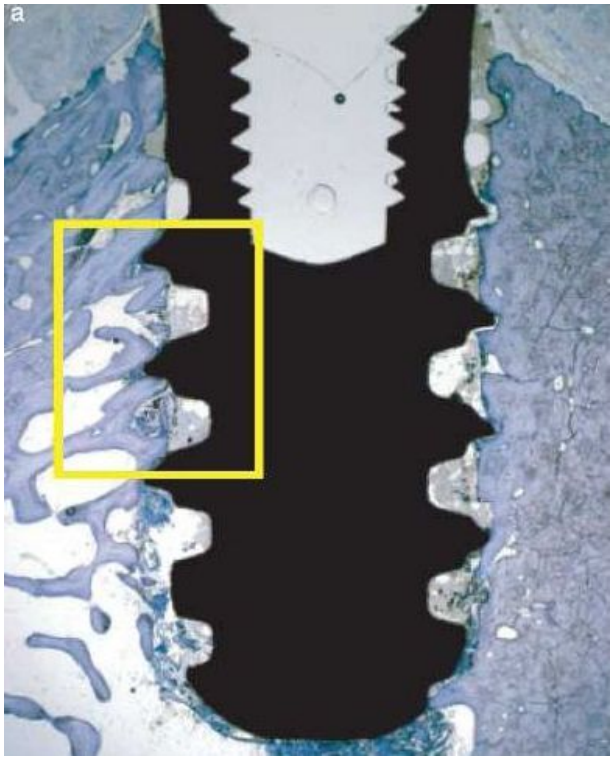

Figure 12.1: Use the whole dental implant as computational domain.

Appendix A

Flow chart of the biological processes

To get a good overview of all the biological processes that play a role in bone-implant healing the following flow chart is produced to easily see the relationships between different cell types, tissues, growth factors and mechanical stimuli.

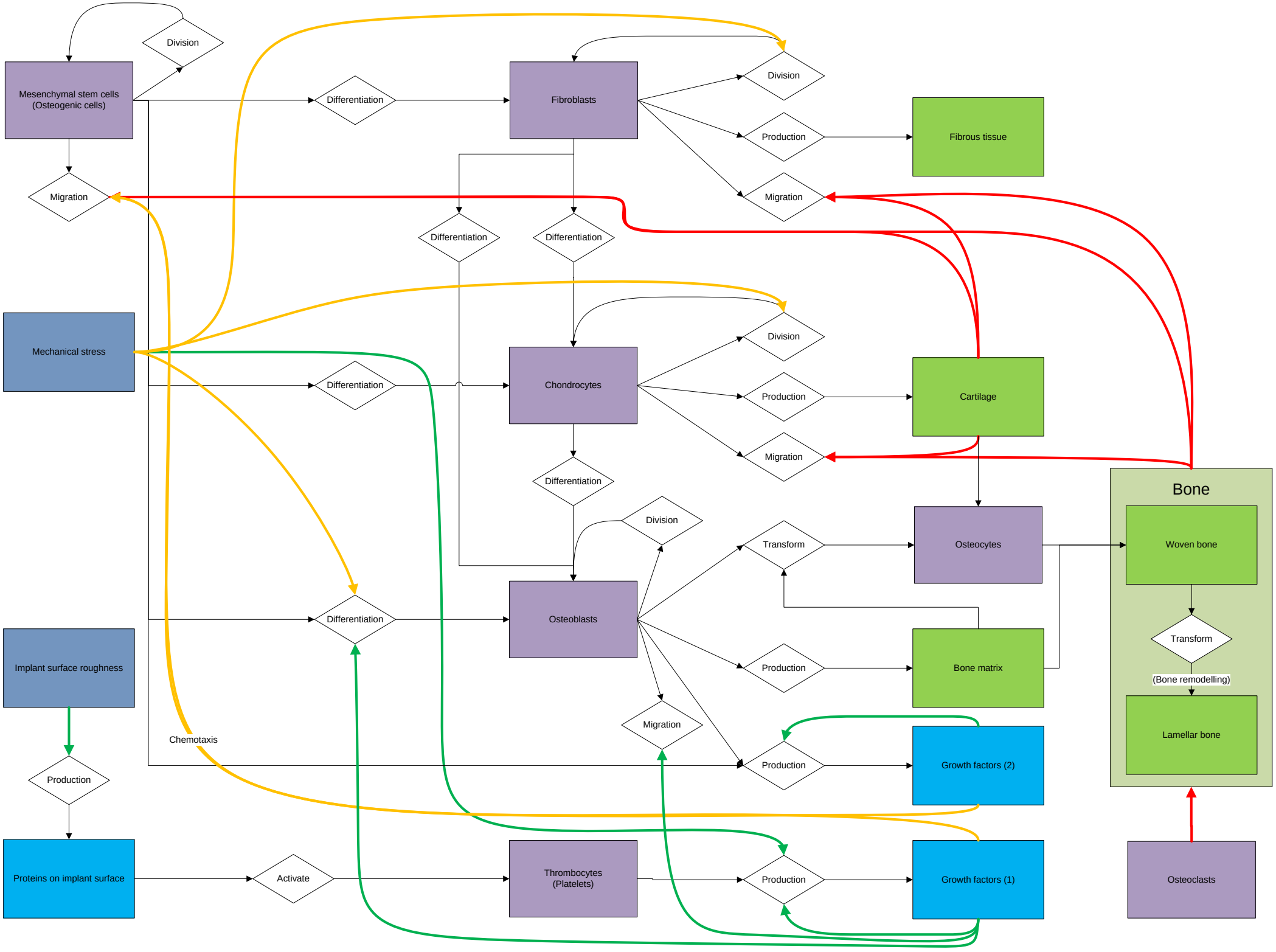
Mesenchymal stem cells (Osteogenic cells)
Division
Migration
Differentiation
Fibroblasts
Division
Production
Migration
Fibrous tissue
Differentiation
Differentiation
Mechanical stress
Differentiation
Chondrocytes
Division
Production
Migration
Cartilage
Differentiation
Division
Differentiation
Osteoblasts
Transform
Production
Migration
Osteocytes
Bone matrix
Bone
Woven bone
Transform
(Bone remodelling)
Lamellar bone
Implant surface roughness
Chemotaxis
Production
Production
Growth factors (2)
Proteins on implant surface
Activate
Thrombocytes (Platelets)
Production
Growth factors (1)
Osteoclasts

Appendix B

Alternative choice in IMEX for 1D FVM model

As mentioned in Section 4.3 an alternative choice in the IMEX method can lead to a more efficient solving method: all non-linear terms (including terms that have some combination of different model variables) are taken at the current time step. This would lead to the following system of equations

$$\mathbf{v}^{i+1} = \left(\frac{M}{\Delta t} - S\right)^{-1} \left(\left(\frac{M}{\Delta t} + T(\mathbf{u}^i)\right)\mathbf{v}^i + \mathbf{f}(\mathbf{u}^i)\right) \tag{B.1}$$

requiring that the matrix inverse only has to be calculated once at the start.

Following this rule, the following discretization is achieved. Only for the osteogenic cell concentration an exception is made because of the chemotaxis term, taking this term on the current time step turns out to lead to great instability.

The differences with the original choice are found in Eq. (B.5)-(B.9).

Platelet concentration

$$\begin{aligned} h\frac{c_n^{i+1} - c_n^i}{\Delta t} = {} & \frac{D_c}{h}\left(c_{n-1}^{i+1} - 2c_n^{i+1} + c_{n+1}^{i+1}\right) + \frac{H_c}{2h}\left[(p_{n-1} - p_n)\, c_{n-1}^{i+1} + (p_{n-1} - 2p_n + p_{n+1})\, c_n^{i+1}\right. \\ & \left. + (p_{n+1} - p_n)\, c_{n+1}^{i+1}\right] - hA_c c_n^{i+1} \end{aligned} \tag{B.2}$$

Osteogenic cells

$$\begin{aligned} h\frac{m_n^{i+1} - m_n^i}{\Delta t} = {} & \frac{D_m}{h}\left(m_{n-1}^{i+1} - 2m_n^{i+1} + m_{n+1}^{i+1}\right) \\ & - \frac{B_{m1}}{2h}\left[\left(s_{1n-1}^i - s_{1n}^i\right) m_{n-1}^{i+1} + \left(s_{1n-1}^i - 2s_{1n}^i + s_{1n+1}^i\right) m_n^{i+1} + \left(s_{1n+1}^i - s_{1n}^i\right) m_{n+1}^{i+1}\right] \\ & - \frac{B_{m2}}{2h}\left[\left(s_{2n-1}^i - s_{2n}^i\right) m_{n-1}^{i+1} + \left(s_{2n-1}^i - 2s_{2n}^i + s_{2n+1}^i\right) m_n^{i+1} + \left(s_{2n+1}^i - s_{2n}^i\right) m_{n+1}^{i+1}\right] \\ & + h\left(\alpha_{m0} + \frac{\alpha_m s_{1n}^i}{\beta_m + s_{1n}^i} + \frac{\alpha_m s_{2n}^i}{\beta_m + s_{2n}^i}\right) m_n^{i+1}(1 - m_n^i) - \frac{\alpha_{mb} s_{1n}^i}{\beta_{mb} + s_{1n}^i} m_n^{i+1} - hA_m m_n^{i+1} \end{aligned} \tag{B.3}$$

Osteoblasts

$$h\frac{b_n^{i+1} - b_n^i}{\Delta t} = \frac{\alpha_{mb} s_{1n}^i}{\beta_{mb} + s_{1n}^i} m_n^i - hA_b b_n^{i+1} \tag{B.4}$$

Growth factors I

$$h\frac{{s_1}_n^{i+1}-{s_1}_n^{i}}{\Delta t}=\frac{D_{s1}}{h}\left({s_1}_{n-1}^{i+1}-2{s_1}_n^{i+1}+{s_1}_{n+1}^{i+1}\right)+\frac{\alpha_{c1}{s_1}_n^{i}}{\beta_{c1}+{s_1}_n^{i}}c_n^i+\frac{\alpha_{c2}{s_2}_n^{i}}{\beta_{c2}+{s_2}_n^{i}}c_n^i-hA_{s1}{s_1}_n^{i+1} \quad \text{(B.5)}$$

Growth factors II

$$h\frac{{s_2}_n^{i+1}-{s_2}_n^{i}}{\Delta t}=\frac{D_{s2}}{h}\left({s_2}_{n-1}^{i+1}-2{s_2}_n^{i+1}+{s_2}_{n+1}^{i+1}\right)+\frac{\alpha_{m2}{s_2}_n^{i}}{\beta_{m2}+{s_2}_n^{i}}m_n^i+\frac{\alpha_{b2}{s_2}_n^{i}}{\beta_{b2}+{s_2}_n^{i}}b_n^i-hA_{s2}{s_2}_n^{i+1} \quad \text{(B.6)}$$

Fibrin network

$$h\frac{{v_f}_n^{i+1}-{v_f}_n^{i}}{\Delta t}=\frac{\alpha_w{s_2}_n^{i}}{\beta_w+{s_2}_n^{i}}b_n^i{v_f}_n^i(1-{v_w}_n^i) \quad \text{(B.7)}$$

Woven bone

$$h\frac{{v_w}_n^{i+1}-{v_w}_n^{i}}{\Delta t}=\frac{\alpha_w{s_2}_n^{i}}{\beta_w+{s_2}_n^{i}}b_n^i{v_f}_n^i(1-{v_w}_n^i)-h\gamma{v_w}_n^i(1-{v_l}_n^i) \quad \text{(B.8)}$$

Lamellar bone

$$h\frac{{v_l}_n^{i+1}-{v_l}_n^{i}}{\Delta t}=h\gamma{v_w}_n^i(1-{v_l}_n^i) \quad \text{(B.9)}$$

Index

Bibliography

P. Moreo Calvo. *Mathematical modelling and computational simulation of the mechanobiological behaviour of bone implants interfaces.* Thesis at the University Zaragoza, Faculty of Computational Mechanics, 2008.

A. Andreykiv. *Simulation of bone ingrowth.* Thesis at the Delft University, Faculty of Mechanical Engineering, 2006.

Y.S. Khoe. *Feasibility study on the acceleration and upscaling of bone ingrowth simulation.* Thesis at the Delft University, Faculty of Mechanical Engineering, 2009.

Pavel Prokharau and Fred Vermolen. Stability analysis for a peri-implant osseointegration model. 2010.

P. Prokharau, F. Vermolen, M.J. Garcia Aznar, M. Doblaré, 2010. On the implementation of mechanical stimulus into peri-implant osseointegration. 2010.

J. van Kan, G. Segal and F. Vermolen. *Numerical Methods in Scientific Computing.* VSSD, 2005.

R. Huiskes, W.D. van Driel, P.J. Prendergast, K. Søballe A biomechanical regulatory model for periprosthetic fibrous-tissue differentiation. *Journal of Materials Science: Materials in Medicine*, 8:785-788, 1997